PHASE BEHAVIOR OF CONCENTRATED PEA PROTEIN ISOLATE-PECTIN MIXTURE AND THEIR APPLICATION

A Dissertation
Submitted to the Graduate Faculty
of the
North Dakota State University
of Agriculture and Applied Science

By

Yang Lan

In Partial Fulfillment of the Requirements
for the Degree of
DOCTOR OF PHILOSOPHY

Major Program:
Cereal Science

August 2020

Fargo, North Dakota

North Dakota State University
Graduate School

Title

PHASE BEHAVIOR OF CONCENTRATED PEA PROTEIN ISOLATE-PECTIN MIXTURE AND THEIR APPLICATION

By

Yang Lan

The Supervisory Committee certifies that this ***disquisition*** complies with North Dakota State University's regulations and meets the accepted standards for the degree of

DOCTOR OF PHILOSOPHY

SUPERVISORY COMMITTEE:

Dr. Jiajia Rao
Chair

Dr. Clifford A. Hall III

Dr. Senay Simsek

Dr. Long Jiang

Approved:

August 27, 2020
Date

Dr. Richard Horsley
Department Chair/Program Coordinator

ABSTRACT

Proteins and polysaccharides are the two major ingredients and often used together in processed food. In aqueous solution, protein–polysaccharide complexation leads to form either in one- or two- phase systems. In recent years, pea protein has received increased attention because of its nutritional value and low price. However, the complexation between pea protein and polysaccharide at concentrated levels and their application have not yet been reported. As such, the overall objectives of this project were: i) to study the phase behaviors of concentrated solutions of pea protein isolate (PPI)–pectin mixtures; ii) to illustrate the microstructure and quantify physicochemical properties of PPI–pectin complexes; and iii) to explore applications of PPI–pectin complexes.

We demonstrated that the state diagram could explicitly identify critical phase transition pH values (pHs) (pH_c, $pH_{\varphi 1}$ and $pH_{\varphi 2}$) of soluble complexes and complex coacervates at concentrated biopolymer system. The pH_{opt} could be recognized at the net charge neutrality or the highest storage modulus of the biopolymer mixture. As the mixing ratio increased from 1:1 to 20:1, the pHs shifted towards higher pH in PPI–pectin mixture. The higher overall charge density of low methoxyl pectin (LMP) favors complex coacervates formation over a wider pH range as compared with high methoxyl pectin (HMP). Electrostatic interaction and hydrogen bonding were the two major bonds attributed to the complexation between PPI and pectin. Additionally, smooth inner pore surfaces with homogeneous large pore size of PPI–sugar beet pectin (SBP) microstructure could be formed at the late stage of coacervates when the environmental pH is near the $pH_{\varphi 2}$ compared to coacervates formed at pH_{opt}. In terms of application, the formation of PPI–pectin soluble complexes could shift minimum protein percentage solubility towards more acidic pH and slightly increase the thermal denaturation temperature of PPI. For application of

hempseed oil (HSO) microencapsulation by means of complex coacervates, the spray-dried microcapsules prepared at late stage of complex coacervates (pH 2.5) had higher drying efficiency and encapsulation efficiency than that coacervates formed at pH 3.5. However, the oxidative stability of HSO microcapsules using the PPI–SBP coacervates fabricated at pH 2.5 was significantly shortened.

ACKNOWLEDGEMENTS

First, I want to thank my advisor, Dr. Jiajia Rao. She gave me tons of excellent suggestions and support in arranging my doctoral study and research work in past four years. I appreciate her encouragement and scientific training on me such as experimental design, problem solving, scientific writing and communication. Without her guidance, I may not complete my study and achieve such accomplishment. I also want to express my gratitude to Dr. Bingcan Chen since he gave me abundant substantial suggestions and assistances in experimental design, performance, and work publishing.

Thank my committee members, Clifford A. Hall, Senay Simsek, and Long Jiang for sharing their valuable suggestions to my study and research. In addition, I am so grateful to Dr. Sanku Mallik in school of pharmacy for sharing his lab resources with me so that I can complete my ITC experiment; to Pawel Borowicz in animal science department for critical suggestions and support in confocal laser scanning microscopy study; and to Dr. Jae-Bom Ohm in USDA-ARS wheat quality lab for his assistance in FTIR study.

Moreover, I really appreciate love, support, and encouragement from my mother, relative, and lab team members, Jin Wan, Minwei Xu, Fengchao Zha, Xiaoxi Qi, Zixuan Gu and Haiyang Jiang, etc. Last, I would thank to China Scholarship Council who provided me with a scholarship for my doctoral study.

TABLE OF CONTENTS

ABSTRACT iii

ACKNOWLEDGEMENTS v

LIST OF TABLES xi

LIST OF FIGURES xii

GENERAL INTRODUCTION 1

CHAPTER 1. LITERATURE REVIEW 4

Pea proteins 4

Chemical composition of pea protein isolate 4

Functionality of PPI 5

Pectin 8

Phase behaviors of protein–polysaccharide complexes 10

Interactions in protein–polysaccharide complexes 10

Factors influencing formation of protein–polysaccharide complexes 13

Methods to identify formation of protein–polysaccharide complexes 18

Turbidimetric method 18

Zeta–potential measurement 19

State diagram 20

Application of protein–polysaccharide complexes 20

Improving functionality of protein 21

Microencapsulation of bioactive compounds 22

Fat replacers 23

References 24

CHAPTER 2. PEA PROTEIN ISOLATE–HIGH METHOXYL PECTIN SOLUBLE COMPLEXES FOR IMPROVING PEA PROTEIN FUNCTIONALITY: EFFECT OF PH, BIOPOLYMER RATIO AND CONCENTRATIONS 35

Abstract 35
Introduction 36
Materials and methods 39
Materials 39
Preparation of pea protein isolate 40
Preparation of PPI and HMP stock solution 40
PPI–HMP mixture preparation 41
Turbidity measurement 41
Particle charge measurement 42
Percent protein solubility 42
Rheological property 42
Differential scanning calorimetry 43
Statistical analysis 43
Results and discussions 43
Identification of suitable pH conditions for forming PPI–HMP soluble complexes at low PPI concentration 43
Identification of PPI–HMP soluble complexes formation as a function of biopolymer mixing ratio at low PPI concentration 46
Identification of PPI–HMP soluble complexes formation as a function of protein concentration 49
pH-dependent protein percent solubility (PS) profiles 52
Flow behavior of PPI–HMP mixture 54
Thermal property of PPI–HMP soluble complexes 57
Conclusions 58
References 58

CHAPTER 3. PHASE BEHAVIOR, THERMODYNAMIC AND MICROSTRUCTURE OF CONCENTRATED PEA PROTEIN ISOLATE–PECTIN MIXTURE: EFFECT OF PH, BIOPOLYMER RATIO AND PECTIN CHARGE DENSITY 65

Abstract 65

Introduction 65

Materials and methods 70

Materials 70

Characterization of pectins 70

Preparation of PPI and pectin stock solutions 72

Preparation of PPI–pectin mixtures 72

Surface charge analysis 73

Confocal laser scanning microscopy (CLSM) 73

Isothermal titration calorimetry (ITC) 74

Fourier transform infrared spectroscopy (FTIR) 74

Statistical analysis 75

Results and discussion 75

Characterization of pectin 75

Effect of pH, mixing ratio and pectin type on phase behaviors of PPI–pectin mixture 76

Microstructural insights into phase behaviors of PPI–pectin mixture 83

Thermodynamic insights into phase behaviors of PPI–pectin complexes 85

FTIR characterization of PPI–pectin complexes 88

Conclusions 90

References 91

CHAPTER 4. PHASE BEHAVIOR AND COMPLEX COACERVATION OF CONCENTRATED PEA PROTEIN ISOLATE–BEET PECTIN SOLUTION 98

Abstract 98

Introduction....98
Materials and methods....101
Materials....101
Fabrication of complex coacervates....102
Surface charge analysis....103
Viscoelastic properties of complex coacervates....104
Quantification of PPI in coacervate phase....104
Isothermal titration calorimetry (ITC)....105
Scanning electron microscopy (SEM)....106
Fourier transform infrared spectroscopy (FTIR)....107
Statistical analysis....107
Results and discussion....107
Effect of pH and mixing ratios on complex coacervation formation....107
Thermodynamic characterization of interactions between PPI and SBP....116
Morphological characterization of complex coacervates (dense colloids *vs* soft colloids)....118
Conclusions....122
References....123
CHAPTER 5. MICROENCAPSULATION OF HEMPSEED OIL BY PEA PROTEIN ISOLATE–SUGAR BEET PECTIN COMPLEX COACERVATION: INFLUENCE OF COACERVATION PH AND WALL/CORE RATIO....130
Abstract....130
Introduction....131
Materials and methods....134
Materials....134
Preparation of microencapsulated hempseed oil in PPI–SBP complex coacervates....135

Physiochemical properties of microcapsules 137
The oxidative stability of microencapsulated hempseed oil 140
Statistical analysis 141
Results and discussion 141
Optimum pH for complex coacervation between PPI and SBP 141
Encapsulation efficiency of microcapsules and their physicochemical properties 145
Morphological properties of microcapsules 151
Oxidative stability of HSO in microcapsules 155
Conclusions 158
References 159
OVERALL CONCLUSION 165
FUTURE WORKS 168
References 169

LIST OF TABLES

Table		Page
2-1.	Thermal property of PPI–HMP soluble complexes.	57
3-1.	The degree of esterification (DE) and galacturonic acid (GalA) content of pectin.	76
3-2.	Thermodymic parameters of binding between PPI and pectins at 25 ℃ in citrate–phosphate buffer (pH 3.5).	87
4-1.	Percentage (%) of PPI in PPI–SBP coacervate phases collected at different mixing ratios during acid titration.	115
5-1.	Formulation and code of microcapsules.	137
5-2.	Powder yield (PY), encapsulation efficiency (EE), pay load (PL) and physical properties of hemp seed oil (HSO) microcapsules.	146
5-3.	Copper and iron content in microcapsules as determined by ICP–OES.	158

LIST OF FIGURES

Figure — Page

1-1. Schematic structure of pectins. Pectin is dominantly composed of galacturonan with 1,4–linked α–D–galacturonic acid units (GalA) in the backbone. The carboxylic acid groups in GalA can be partly methyl esterified. Adapted from Izydorczyk, Cui, and Wang (2005). 10

1-2. Possible interactions between charged proteins and polysaccharides in liquid. P_r, and P_s represents protein and polysaccharide solution, respectively. Adapted from Matalanis, et al. (2011). 12

1-3. Schematic phase transition of protein–polysaccharide mixture as function of pH. 15

1-4. Phase behaviors of concentrated solutions of protein-polysaccharide mixtures. Adapted from Lan, Ohm, Chen, and Rao (2020). 20

2-1. (a) Turbidity curves of PPI (0.05 wt %), HMP (0.05 wt%), and mixed (1:1 ratio) PPI–HMP system during acid titration from pH 8–2. $pH_{\varphi 1}$was determined by extending tangent lines on either side of inflection points. (b) Dependence of ζ–potential of PPI (0.05 wt %), HMP (0.05 wt %), and mixed (1:1 ratio) PPI–HMP system on pH. (c) Dependence of PPI and mixed (1:1 ratio) PPI–HMP appearance on pH. 44

2-2. (a) $pH_{\varphi 1}$of PPI-HMP mixture at different biopolymer mixing ratio. (b) Dependence of ζ–potential on pH and biopolymer mixing ratio. The PPI concentration was fixed at 0.05 wt%. 47

2-3. State diagram of PPI–HMP mixture in the presence of 0.05 wt% of PPI (a) and 1.00 wt% of PPI (b). (c) The appearance of PPI–HMP mixture (ratio 5:1) as function of pH. ○ represents translucent/transparent solution; □ represents cloudy/milky solution; ▲ represents precipitation and cloudy solution; ■ represents precipitation and clear solution. 50

2-4. Dependence of ζ–potential on pH and biopolymer mixing ratio. The PPI concentration was fixed at 1 wt%. 52

2-5. Percent protein solubility as function of pH and biopolymer ratio. The PPI concentration was fixed at 1 wt%. 53

2-6. (a) Apparent viscosity versus applied shear rate of mixed PPI–HMP system (ratio 2:1) at different pH; (b) Apparent viscosity versus applied shear rate of PPI–HMP soluble complex mixtures, PPI and HMP solution at pH 6. 55

3-1. State diagram of PPI–pectin mixture as function of pH and mixing ratio (a) HMP; (b) LMP. The appearance of PPI–pectin mixture (ratio 5:1) as function of pH (c) HMP, and (d) LMP. The PPI concentration was fixed at 1 wt%. The appearance was observed after 24 h standing. ○ represents translucent solution; □ represents turbid solution; ▲ represents precipitation & cloudy solution; ■ represents precipitation & clear solution; ● represents precipitation & clear solution that has higher volume of precipitation than ■. 77

3-2. The effect of degree of esterification (DE) on pHs values associated with co-solubility, soluble complex and complex coacervate of PPI–pectin mixture. Four pHs (pH_c, $pH_{\varphi 1}$, pH_{opt} and $pH_{\varphi 2}$) of phase transition were included. The PPI–pectin mixing ratio was fixed at 5:1, and PPI concentration was fixed at 1 wt%. The measurements were repeated three times. The bars with different letters are significantly different ($p < 0.05$). 80

3-3. Dependence of Zeta (ζ)–potential on pH and biopolymer mixing ratio (a) HMP; (b) LMP. The strength of electrostatic interaction (SEI) of PPI to PPI, PPI to HMP, and PPI to LMP was presented in grey color. (c) Plot of isoelectric point (IEP) as function of PPI–pectin mixing ratio. The PPI concentration was fixed at 1.0 wt%. 81

3-4. Confocal images of PPI (a), HMP (b), and LMP (c) dispersions at pH 7; PPI–HMP mixtures at pH 7 (d), pH 5.5 (e), and pH 3.5 (f); PPI–LMP mixtures at pH 8 (g), pH 6 (h), and pH 3.5 (i). The PPI–pectin mixing ratio was fixed at 5:1, and PPI concentration was fixed at 1 wt%. Red color represents the protein phase in the CLSM image. Bar represents 5 µm..... 84

3-5. Thermogram (top panel) and binding isotherm (bottom panel) corresponding to the titration of PPI dispersion with HMP at pH 5.5 (a), LMP at pH 6 (b), HMP at pH 3.5 (c), and LMP at pH 3.5 (d) at 25 °C. The concentration of PPI, HMP, LMP in citrate–phosphate buffer was 48.31, 7.58 and 10.97 µM, respectively. 86

3-6. FTIR spectra of PPI, HMP, LMP, PPI–HMP and PPI–LMP complexes prepared at selected pH conditions. The PPI–pectin mixing ratio was fixed at 5:1, and PPI concentration was fixed at 1 wt%. 88

4-1. (a) State diagram of PPI, and PPI–SBP mixtures at different mixing ratios during acid titration. (b) The appearance of PPI–SBP mixture (5:1 mixing ratio) as function of pH. The PPI concentration was fixed at 1 wt%. The appearance was observed after 24 h standing. ○ represents translucent solution; □ represents turbid solution; ▲ represents precipitation and cloudy solution; ■ represents precipitation and clear solution; ● represents precipitation and clear solution that has higher volume of precipitation than ■. 108

4-2. (a) Zeta (ζ)–potential changes of PPI, SBP, PPI–SBP mixtures at different mixing ratios and the strength of electrostatic interaction (SEI) of PPI–PPI and PPI–SBP during acid titration. (b) Plot of isoelectric point (IEP) against PPI–SBP mixing ratio (including data points of pure SBP and PPI). The PPI concentration was fixed at 1 wt%. 111

4-3. The (a) storage modulus G′ and (b) loss modulus G″ versus angular frequency for PPI–SBP coacervates prepared at different pH values (the PPI–SBP mixing ratio was fixed at 5:1). The (c) G′ and (d) G″ of coacervates prepared at different mixing ratios and at the pH that the highest G′ occurred within each mixing ratio. The PPI concentration was fixed at 1 wt%. 114

4-4. Thermogram (top panel) and binding isotherm (bottom panel) corresponding to the titration of PPI (48.31 μM) with SBP (7.41 μM) dispersion in citrate–phosphate buffer (pH 3.5) at 25 °C. 117

4-5. SEM micrographs (5000×) of (a) PPI collected at pH 4.5, (b) SBP powder, and PPI–SBP coacervates collected at (c) pH 3.5 and (d) pH 2.5; (e) FTIR spectra of the coacervates prepared at pH 3.5 and 2.5. The PPI–SBP mixing ratio was fixed at 5:1, and PPI concentration was fixed at 1 wt%. Bar in SEM images represents 5 μm. 119

5-1. (a) State diagram of pea protein isolate (PPI)–sugar beet pectin (SBP) mixtures as function of pH (5.0–2.0) and wall/core mass ratios (4:1 to 1:1). (b) The appearance of PPI–SBP mixture (at wall/core ratio of 4:1) as function of pH observed after 24 h static standing at 4 ℃. For all mixtures, PPI to SBP mixing ratio and the total biopolymer concentration was fixed at 5:1 and 1.20 wt%, respectively. Nile red (lipophilic dye) was added into both water &hem seed oil (HSO) mixture (control) and the microencapsulated HSO in PPI–SBP complex coacervate (pink color tubes) to aid for visualizing oil distribution during phase separation. Three symbols ▲, ■, and ● represents (i) precipitation & cloudy solution, (ii) precipitation & clear solution, and (iii) precipitation & clear solution containing higher volume of precipitation than ■, respectively. 142

5-2. Impact of wall/core ratios on storage modulus (G′) and loss modulus (G″) of hemp seed oil (HSO) microcapsules by means of PPI–SBP coacervates at 1 rad/s frequency as a function of pH. 144

5-3. Particle size distribution of spray-dried hemp seed oil (HSO) microcapsules. F1-F9 represent nine formulations listed in Table 5-1. 148

5-4. ATR–FTIR spectra of the hemp seed oil (HSO), PPI, SBP, PPI–SBP microcapsules (F1 and F4) and PPI microcapsules (F7). F1, F4, and F7 represent formulations listed in Table 5-1. 150

5-5. SEM of spray-dried HSO microcapsules by means of PPI–SBP coacervates (a–d) and HSO microcapsules by means of PPI as wall material (e–f). Bar represents 5 μm. Arrow was pointed as hollow and uncompleted particles. F1-F8 represent formulations listed in Table 5-1. 152

5-6. Three-dimensional confocal images of HSO microcapsules by means of PPI–SBP coacervates presented in full size (abef; size of 650×650×15 μm in x, y and z directions respectively) and smaller size (cdgh; 90×90×15 μm in x, y and z directions respectively). PPI and HSO were labelled as red and green color, respectively. Arrow was pointed as hollow and uncompleted particles. F1, F2, F4, and F5 represent formulations listed in Table 5-1. 154

5-7. Formation of secondary oxidation product hexanal (a) and propanal (b) in HSO microcapsules by means of PPI–SBP coacervate as a function of storage time during storage at 37 °C. Some of standard error bars are within the data points. The lag phase of variants was calculated and inserted as table. F1, F2, F4, and F5 represent formulations listed in Table 5-1. 156

GENERAL INTRODUCTION

The phase behavior of protein and polysaccharide in a solution can be either as one phase system (co-solubility and soluble complexes) or two phases system (complex coacervates), depending on strength of attractive electrostatic interaction between charged functional groups of biopolymers (Wijaya, Patel, Setiowati, & Van der Meeren, 2017). Such strength is prominently impacted by factors such as pH, biopolymer mixing ratio and concentrations, charge density of polysaccharide (Jones, Decker, & McClements, 2009). According to previous reports, the formation of protein–polysaccharide soluble complexes/complex coacervates is a promising method to improve functional properties of protein, such as protein solubility, thermal stability, foaming and emulsifying properties (Braudo, Plashchina, & Schwenke, 2001; Moschakis & Biliaderis, 2017; Rodriguez, Binks, & Sekine, 2018; Wagoner & Foegeding, 2017), as wall material to encapsulate bioactive compounds (Devi, Sarmah, Khatun, & Maji, 2017), purify proteins (Li, Long, et al., 2018) and to fabricate films (Eghbal, et al., 2016), etc.

Recently, there has been an increased interest in the consumption of pea (*Pisum sativum* L.) protein due to its low cost, high production yield, sustainable source with a low carbon footprint, high nutritional value, allergen-free and gluten-free that can be claimed in food labelling (Adebiyi & Aluko, 2011; FAOSTAT; Havemeier, Erickson, & Slavin, 2017; Lam, Can Karaca, Tyler, & Nickerson, 2018). Nevertheless, the application of pea protein in food industry is still changeling due to its low solubility and some limited functionality (Cui, et al., 2020; Wagoner, et al., 2017).

In the past, the phase behaviors between pea protein and polysaccharide have been investigated at low biopolymer concentrations (below 0.30 %) (Aryee & Nickerson, 2012; Liu, Shim, Shen, Wang, & Reaney, 2017; Liu, et al., 2010). However, protein–polysaccharide

complexes generally require higher biopolymer concentration in the purpose of application such as microencapsulation. As such, it is extremely important to understand the phase behaviors, as well as physiochemical properties of pea protein–polysaccharide complexes at higher biopolymer concentrations and their application. One of the reasons for limited research on protein–polysaccharide complexes at concentrated solution is the restriction of analytical tool for identifying critical phase transition pH values (pHs) (pH_c, $pH_{\varphi 1}$, $pH_{\varphi 2}$) at concentrated biopolymer solutions. In the past, turbidimetric methods have been widely adopted to distinguish phase behaviors via measuring the turbidity changes as function of pH (Aryee, et al., 2012; Liu, et al., 2017; Liu, et al., 2010). However, this traditional turbidimetric method is invalid for identifying phase behaviors and pHs (i.e. $pH_{\varphi 1}$, $pH_{\varphi 2}$ and pH_{opt}) of concentrated binary biopolymer system because the initial turbidity of the system is so high (OD_{600nm} >1). Additionally, the phase transition pHs tend to shift towards higher pH values as rise of biopolymer concentrations (Niu, et al., 2014). As such, the development of an alternative method to identify the phase transition pHs at concentrated biopolymer systems is utmost important for the commercial practicality of pea protein–polysaccharide complexes.

Therefore, the initial objective of this project was to develop alternative methods (i.e. state diagram, zeta–potential and rheological measurement) to identify pHs for a concentrated pea protein–pectin biopolymer system, and to study the factors such as biopolymer concentrations and mixing ratios influenced on the pHs. And then, the microstructure and physicochemical properties of PPI–pectin complexes including soluble complex and complex coacervates were elucidated in a concentrated mixture system by scanning electron microscopy (SEM), isothermal titration calorimetry (ITC), and Fourier transform infrared spectroscopy

(FTIR). Finally, the objective was to explore applications of PPI–pectin complexes in terms of improving PPI functionality and microencapsulation of hempseed oil (HSO).

CHAPTER 1. LITERATURE REVIEW

Pea proteins

Chemical composition of pea protein isolate

Recently, pea (*Pisum sativum* L.) protein has garnered considerable interest because of its low cost and high production yield (dry peas make up 15% of world pulses production), environmental sustainability, high nutritional value (rich in protein and fiber), allergen-free and gluten-free that can be claimed in food labelling (Adebiyi, et al., 2011; FAOSTAT; Havemeier, et al., 2017; Lam, et al., 2018). Pea contains approximately 18–30% protein, 60–70% carbohydrates (35–40% starch and 10–15% dietary fiber), 1.6–3.2% fat and other minor components (minerals, phytic acid, saponins, etc.) depending on the variety and growing conditions (Boye, Zare, & Pletch, 2010; Karaca, Low, & Nickerson, 2011). Therefore, it can be considered as good sources of material for extracting protein. In general, PPI is commonly extracted from the defatted pea flour using method of alkaline extraction followed by isoelectric precipitation (AE–IEP), which take advantages of high solubility of proteins in alkaline conditions and their minimal solubility at their isoelectric point (IEP) between pH 4 and 5 (Lam, et al., 2018). Briefly, AE–IEP method started by stirring defatted pea flour in water at a 1:15 (w/v) ratio, followed by adjusting pH to 8.5–9.5 using NaOH and then stirred for about 1 h at room temperature. Afterwards, the mixture is centrifuged to collect supernatant, and then the proteins are precipitated from the supernatant by adjusting pH to IEP of PPI. Finally, the precipitates are collected, re-suspended in water, neutralized, and dried (Shevkani, Singh, Kaur, & Rana, 2015; Stone, Karalash, Tyler, Warkentin, & Nickerson, 2015). The protein content of PPI extracted using AE–IEP method is commonly ranging from 78% to 86% due to variations in extraction conditions, pea cultivars and other factors (Cui, et al., 2020). The extracted PPI

primarily consists of two classes of proteins according to Osbourne classification, globulins (salt-soluble) and albumins (water-soluble), taking up approximately 70–80% and 10–20% of the total protein, respectively (Zha, Dong, Rao, & Chen, 2019). Based on sedimentation coefficients, globulins can be further subdivided into legumin (hexameric protein, 300–400 kDa, 11S), vicilin (trimeric protein, 150–170 kDa, 7S), and convicilin (composed of three ~70 kDa sub-units, 7S) (Lam, et al., 2018). Legumin is a hexameric protein molecule which consists of six subunit pairs of 60 kDa and each pair has an acidic (α, 40 kDa) and a basic (β, 20 kDa) subunit linked via covalent bonds. Vicilin is a trimer protein with a molecular mass between 150 to 170 kDa. Comparing with legumin, vicilin is more water soluble due to surface that is more hydrophilic than hydrophobic (Stone, et al., 2015). As such, the physicochemical and functional properties of pea protein are highly related to their protein composition (Sikorski, 2001). In terms of amino acid profile of pea protein, pea proteins are rich in glutamic acid, aspartic acid, arginine, leucine, and lysine (a limiting amino acid in most cereals), whereas sulfur-containing amino acids such as methionine and cysteine are lacking (Gorissen, et al., 2018).

Functionality of PPI

Functional properties of pea protein are strongly influenced by its physiochemical properties such as molecular rigidity/flexibility, amino acid composition and sequence, hydrophobicity/hydrophilicity ratio, net charge and charge distributions, etc. (Nakai & Modler, 1996). Thus, it ultimately determines the performance of protein in food application in terms of texture and organoleptic characteristics (Boye, et al., 2010). The major functional properties of PPI including solubility, foaming, emulsifying, and rheological properties are discussed in this section.

Solubility

Solubility is one of the protein functionalities that critically affects protein applications in high moisture food product and other functionalities such as foaming and emulsifying properties. The most commonly used solvents in evaluation of protein solubility are water or phosphate buffer. High protein solubility means that it is easy to incorporate and distribute proteins uniformly in high moisture-based food products. It also means proteins have better emulsifying, foaming and gelling properties (Adebiyi, et al., 2011; Liang & Tang, 2013). Generally, the solubility of pea protein is correlated to the average surface hydrophobicity and charge density of the protein. The solubility increases when the average hydrophobicity decreases or charge density increases (Nakai, et al., 1996). Generally, environmental conditions such as pH, ionic strength and protein extraction methods impacted on protein surface hydrophobicity and charge density, thus the solubility of protein (Nakai, et al., 1996). For instance, neutral salts, such as NaCl and $CaCl_2$, which are able to control the ionic strength of the protein solution, have a two-fold effect of protein solubility via their effect on electrostatic forces (Nakai, et al., 1996). Normally, solubility increases at low salt concentrations (also called “salting-in”) by suppressing the electrostatic attractive forces between proteins, while solubility decreases at higher salt concentrations (so called “salting-out”) due to ion hydration tendency of the salts. In addition, proteins are generally soluble in strong polar solvents such as water and glycerol while rarely soluble in weak polar solvents such as ethanol or organic solvents such as acetone (Belitz, Burghagen, Grosch, & Schieberle, 2013).

In terms of solubility of PPI as function of pH, PPI displays U-shaped pH dependent solubility profile, which means solubility of PPI is higher at very acidic or alkaline condition, and the lowest solubility existed at the IEP of PPI (~pH 4.5). For example, 82% of PPI solubility

was reported at pH 7–8, whereas only 44% of solubility of PPI was measured at pH 3 (Cui, et al., 2020). The lower solubility at pH 3 could be attributed to protonation of carboxylic acid groups of PPI. As a result, hydrophobic interaction was enhanced, and electrostatic repulsion between protein molecules was reduced (Taherian, et al., 2011).

Foaming and emulsifying properties

Because of the amphiphilic molecule properties of protein, protein molecules can partly unfold and reorient buried hydrophobic groups towards hydrophobic phase and charged groups (hydrophilic groups) towards hydrophilic phase during emulsion and foam preparation (Belitz, et al., 2013). Therefore, proteins have a capability to decrease interfacial tension or surface tension between two immiscible phases (water–oil interface of emulsion droplet or water–air interface of air bubbles) by forming cohesive and viscous intermediate layer between two immiscible phases (Belitz, et al., 2013). Generally, emulsifying capacity (EC) and emulsifying stability (ES) are the two frequently used indicators for evaluating emulsifying property of protein. EC indicates the maximum grams of oil encapsulated by per unit of protein to form oil-in-water (O/W) emulsion system, whereas ES measures how well the emulsion can resist changes to its structure over a time period (Stone, et al., 2015). Stone et al. reported that the EC and ES of 1% (w/v) PPI (prepared by AE–IEP, freeze-dried) was 187 g/g and 96%, respectively (Stone, et al., 2015). The second commonly used method to determine protein emulsifying stability is to measure the change of droplet diameters as a functional time to represent a long term storage stability of emulsion (Yao, et al., 2016).

Foam capacity (FC) and foam stability (FS) are the two most common parameters used to characterize the protein foaming properties (Boye, et al., 2010). FC is parameter to represent the ability of protein to form foams under certain conditions (e.g. protein concentration and pH),

whereas FS indicates the ability of a protein to retain the foam volume during a period of time (Stone, et al., 2015). The features of proteins, such as solubility, surface hydrophobicity, molecular weight, and net charge of proteins determines the FC and FS of protein (Belitz, et al., 2013). For measurement of FC and FS, foam is formed by stirring protein solution at high speed for about 5 min (low temperature) and foam volume is recorded at 0 and 30 min. FC is measured by volume growth before and after whipping whereas FS is calculated as the foam volume change during 0–30 min. For example, the FC and FS of 1% (w/v) PPI (extracted using AE–IEP, freeze-dried) was reported as 87–132% and 94–96%, respectively (Shevkani, et al., 2015). A lower FS value (68%) of a 1% PPI obtained from same protein extraction method was also reported (Stone, et al., 2015).

Viscosity

The rheological property of pea proteins is also an important functional property, which affects their utilization in foods. Taherian et al. measured the apparent viscosity of 10 wt% PPI using a rheometer with a cone (60 mm diameter) under a shear rate of 0.1–100 s^{-1} and reported that its apparent viscosity was highly dependent on protein purity and solubility of PPI (Taherian, et al., 2011). Moreover, PPI showed a shear-thinning behavior, which means a high viscosity at low shear rates and lower viscosity with increasing shear rates (McCarthy, et al., 2016; Taherian, et al., 2011).

Pectin

Pectin is an anionic polysaccharide and is a mainly existed in plant cell wall. It has been worldwide employed in food industry as a gelling and thickening agent in jams or a stabilizer in acidic protein products (Ru, Wang, Lee, Ding, & Huang, 2012). Commercially available pectin is isolated from plant materials (e.g. citrus peel, apple pulp and sugar beet) by means of acid

extractions (Sperber, Schols, Stuart, Norde, & Voragen, 2009). After acid extraction, pectin has Mw of 60–180 kDa varied from its origin. It is predominantly composed of galacturonan with 1,4–linked α–D–galacturonic acid (GalA) units in the backbone (**Fig. 1-1**) (Fishman, Gillespie, Sondney, & El-Atawy, 1991; Sperber, et al., 2009). The carboxylic acid groups in GalA residues can be methyl esterified to change the charge density of pectin, thus the functionality of pectin. For instance, un-esterified residues (carboxylic acid) carry negative charges when the solution pH is above the pK_a of carboxyl moieties (ranging from 2.9 to 3.3 depending on pectin sources) (Wagoner, et al., 2017). According to the structure of pectin, pectin can be classified by two parameters: the degree of esterification (DE) of the carboxylic acid groups in galacturonan and the degree of blockiness (DB). The DE determines the overall charge density, while DB give information to local charge density of the pectin molecules as DB denotes the distribution pattern of un-esterified blocks of GalA along the pectin backbone (Ru, et al., 2012; Xu, et al., 2018). Based on DE, pectin can be categorized as low methyl (DE < 50%) pectin (LMP) with high overall charge density, and high methyl (DE ≥ 50%) pectin (HMP) with low overall charge density (Xu, et al., 2018). For example, a widely used sugar beet pectin (SBP) typically has DE around 55% (Wang, Ren, Ding, Xu, & Chen, 2018; Xiao, Qi, & Wickham, 2018). A high DB value typically means that the un-esterified blocks of GalA are distributed in a blockwise manner along the pectin backbone (more sections of the chain contain contiguous charged residues), representing a high local charge density; a low DB value means a random distribution, indicating a low local charge density (Xu, et al., 2018).

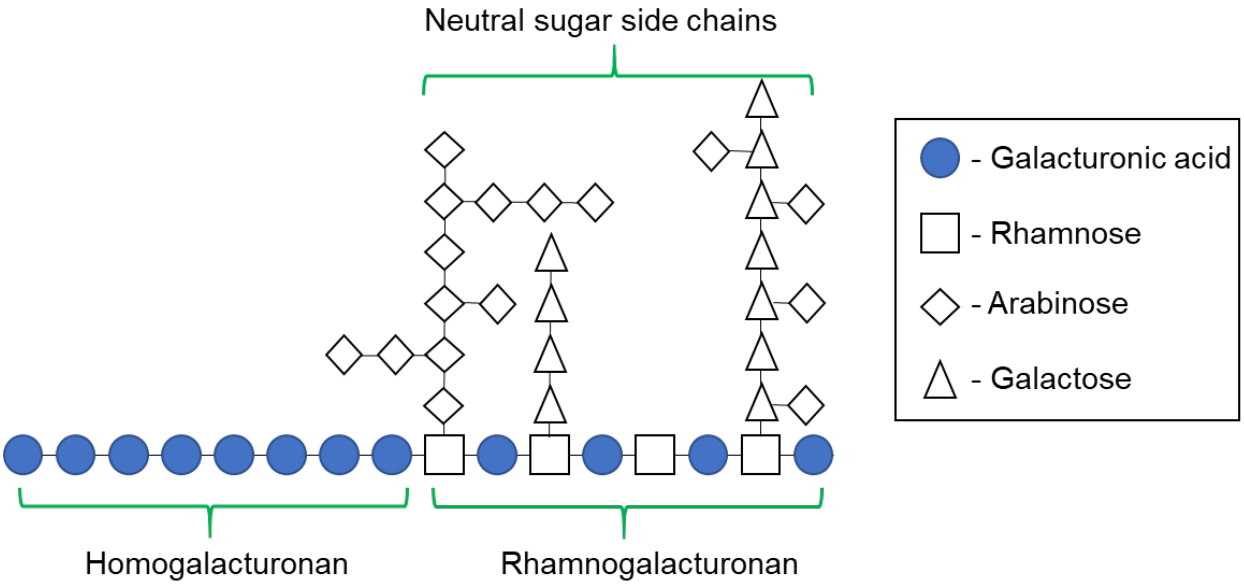

Figure 1-1. Schematic structure of pectins. Pectin is dominantly composed of galacturonan with 1,4–linked α–D–galacturonic acid units (GalA) in the backbone. The carboxylic acid groups in GalA can be partly methyl esterified. Adapted from Izydorczyk, Cui, and Wang (2005).

Phase behaviors of protein–polysaccharide complexes

Protein and polysaccharide are often used in processed food for numerous reasons such as improved protein functionality and food texture. In a mixed biopolymer (protein and polysaccharide) systems, either one- or two-phase behaviors can occur depending on the biopolymer characteristics (e.g., type and distribution of reactive groups, molecular weight), biopolymer concentration, ratio and environmental conditions (i.e., pH, salt and temperature).

Interactions in protein–polysaccharide complexes

Electrostatic interactions

In a solution of protein–polysaccharide, both biopolymers generally interact by non-covalent bonds, and three molecular interaction forces, i.e., electrostatic interactions, hydrogen bonding and hydrophobic interactions (Wijaya, Patel, et al., 2017). Among the three interactions, electrostatic interactions (ion to ion) is dominant. Electrostatic interactions can be divided into attractive electrostatic interaction and repulsive electrostatic interaction, resulting in associative

phase separation and segregative phase separation, respectively (**Fig. 1-2**). These separation type depends on the biopolymer characteristics, biopolymer concentrations and ratios, and environmental conditions (e.g., pH, ionic strength, charge density and temperature) (Matalanis, Jones, & McClements, 2011). Repulsive electrostatic interactions occur when both biopolymers (proteins and polysaccharides) in a solution carry charges have the same sign, contributing to phase behaviors of co-solubility at low biopolymer concentrations or incompatibility at high biopolymer concentrations (**Fig. 1-2**) (Wijaya, Patel, et al., 2017). In contrast, attractive electrostatic interactions take place where oppositely charged biopolymers mix in a solution. This interaction could be weak or strong and contribute to formation of soluble or insoluble complexes (complex coacervates), respectively (**Fig. 1-2**). For anionic polysaccharide–protein mixture system, soluble complexes are formed due to weak electrostatic binding of anionic polysaccharides to cationic reactive sites of proteins, and the resulting net charge allows the colloidal particles to be relatively stable suspended in the solution. Furthermore, insoluble complexes (coacervates) are formed as the increase of attractive electrostatic interaction strength between anionic carboxyl groups on the polysaccharides and cationic amino groups on the protein surface (Wijaya, Patel, et al., 2017).

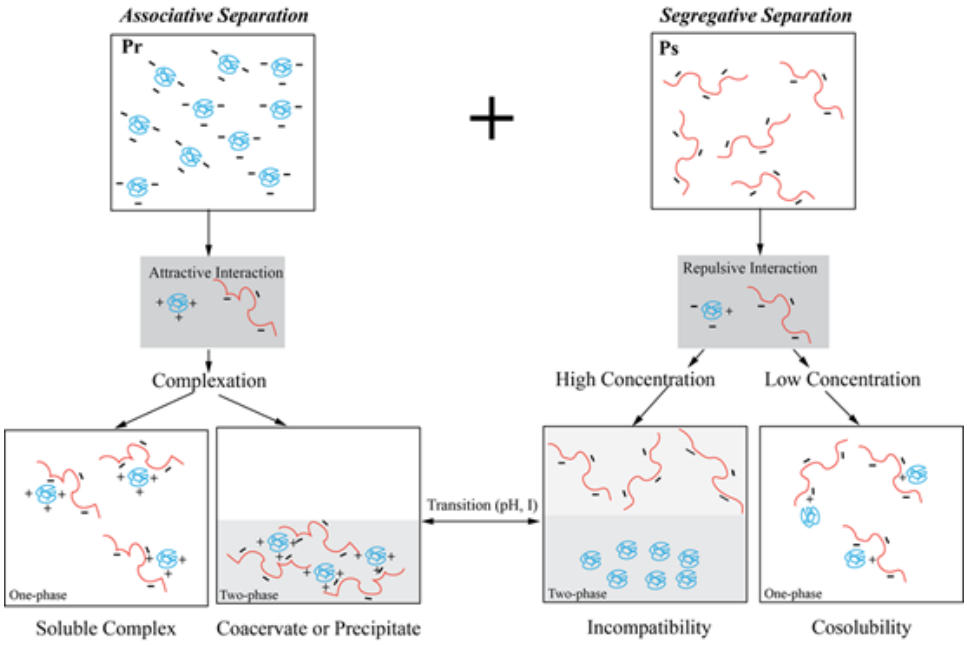

Figure 1-2. Possible interactions between charged proteins and polysaccharides in liquid. P_r, and P_s represents protein and polysaccharide solution, respectively. Adapted from Matalanis, et al. (2011).

Hydrogen bonds

Hydrogen bonds are formed between a hydrogen atom of one molecule and an electronegative atom on a neighboring group (i.e. nitrogen, oxygen, sulfur and oxygen on carbonyl/carboxyl group) (McClements, 2015). Typically, bond strengths and lengths of hydrogen bond are 10–40 kJ/mol and 0.18 nm, respectively. As the two biopolymers carry charges have the same sign, hydrogen bonding between proteins and polysaccharides can be occurred (Wijaya, Patel, et al., 2017). For example, hydrogen bonding could be presented when soluble complexes of protein and sulphated polysaccharides are fabricated at pH values above the IEP of the protein (Ye, 2008). Hydrogen bonding was also reported in gelatin–pectin complexes system (Schmitt, Sanchez, Desobry-Banon, & Hardy, 1998).

Hydrophobic interactions

Hydrophobic interactions is a strong attractive force that acts between nonpolar groups for avoiding contact with water (McClements, 2015). In general, hydrophobic interactions in

protein–polysaccharide complexes become stronger as an increase of temperature. This is because the increased temperature results in conformational and structural changes of the biopolymers, thereby the interaction of hydrophobic segments of biopolymers was also increased (Schmitt, et al., 1998). The hydrophobic interactions can be applied for increasing thermal stability of protein by using protein–polysaccharide complexes. For instance, it has been evidenced by increased thermal stability of β-lactoglobulin–SBP complexes at the pH conditions of 5 to 7 and salt concentrations (0 to 200 mM NaCl) after a heat treatment at 80 °C for 15 min (Jones & McClements, 2008).

Factors influencing formation of protein–polysaccharide complexes

As stated aforementioned, the phase behavior of protein–polysaccharide is primarily driven by electrostatic interaction (Jones & McClements, 2011). Therefore, pH, ionic strength, protein to polysaccharide ratio and biopolymer concentrations, biopolymer type are the major factors affecting either one phase or two phases of protein–polysaccharide mixture due to their great potential to influence the strength of electrostatic interactions (Jones, et al., 2009).

pH

The formation of soluble complexes or complex coacervates is mostly dependent on solution pH due to its influence on the ionization degree of functional groups (i.e. amino and carboxyl groups) on the biopolymer backbone (Pathak, Priyadarshini, Rawat, & Bohidar, 2017). The influence of pH on formation of protein–polysaccharide complexes is usually investigated by turbidimetric analysis based on the optical properties of biopolymer mixtures at low total concentrations (i.e. below 0.3 wt%) (Aryee, et al., 2012; Liu, et al., 2017; Liu, et al., 2010). When reducing pH of a mixed biopolymer (i.e. protein–anionic polysaccharide) solution to acidic pH, four pH regions corresponded to four phase behaviors can be identified using three

pHs (pH_c, $pH_{\varphi 1}$, $pH_{\varphi 2}$) (**Fig. 1-3**) (Moschakis, et al., 2017; Niu, et al., 2014). Initially, both the protein and anionic polysaccharide molecules have a sufficiently strong negative charge at higher pH values which prevents them from becoming close enough to associate. When the pH is reduced below a critical value, which refer to as pH_c, then the protein and polysaccharide weakly associates with each other to form soluble complexes. Therefore, the pH_c is identified as the onset pH of soluble complex formation due to a slope change in the turbidity curve as function of pH (Jones, et al., 2011). Upon further reduction of the pH, another critical value is reached, which refer to as $pH_{\varphi 1}$, where the protein–polysaccharide associates to form coacervates. Typically, the coacervate phase is a highly viscous or gel-like material. The $pH_{\varphi 1}$ is the onset of complex coacervates formation because of turbidity increased sharply due to increased electrostatic attractive interaction. When the electrostatic attraction between the protein and polysaccharide molecules is sufficiently strong, the biopolymer molecules are packed densely and sediment very quickly to the bottom of solution. The turbidity (optical density) reaches a maximum at pH_{opt} where the coacervates yield is maximum at this pH due to charge neutrality between the biopolymers. When the pH below the pKa value of anionic groups on the polysaccharide molecules, there is no association between polysaccharide molecule and protein This pH is referred as $pH_{\varphi 2}$. For example, Liu et al. reported values of pH_c, $pH_{\varphi 1}$, pH_{opt}, $pH_{\varphi 2}$ at pH 4.2, 3.7, 3.5 and 2.5, respectively, when PPI and gum arabic (GA) mixed at a total biopolymer concentration of 0.05% and their weight ratio of 1:1 (Liu, Low, & Nickerson, 2009). When PPI is mixed with another anionic polysaccharides (alginate) at ratio of 1:1 and total concentration of 0.1%, different values of pH_c, $pH_{\varphi 1}$, pH_{opt} at pH 5, 3, and 2, respectively, were reported by Klemmer et al (Klemmer, Waldner, Stone, Low, & Nickerson, 2012).

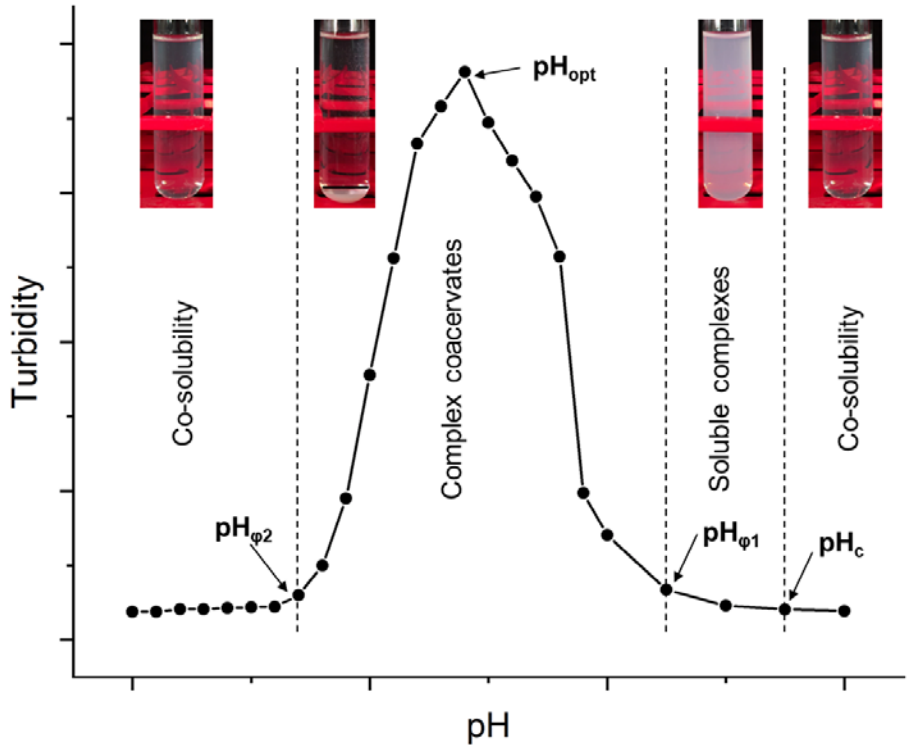

Figure 1-3. Schematic phase transition of protein–polysaccharide mixture as function of pH.

Protein–polysaccharide concentration and ratio

The influence of biopolymer ratio on the protein-polysaccharide complex formation is widely investigated using turbidimetric method by comparing changes in turbidity profile at low total biopolymer concentration. The total biopolymer concentration of complexes in reported literatures is typically 0.05–0.3 wt%, and the ratio of proteins to polysaccharides ranges from 1:1 to 30:1 (Elmer, Karaca, Low, & Nickerson, 2011; Klemmer, et al., 2012; Stone, Cheung, Chang, & Nickerson, 2013). In general, mixing ratios influence biopolymer surface charge, and thus impact on critical pH range of protein–polysaccharide complex formation. There is an agreement from studies on the relationship between pHs (pH_c, $pH_{\varphi 1}$ and $pH_{\varphi 2}$) and protein to polysaccharide ratios. The critical pH shifts to higher pH values as protein to polysaccharide ratios increase due to the presence of more positively charged protein molecules (Elmer, et al., 2011; Klassen, Elmer, & Nickerson, 2011; Liu, et al., 2017; Liu, et al., 2009). For example, at fixed total

biopolymer concentration of 0.05 wt%, the pH_c, $pH_{\varphi 1}$ and $pH_{\varphi 2}$ shifted from 4.4, 4.1, 2.3 to higher pH values of 4.9, 4.5, 3.2, respectively, as the mixing ratio of ovalbumin (OVA) to GA increased from 2:1 to 8:1 (Niu, et al., 2014). Similarly, abovementioned three pHs shifted from 4.2, 3.7, 2.5 to 4.7, 4.4, 2.8, respectively, as the mixing ratio of PPI to GA increased from 1:1 to 10:1 (Liu, et al., 2009). Similar shift in pHs was widely reported in other mixed systems, such as PPI–alginate (Klemmer, et al., 2012) and PPI–pectins (Pillai, et al., 2019; Warnakulasuriya, Pillai, Stone, & Nickerson, 2018). Although the pH_c was not affected by protein–polysaccharide ratios in some biopolymer systems, $pH_{\varphi 1}$ and $pH_{\varphi 2}$ presented similar abovementioned shift trend as the increase of ratios (Liu, Shim, Tse, Wang, & Reaney, 2018; Vinayahan, Williams, & Phillips, 2010).

The influence of biopolymer concentration on complex formation is currently investigated by measuring turbidity changes at constant biopolymer mixing ratios at low biopolymer mixture concentrations. Generally, the maximum turbidity increases remarkably as total biopolymer concentrations increase from very low value of 0.05% to 0.5%, while no significant turbidity rises could be visible from concentration of 0.5% to 3% (Niu, et al., 2014). In addition, as rise of biopolymer concentrations, pH_c and $pH_{\varphi 1}$ tend to shift towards higher pH values and the region of complex coacervates formation pH becomes broader (Niu, et al., 2014). Moreover, high biopolymer concentrations may cause phase separation through thermodynamic incompatibility due to the contest between macromolecules and solvent (Schmitt, et al., 1998).

Charge density

The charge density of biopolymers is a measure of the number of electric charges present on the surface of biopolymer per unit length (Schmitt, et al., 1998). The non-charged pullulan can be carboxylated to form four fractions with different charge densities (Ganzevles, Kosters,

van Vliet, Stuart, & de Jongh, 2007). In addition, as aforementioned, LMP possesses more charged carboxyl groups than HMP, so LMP has higher overall charge density. Because of higher charge density of LMP than that of HMP, protein–LMP system is more prone to form complex coacervates at higher pH with greater interactions at the optimal mixing conditions. For example, maximum electrostatic attractive interactions between PPI–LMP occurred at higher pH (3.7–3.8) with greater strength as compared to lower pH_{opt} values (pH 3.4–3.5) of PPI–HMP (Warnakulasuriya, et al., 2018). Compared to system of protein–HMP, the pHs shifted to higher values when LMP interacts with either PPI (Warnakulasuriya, et al., 2018) or β-lactoglobulin (Sperber, et al., 2009). Similar phenomena could be observed in other polysaccharides that have different charge density. Xiong et al studied the complex coacervate formation between OVA and carboxymethylcellulose (CMC) with different degrees of substitution (CMC 0.7 and CMC 1.2) (Xiong, et al., 2017). They found that due to higher charge density of CMC 1.2 than CMC 0.7, OVA and CMC 1.2 had stronger binding capacity and resistance to salt ion shielding effect, and the obtained complex coacervates showed more compact microstructure and stronger viscoelastic properties. In another example, ι-carrageenan has higher charge density than κ-carrageenan due to presence of more sulphate groups, so the former has higher binding constant to casein molecules (Burova, et al., 2007).

Ionic strength

Ionic strength of a solution is the concentration of all ions present in that solution (Wilkinson & McNaught, 1997). The complexation between protein and polysaccharide is strongly dependent on ionic strength because it affects the strength of electrostatic interactions. At low ionic strength, addition of ions might not affect complex formation. However, the net charges carried by protein and polysaccharide could be screened at high ionic strength, resulting

in reduced electrostatic interactions between biopolymers (Klassen, et al., 2011; Liu, et al., 2009), thus the complex formation condition is also changed. Liu et al. studied the effects of NaCl (0–50 mM) on the formation of PPI–GA complexes (Liu, et al., 2009). They reported that there was no effect on biopolymer interactions at NaCl level <7.5 mM, while there was a great interference on the interaction at a level of higher than 7.5 mM because of PPI aggregation. This kind of effect may have varied from proteins or polysaccharides. Jones and McClements reported that 0–200 mM NaCl had little effect on the β-lactoglobulin–sugar beet pectin complex formation (Jones, et al., 2008). Weinbreck et al. reported a self-repression of whey protein–GA complex formation at an ionic strength of 70 mM NaCl (Weinbreck, de Vries, Schrooyen, & de Kruif, 2003). Aryee and Nickerson investigated impacts of different salt types (NaCl, KCl and $CaCl_2$) on complexes formation. They reported that all salts suppressed the formation of complexes at higher concentration, and there was no difference between NaCl and KCl at same concentration, but the addition of a divalent ion ($CaCl_2$) led to increased suppression for the formation of complexes (Aryee & Nickerson, 2014).

Methods to identify formation of protein–polysaccharide complexes

Turbidimetric method

The formation of protein–polysaccharide soluble complexes and complex coacervates is dominantly driven by attractive electrostatic interaction. As a result, the formation is highly dependent on strength of electrostatic interaction between biopolymers, which is most remarkably influenced by the pH of mixed solution for a mixture at specific biopolymer concentration, mixing ratios, charge density and ionic strength. Traditionally, complex formation and mechanism studies were mostly performed at low biopolymer concentrations of below 0.30 % (Aryee, et al., 2012; Liu, et al., 2017; Liu, et al., 2010). Turbidity measurement has been

long applied to identify boundary pH for complex formation where phase behaviors are defined on the basis of optical properties (Elmer, et al., 2011; Wagoner, Vardhanabhuti, & Foegeding, 2016). Typically, three pHs (pH_c, $pH_{\varphi1}$, $pH_{\varphi2}$) were identified from turbidity curves (**Fig. 1-3**) during titration from neutral to acidic pH, corresponding to four different phase behaviors (pH > pH_c, co-solubility; pH_c~ $pH_{\varphi1}$, soluble complexes; $pH_{\varphi1}$~ $pH_{\varphi2}$, complex coacervates; pH<$pH_{\varphi2}$ dissolution of complexes) (Li, Zhang, Zhao, Ding, & Lin, 2018). Between $pH_{\varphi1}$ and $pH_{\varphi2}$, a maximum optical density could be normally observed and defined as pH_{opt} which was believed to be the pH where highest amount of coacervates were produced (Hosseini, et al., 2013; Ye, Flanagan, & Singh, 2006). The main drawback of this method is that the pHs (pH_c, $pH_{\varphi1}$, $pH_{\varphi2}$) cannot be identified at high biopolymer concentrations.

Zeta–potential measurement

Recently, zeta–potential measurement has been proposed as an alternative model to determine phase transitions of complex formation based on surface charge at the molecular level with function of pH, which use absolute ζ–potential value ranges to describe different protein–polysaccharide phase behaviors (Adal, et al., 2017; Li, et al., 2012). For example, Li et al identified five key regions, that is, co-solubility, stable and quasistable soluble complexes, complex coacervates, and stable mixed polymers below the pKa of SBP based on value ranges of ζ–potential in bovine serum albumin (BSA)–SBP mixture (Li, et al., 2012). In addition, as described earlier, between $pH_{\varphi1}$ and $pH_{\varphi2}$, a maximum optical density can be found and defined as the pH_{opt}. Alternative to turbidity measurement, the pH_{opt} could also be determined by zero net zeta–potential value of liquid complexes (Eghbal, et al., 2016), or highest viscoelasticity of complex coacervates (Raei, Rafe, & Shahidi, 2018).

State diagram

In contrast to low concentrations of protein and saccharides, determining mechanisms and boundary pH ranges of the protein–polysaccharide complexes at higher protein and saccharide concentrations cannot use classical turbidimetric methods due to initial turbidity being too high (Klemmer, et al., 2012; Stenger, Zeeb, Hinrichs, & Weiss, 2017). Considering this situation, an alternative approach to identify phase behaviors or approximate boundary formation pH values is through the use of state diagrams (Azarikia & Abbasi, 2016; Rahmati, Koocheki, Varidi, & Kadkhodaee, 2018; Yuan, Wan, Yang, & Yin, 2014). This method is to distinguish different visible phase behaviors by observing protein-polysaccharide mixture at static status and applying different markers to represent the difference, such as clear solution, cloudy solution, part or complete phase separation behaviors (**Fig. 1-4**). However, the pH_{opt} can be only identified either by measuring zero net zeta–potential value of liquid complexes (Eghbal, et al., 2016), or the highest viscoelasticity of complex coacervates (Raei, et al., 2018).

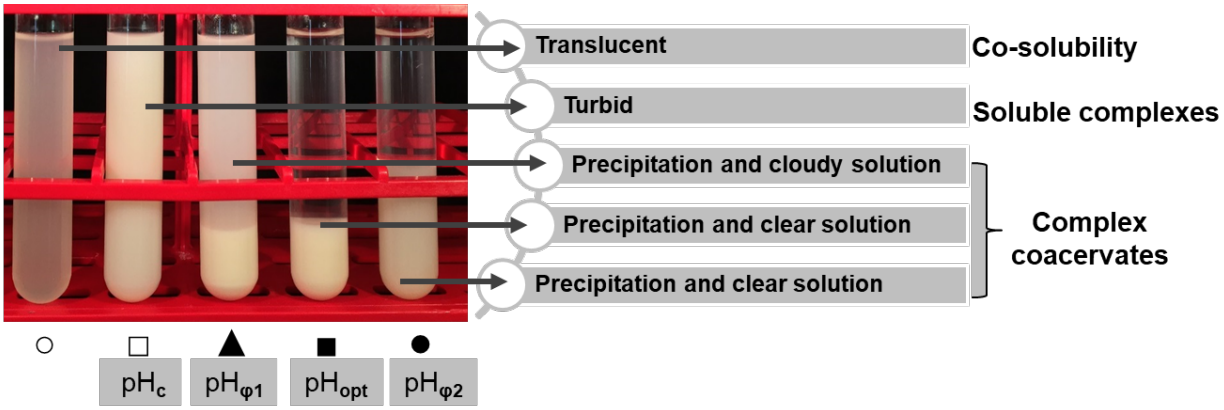

Figure 1-4. Phase behaviors of concentrated solutions of protein-polysaccharide mixtures. Adapted from Lan, Ohm, Chen, and Rao (2020).

Application of protein–polysaccharide complexes

A number of applications about soluble complexes and complex coacervates have been developed in food science and pharmaceutical science, such as improvement of protein

functionality (Wagoner, et al., 2017), to act as stabilizers for emulsion and foam (Rodriguez, et al., 2018), microencapsulation of active compounds (Gomez-Mascaraque, Llavata-Cabrero, Martinez-Sanz, Fabra, & Lopez-Rubio, 2018) and as fat replacers (Krzeminski, Prell, Busch-Stockfisch, Weiss, & Hinrichs, 2014).

Improving functionality of protein

Protein–polysaccharide complexes are widely reported to show enhanced functional properties than that of single biopolymer. The particular application of protein–polysaccharide complexes for improving protein functionalities include solubility, viscosity, thermal stability, and interfacial (foaming and emulsifying) properties. Typically, a significant solubility improvement around protein IEP is observed in protein–polysaccharide system (Wagoner, et al., 2016). Protein–polysaccharide complexes generally present improved viscosity as polysaccharide dispersions generally display higher viscosities than protein solution and entities of larger sizes are formed (Schmitt & Turgeon, 2011). Therefore, it can be used for improving food texture. In addition, protein–polysaccharide complexes can increase protein thermal stability by inhibiting thermal aggregation of protein via limiting the number of accessible protein reactive sites and lowing biopolymer diffusion coefficients (Schmitt, et al., 1998). One example is found in β-lactoglobulin–pectin complexes (Jones, et al., 2009). In this case, the existence of pectin (0.1 wt%) enhanced the thermal aggregation temperature of the protein after the formation of β-lactoglobulin–pectin soluble complexes.

Additionally, due to combining physicochemical properties of individual biopolymers, protein–polysaccharide soluble complexes and coacervates act as a stabilizer displayed improved stable emulsions and/or foams against droplet flocculation and coalescence (Moschakis, et al., 2017). The stabilization performance is dependent on the environmental conditions, such as pH,

ionic strength, biopolymer concentration and mixing ratios, etc. One example of improved emulsion stabilization could be found in formation of β-lactoglobulin–pectin complexes (Guzey & McClements, 2007). Compared to 0.1% corn -in -water emulsion (O/W) containing β-lactoglobulin–coated droplets, complex coacervation of β-lactoglobulin-pectin stabilized emulsion at pH 4 demonstrated an improved emulsion stability with the addition of NaCl. In another example, high internal O/W phase emulsion (an emulsified system that has high oil fraction (φ_{oil})) at φ_{oil} of 0.82 can be stabilized by whey protein isolate (WPI)–LMP complex coacervates at low total biopolymer concentrations of 0.3 wt% (Wijaya, Van der Meeren, Wijaya, & Patel, 2017). In addition, protein–polysaccharide complexes improved foam stabilization in lentil protein–guar gum/xanthan gum/pectin (Jarpa-Parra, Tian, Temelli, Zeng, & Chen, 2016) and egg albumin–xanthan systems (Miquelim, Lannes, & Mezzenga, 2010). This is because surface tension at air/water interface was reduced appreciable as Miquelim et al founded in egg albumin–polysaccharide complexes system (Miquelim, et al., 2010).

Microencapsulation of bioactive compounds

Attributed to improved interfacial properties of protein–polysaccharide complexes, microencapsulation of bioactive compounds by means of complex coacervation is one of the most widely reported application areas. In this method, complex coacervates can be used as wall materials to encapsulate bioactive compounds (i.e. enzymes, essential oils, polyphenols, and bacteria) that are sensitive to loss their biological activity during food processing or storage conditions (i.e. heat, air, pH variations and interactions with other components) (Eratte, Dowling, Barrow, & Adhikari, 2018). The typical processing steps are involved in emulsification, complex coacervation and drying process. Firstly, hydrophobic bioactive compound is mixed with protein–polysaccharide solutions at a proper mass ratio to form O/W emulsion. After that, pH

adjustment is performed to promote complex coacervation between protein–polysaccharide. The pH adjustment is aimed for controlling electrostatic interaction between two biopolymers to the appropriate strength. The final step usually involves solidifying liquid complex coacervates using drying techniques like spray drying or freeze drying (Timilsena, Adhikari, Barrow, & Adhikari, 2016). For example, freeze dried OVA–HMP complex coacervate powder encapsulated linoleic acid showed good water dispersion behavior and linoleic acid oxidative stability during a 13-day storage (Sponton, Perez, & Santiago, 2017). Ifeduba and Akoh reported a good oxidative stability (14-day storage at 4 ºC) of soybean oil was achieved by encapsulated soybean oil in gelatin–GA coacervates that was and added to yogurts (Ifeduba & Akoh, 2015).

Fat replacers

Due to potential health concerns like obesity caused by over-consumption of fat, consumers have increased demand for low-fat foods, leading to development of fat replacers with natural or chemical methods (Jones, et al., 2011). However, fat contributes to food flavor, texture, and mouthfeel such as creaminess and smoothness (Schmitt, et al., 1998). Developing fat replacers using protein–polysaccharide complexes has high potential because of protein–polysaccharide complex system provides new food texturization and sensory attributes (Krzeminski, et al., 2014). For example, whey protein (WP)–pectin complexes are used as fat replacers and texturizing elements in reduced-fat yogurt (Krzeminski, et al., 2014). Starting from WP–pectin complex formation, then skim milk was added into the complexes, followed by heating, cooling, and fermentation process. After that, this low-fat yogurt was evaluated based on the sensory and structural characteristics. Results revealed that addition of a non-heated whey protein–HMP mixture into skim milk formulations resembled a yogurt texture similar with the

full-fat yogurt regarding grainy, viscous, and creamy sensory attributes (Krzeminski, et al., 2014).

References

Adal, E., Sadeghpour, A., Connell, S., Rappolt, M., Ibanoglu, E., & Sarkar, A. (2017). Heteroprotein complex formation of bovine lactoferrin and pea protein isolate: A multiscale structural analysis. *Biomacromolecules, 18*(2), 625-635.

Adebiyi, A. P., & Aluko, R. E. (2011). Functional properties of protein fractions obtained from commercial yellow field pea (*Pisum sativum* L.) seed protein isolate. *Food Chemistry, 128*(4), 902-908.

Aryee, F. N. A., & Nickerson, M. T. (2012). Formation of electrostatic complexes involving mixtures of lentil protein isolates and gum arabic polysaccharides. *Food Research International, 48*(2), 520-527.

Aryee, F. N. A., & Nickerson, M. T. (2014). Effect of pH, biopolymer mixing ratio and salts on the formation and stability of electrostatic complexes formed within mixtures of lentil protein isolate and anionic polysaccharides (kappa-carrageenan and gellan gum). *International Journal of Food Science and Technology, 49*(1), 65-71.

Azarikia, F., & Abbasi, S. (2016). Mechanism of soluble complex formation of milk proteins with native gums (*tragacanth and Persian gum*). *Food Hydrocolloids, 59*, 35-44.

Belitz, H. D., Burghagen, M., Grosch, W., & Schieberle, P. (2013). *Food chemistry*: Springer Berlin Heidelberg.

Boye, J., Zare, F., & Pletch, A. (2010). Pulse proteins: Processing, characterization, functional properties and applications in food and feed. *Food Research International, 43*(2), 414-431.

Braudo, E. E., Plashchina, I. G., & Schwenke, K. D. (2001). Plant protein interactions with polysaccharides and their influence on legume protein functionality A Review. *Food / Nahrung, 45*(6), 382-384.

Burova, T. V., Grinberg, N. V., Grinberg, V. Y., Usov, A. I., Tolstoguzov, V. B., & de Kruif, C. G. (2007). Conformational changes in ι- and κ-carrageenans induced by complex formation with bovine β-casein. *Biomacromolecules, 8*(2), 368-375.

Cui, L., Bandillo, N., Wang, Y., Ohm, J.-B., Chen, B., & Rao, J. (2020). Functionality and structure of yellow pea protein isolate as affected by cultivars and extraction pH. *Food Hydrocolloids, 108*, 106008.

Devi, N., Sarmah, M., Khatun, B., & Maji, T. K. (2017). Encapsulation of active ingredients in polysaccharide-protein complex coacervates. *Advances in Colloid and Interface Science, 239*, 136-145.

Eghbal, N., Yarmand, M. S., Mousavi, M., Degraeve, P., Oulahal, N., & Gharsallaoui, A. (2016). Complex coacervation for the development of composite edible films based on LM pectin and sodium caseinate. *Carbohydrate Polymers, 151*, 947-956.

Elmer, C., Karaca, A. C., Low, N. H., & Nickerson, M. T. (2011). Complex coacervation in pea protein isolate-chitosan mixtures. *Food Research International, 44*(5), 1441-1446.

Eratte, D., Dowling, K., Barrow, C. J., & Adhikari, B. (2018). Recent advances in the microencapsulation of omega-3 oil and probiotic bacteria through complex coacervation: A review. *Trends in Food Science & Technology, 71*, 121-131.

FAOSTAT. http://www.fao.org/faostat/en/#data/QC. In: Accessed 6/1/2020.

Fishman, M. L., Gillespie, D. T., Sondney, S. M., & El-Atawy, Y. S. (1991). Intrinsic viscosity and molecular weight of pectin components. *Carbohydrate Research, 215*(1), 91-104.

Ganzevles, R. A., Kosters, H., van Vliet, T., Stuart, M. A. C., & de Jongh, H. H. J. (2007). Polysaccharide charge density regulating protein adsorption to air/water interfaces by protein/polysaccharide complex formation. *Journal of Physical Chemistry B, 111*(45), 12969-12976.

Gomez-Mascaraque, L. G., Llavata-Cabrero, B., Martinez-Sanz, M., Fabra, M. J., & Lopez-Rubio, A. (2018). Self-assembled gelatin-iota-carrageenan encapsulation structures for intestinal-targeted release applications. *Journal of Colloid and Interface Science, 517*, 113-123.

Gorissen, S. H. M., Crombag, J. J. R., Senden, J. M. G., Waterval, W. A. H., Bierau, J., Verdijk, L. B., & van Loon, L. J. C. (2018). Protein content and amino acid composition of commercially available plant-based protein isolates. *Amino Acids, 50*(12), 1685-1695.

Guzey, D., & McClements, D. J. (2007). Impact of electrostatic interactions on formation and stability of emulsions containing oil droplets coated by β-lactoglobulin−pectin complexes. *Journal of Agricultural and Food Chemistry, 55*(2), 475-485.

Havemeier, S., Erickson, J., & Slavin, J. (2017). Dietary guidance for pulses: the challenge and opportunity to be part of both the vegetable and protein food groups. *Annals of the New York Academy of Sciences, 1392*(1), 58-66.

Hosseini, S. M. H., Emam-Djomeh, Z., Razavi, S. H., Moosavi-Movahedi, A. A., Saboury, A. A., Atri, M. S., & Van der Meeren, P. (2013). β-Lactoglobulin–sodium alginate interaction as affected by polysaccharide depolymerization using high intensity ultrasound. *Food Hydrocolloids, 32*(2), 235-244.

Ifeduba, E. A., & Akoh, C. C. (2015). Microencapsulation of stearidonic acid soybean oil in complex coacervates modified for enhanced stability. *Food Hydrocolloids, 51*, 136-145.

Izydorczyk, M., Cui, S. W., & Wang, Q. (2005). *Polysaccharide gums: structures, functional properties, and applications*: Taylor & Francis Group.

Jarpa-Parra, M., Tian, Z., Temelli, F., Zeng, H. B., & Chen, L. (2016). Understanding the stability mechanisms of lentil legumin-like protein and polysaccharide foams. *Food Hydrocolloids, 61*, 903-913.

Jones, O. G., Decker, E. A., & McClements, D. J. (2009). Formation of biopolymer particles by thermal treatment of β-lactoglobulin–pectin complexes. *Food Hydrocolloids, 23*(5), 1312-1321.

Jones, O. G., & McClements, D. J. (2008). Stability of biopolymer particles formed by heat treatment of β-lactoglobulin-beet pectin electrostatic complexes. *Food Biophysics, 3*(2), 191-197.

Jones, O. G., & McClements, D. J. (2011). Recent progress in biopolymer nanoparticle and microparticle formation by heat-treating electrostatic protein-polysaccharide complexes. *Advances in Colloid and Interface Science, 167*(1-2), 49-62.

Karaca, A. C., Low, N., & Nickerson, M. (2011). Emulsifying properties of chickpea, faba bean, lentil and pea proteins produced by isoelectric precipitation and salt extraction. *Food Research International, 44*(9), 2742-2750.

Klassen, D. R., Elmer, C. M., & Nickerson, M. T. (2011). Associative phase separation involving canola protein isolate with both sulphated and carboxylated polysaccharides. *Food Chemistry, 126*(3), 1094-1101.

Klemmer, K. J., Waldner, L., Stone, A., Low, N. H., & Nickerson, M. T. (2012). Complex coacervation of pea protein isolate and alginate polysaccharides. *Food Chemistry, 130*(3), 710-715.

Krzeminski, A., Prell, K. A., Busch-Stockfisch, M., Weiss, J., & Hinrichs, J. (2014). Whey protein–pectin complexes as new texturising elements in fat-reduced yoghurt systems. *International Dairy Journal, 36*(2), 118-127.

Lam, A. C. Y., Can Karaca, A., Tyler, R. T., & Nickerson, M. T. (2018). Pea protein isolates: Structure, extraction, and functionality. *Food Reviews International, 34*(2), 126-147.

Lan, Y., Ohm, J. B., Chen, B. C., & Rao, J. J. (2020). Phase behavior and complex coacervation of concentrated pea protein isolate-beet pectin solution. *Food Chemistry, 307*, 125536.

Li, X., Long, J., Hua, Y., Chen, Y., Kong, X., & Zhang, C. (2018). Protein separation coacervation with carboxymethyl cellulose of different substitution degree: noninteracting behavior of bowman-birk chymotrypsin inhibitor. *Journal of Agricultural and Food Chemistry, 66*(17), 4439-4448.

Li, X. Y., Fang, Y. P., Al-Assaf, S., Phillips, G. O., Yao, X. L., Zhang, Y. F., Zhao, M., Zhang, K., & Jiang, F. T. (2012). Complexation of Bovine Serum Albumin and Sugar Beet Pectin: Structural Transitions and Phase Diagram. *Langmuir, 28*(27), 10164-10176.

Li, Y., Zhang, X., Zhao, Y., Ding, J., & Lin, S. (2018). Investigation on complex coacervation between fish skin gelatin from cold-water fish and gum arabic: Phase behavior, thermodynamic, and structural properties. *Food Research International, 107*, 596-604.

Liang, H. N., & Tang, C. H. (2013). pH-dependent emulsifying properties of pea (*Pisum sativum* L.) proteins. *Food Hydrocolloids, 33*(2), 309-319.

Liu, J., Shim, Y. Y., Shen, J. H., Wang, Y., & Reaney, M. J. T. (2017). Whey protein isolate and flaxseed *(Linum usitatissimum* L.) gum electrostatic coacervates: Turbidity and rheology. *Food Hydrocolloids, 64*, 18-27.

Liu, J., Shim, Y. Y., Tse, T. J., Wang, Y., & Reaney, M. J. T. (2018). Flaxseed gum a versatile natural hydrocolloid for food and non-food applications. *Trends in Food Science & Technology, 75*, 146-157.

Liu, S. H., Cao, Y. L., Ghosh, S., Rousseau, D., Low, N. H., & Nickerson, M. T. (2010). Intermolecular interactions during complex coacervation of pea protein isolate and gum arabic. *Journal of Agricultural and Food Chemistry, 58*(1), 552-556.

Liu, S. H., Low, N. H., & Nickerson, M. T. (2009). Effect of pH, salt, and biopolymer ratio on the formation of pea protein isolate-gum arabic complexes. *Journal of Agricultural and Food Chemistry, 57*(4), 1521-1526.

Matalanis, A., Jones, O. G., & McClements, D. J. (2011). Structured biopolymer-based delivery systems for encapsulation, protection, and release of lipophilic compounds. *Food Hydrocolloids, 25*(8), 1865-1880.

McCarthy, N. A., Kennedy, D., Hogan, S. A., Kelly, P. M., Thapa, K., Murphy, K. M., & Fenelon, M. A. (2016). Emulsification properties of pea protein isolate using homogenization, microfluidization and ultrasonication. *Food Research International, 89*, 415-421.

McClements, D. J. (2015). *Food emulsions: principles, practices, and techniques*: CRC press.

Miquelim, J. N., Lannes, S. C. S., & Mezzenga, R. (2010). pH Influence on the stability of foams with protein-polysaccharide complexes at their interfaces. *Food Hydrocolloids, 24*(4), 398-405.

Moschakis, T., & Biliaderis, C. G. (2017). Biopolymer-based coacervates: Structures, functionality and applications in food products. *Current Opinion in Colloid & Interface Science, 28*, 96-109.

Nakai, S., & Modler, H. W. (1996). *Food proteins: Properties and characterization*: Wiley.

Niu, F., Su, Y., Liu, Y., Wang, G., Zhang, Y., & Yang, Y. (2014). Ovalbumin–gum arabic interactions: Effect of pH, temperature, salt, biopolymers ratio and total concentration. *Colloids and Surfaces B: Biointerfaces, 113*, 477-482.

Pathak, J., Priyadarshini, E., Rawat, K., & Bohidar, H. B. (2017). Complex coacervation in charge complementary biopolymers: Electrostatic versus surface patch binding. *Advances in Colloid and Interface Science, 250*, 40-53.

Pillai, P. K. S., Stone, A. K., Guo, Q., Guo, Q., Wang, Q., & Nickerson, M. T. (2019). Effect of alkaline de-esterified pectin on the complex coacervation with pea protein isolate under different mixing conditions. *Food Chemistry, 284*, 227-235.

Raei, M., Rafe, A., & Shahidi, F. (2018). Rheological and structural characteristics of whey protein-pectin complex coacervates. *Journal of Food Engineering, 228*, 25-31.

Rahmati, N. F., Koocheki, A., Varidi, M., & Kadkhodaee, R. (2018). Thermodynamic compatibility and interactions between Speckled Sugar bean protein and xanthan gum for production of multilayer O/W emulsion. *Journal of Food Science and Technology, 55*(3), 1143-1153.

Rodriguez, A. M. B., Binks, B. P., & Sekine, T. (2018). Emulsion stabilisation by complexes of oppositely charged synthetic polyelectrolytes. *Soft Matter, 14*(2), 239-254.

Ru, Q. M., Wang, Y. W., Lee, J., Ding, Y. T., & Huang, Q. R. (2012). Turbidity and rheological properties of bovine serum albumin/pectin coacervates: Effect of salt concentration and initial protein/polysaccharide ratio. *Carbohydrate Polymers, 88*(3), 838-846.

Schmitt, C., Sanchez, C., Desobry-Banon, S., & Hardy, J. (1998). Structure and technofunctional properties of protein-polysaccharide complexes: A review. *Critical Reviews in Food Science and Nutrition, 38*(8), 689-753.

Schmitt, C., & Turgeon, S. L. (2011). Protein/polysaccharide complexes and coacervates in food systems. *Advances in Colloid and Interface Science, 167*(1-2), 63-70.

Shevkani, K., Singh, N., Kaur, A., & Rana, J. C. (2015). Structural and functional characterization of kidney bean and field pea protein isolates: A comparative study. *Food Hydrocolloids, 43*, 679-689.

Sikorski, Z. E. (2001). *Chemical and functional properties of food protein*: Technical Publishing Company, Inc.

Sperber, B., Schols, H. A., Stuart, M. A. C., Norde, W., & Voragen, A. G. J. (2009). Influence of the overall charge and local charge density of pectin on the complex formation between pectin and beta-lactoglobulin. *Food Hydrocolloids, 23*(3), 765-772.

Sponton, O. E., Perez, A. A., & Santiago, L. G. (2017). Protein-polysaccharide associative phase separation applied to obtain a linoleic acid dried ingredient. *Food Hydrocolloids, 71*, 158-167.

Stenger, C., Zeeb, B., Hinrichs, J., & Weiss, J. (2017). Formation of concentrated biopolymer particles composed of oppositely charged WPI and pectin for food applications. *Journal of Dispersion Science and Technology, 38*(9), 1258-1265.

Stone, A. K., Cheung, L., Chang, C., & Nickerson, M. T. (2013). Formation and functionality of soluble and insoluble electrostatic complexes within mixtures of canola protein isolate and (*kappa-*, *iota-* and *lambda*-type) carrageenan. *Food Research International, 54*(1), 195-202.

Stone, A. K., Karalash, A., Tyler, R. T., Warkentin, T. D., & Nickerson, M. T. (2015). Functional attributes of pea protein isolates prepared using different extraction methods and cultivars. *Food Research International, 76,* 31-38.

Taherian, A. R., Mondor, M., Labranche, J., Drolet, H., Ippersiel, D., & Lamarche, F. (2011). Comparative study of functional properties of commercial and membrane processed yellow pea protein isolates. *Food Research International, 44*(8), 2505-2514.

Timilsena, Y. P., Adhikari, R., Barrow, C. J., & Adhikari, B. (2016). Microencapsulation of chia seed oil using chia seed protein isolate-chia seed gum complex coacervates. *International Journal of Biological Macromolecules, 91,* 347-357.

Vinayahan, T., Williams, P. A., & Phillips, G. O. (2010). Electrostatic interaction and complex formation between gum arabic and bovine serum albumin. *Biomacromolecules, 11*(12), 3367-3374.

Wagoner, T., Vardhanabhuti, B., & Foegeding, E. A. (2016). Designing whey protein-polysaccharide particles for colloidal stability. In M. P. Doyle & T. R. Klaenhammer (Eds.), *Annual Review of Food Science and Technology* (Vol. 7, pp. 93-116). Palo Alto: Annual Reviews.

Wagoner, T. B., & Foegeding, E. A. (2017). Whey protein–pectin soluble complexes for beverage applications. *Food Hydrocolloids, 63,* 130-138.

Wang, Q., Ren, Y., Ding, Y., Xu, M., & Chen, B. (2018). The influence of pH and enzyme cross-linking on protein delivery properties of WPI-beet pectin complexes. *Food Research International, 105,* 678-685.

Warnakulasuriya, S., Pillai, P. K. S., Stone, A. K., & Nickerson, M. T. (2018). Effect of the degree of esterification and blockiness on the complex coacervation of pea protein isolate and commercial pectic polysaccharides. *Food Chemistry, 264*, 180-188.

Weinbreck, F., de Vries, R., Schrooyen, P., & de Kruif, C. G. (2003). Complex coacervation of whey proteins and gum arabic. *Biomacromolecules, 4*(2), 293-303.

Wijaya, W., Patel, A. R., Setiowati, A. D., & Van der Meeren, P. (2017). Functional colloids from proteins and polysaccharides for food applications. *Trends in Food Science & Technology, 68*, 56-69.

Wijaya, W., Van der Meeren, P., Wijaya, C. H., & Patel, A. R. (2017). High internal phase emulsions stabilized solely by whey protein isolate-low methoxyl pectin complexes: effect of pH and polymer concentration. *Food & Function, 8*(2), 584-594.

Wilkinson, A., & McNaught, A. (1997). IUPAC Compendium of Chemical Terminology,(the" Gold Book"). *International Union of Pure and Applied Chemistry: Zürich, Switzerland*.

Xiao, Y., Qi, P. X., & Wickham, E. D. (2018). Interactions, induced by heating, of whey protein isolate (WPI) with sugar beet pectin (SBP) in solution: Comparisons with a dry-state Maillard reaction. *Food Hydrocolloids, 83*, 61-71.

Xiong, W. F., Ren, C., Tian, M., Yang, X. J., Li, J., & Li, B. (2017). Complex coacervation of ovalbumin-carboxymethylcellulose assessed by isothermal titration calorimeter and rheology: Effect of ionic strength and charge density of polysaccharide. *Food Hydrocolloids, 73*, 41-50.

Xu, A. Y., Melton, L. D., Ryan, T. M., Mata, J. P., Rekas, A., Williams, M. A. K., & McGillivray, D. J. (2018). Effects of polysaccharide charge pattern on the

microstructures of beta-lactoglobulin-pectin complex coacervates, studied by SAXS and SANS. *Food Hydrocolloids, 77*, 952-963.

Yao, X. L., Xiang, S. P., Nie, K., Gao, Z. M., Zhang, W. Q., Fang, Y. P., Nishinari, K., Phillips, G. O., & Jiang, F. T. (2016). Whey protein isolate/gum arabic intramolecular soluble complexes improving the physical and oxidative stabilities of conjugated linoleic acid emulsions. *Rsc Advances, 6*(18), 14635-14642.

Ye, A. Q. (2008). Complexation between milk proteins and polysaccharides via electrostatic interaction: principles and applications - a review. *International Journal of Food Science and Technology, 43*(3), 406-415.

Ye, A. Q., Flanagan, J., & Singh, H. (2006). Formation of stable nanoparticles via electrostatic complexation between sodium caseinate and gum arabic. *Biopolymers, 82*(2), 121-133.

Yuan, Y., Wan, Z.-L., Yang, X.-Q., & Yin, S.-W. (2014). Associative interactions between chitosan and soy protein fractions: Effects of pH, mixing ratio, heat treatment and ionic strength. *Food Research International, 55*, 207-214.

Zha, F., Dong, S., Rao, J., & Chen, B. (2019). Pea protein isolate-gum arabic Maillard conjugates improves physical and oxidative stability of oil-in-water emulsions. *Food Chemistry, 285*, 130-138.

CHAPTER 2. PEA PROTEIN ISOLATE–HIGH METHOXYL PECTIN SOLUBLE COMPLEXES FOR IMPROVING PEA PROTEIN FUNCTIONALITY: EFFECT OF PH, BIOPOLYMER RATIO AND CONCENTRATIONS

Abstract

Recently, the interest in incorporating of pea protein, as a preferred alternative animal protein, into protein fortified beverage is growing because of its inexpensive price, sustainably produced and gluten free. However, poor functionality such as acidic solubility and thermal stability limits the application of pea protein in beverages. The aim of this study was to enhance the functionality of pea protein isolate (PPI) by forming soluble complexes with high methoxyl pectin (HMP). The effect of PPI–HMP mixing ratio (1:1–20:1) and PPI concentrations (0.05 and 1.00 wt %) on $pH_{\varphi 1}$, a key parameter associated with soluble complexes formation were investigated using turbidimetric analysis, state diagram and ζ–potential. The $pH_{\varphi 1}$ decreased to pH 3.5 as PPI–HMP mixing ratio decreased from 20:1 to 1:1. The ζ–potential results showed a shift in net charge neutrality from pH 4.8 in homogenous PPI solutions to pH 3 for the 1:1 mixture. However, HMP induced phase separation of PPI–HMP mixtures at both higher biopolymer concentration (> 1.50 wt %) and neutral pH values were observed presumably via a thermal incompatibility mechanism. The pH–percentage solubility of PPI–HMP mixtures at fixed 1.00 wt % PPI were biopolymer mixing ratio dependent. The pH–percentage solubility minimum was shifted towards more acidic pH compared to PPI alone when increasing HMP concentration. Apparent viscosity and thermal denaturation temperature of soluble complexes at fixed PPI concentration (1.00 wt %) slightly increased due to the formation of new net structure in the PPI–HMP systems. The findings derived from this research could provide useful information in the design of pea protein fortified beverage with enhanced pea protein stability.

Introduction

In recent years, there is a strong interest in the consumption of plant proteins as a preferred alternative to animal-based sources (e.g., gelatin, whey and casein) due to the low cost and more sustainable source with a lower carbon footprint (Adebiyi & Aluko, 2011; Dijkink & Langelaan, 2002). Moreover, plant-based diets have been shown to deliver health benefits by lowering cholesterol level and blood pressure, balancing blood sugar, and even reducing certain cancer risk (McCarty, 1999). Consequently, significant number of researchers and companies have been interested in applying pulse to food formula due to the abovementioned advantages along with allergen and gluten free claims that can be made on that food (Havemeier, Erickson, & Slavin, 2017). Dry peas (*Pisum sativum L.*) are the second most important leguminous crop which constitute the largest percentage (36 %) of total pulse production (Dahl, Foster, & Tyler, 2012). Currently, the vast majority of commercially available pulse protein isolate is PPI that is extracted from split yellow field pea. Depending on the variety, protein content in yellow field pea ranges from 18–30 % with higher levels of lysine and tryptophan (Adebiyi, et al., 2011). The main protein found in yellow pea are albumins and globulins (Taherian, et al., 2011). They contribute to the surface properties of pea protein such as hydrophobicity, emulsification, and oil binding capacity (Boye, Zare, & Pletch, 2010; Freitas, Ferreira, & Teixeira, 2000). However, the applications of processed yellow pea protein in food or beverage formula are still challenging due to their poor functional performance (Nosworthy, Tulbek, & House, 2017).

One particular interest and challenge is pea protein fortified beverages, including protein shake, sports drink, and protein juice blend. In general, the functional properties of yellow pea proteins applied to food and/or beverage formula have been classified into three major groups: (i) properties related to hydration (e.g., solubility and wettability) (Beck, Knoerzer, Sellahewa,

Emin, & Arcot, 2017), (ii) properties related to the rheological characteristics and thermal stability (e.g., viscosity, elasticity, aggregation and gelification) (Ben-Harb, et al., 2018), and (iii) properties related to the surface active characteristics (e.g., emulsifying and foaming) (Lam & Nickerson, 2013). The most important functional properties related with protein fortified beverage include its solubility, thermal stability and rheological behaviors. In general, protein beverages require thermal processing such as UHT (ultra-high temperature processing) or retorting for safety and shelf life stability purpose. Currently, the protein beverage or protein juice blend beverage are ideally formulated around pH 4–6 to avoid astringency sensorial defects (Wagoner & Foegeding, 2017). At neutral pH, pea proteins have negative charge and are mutually repellent each other in solution. Nevertheless, pea protein loses their negative charge during acidification and has the lowest negative charge and weakest hydration around isoelectric point (pH value around 4.8). Therefore, when acidified pea protein products are heated, the pea protein will quickly aggregate and are subject to sedimentation in the final products.

One promising way to improve protein solubility and thermal stability at acidic environmental is through the formation of protein and polysaccharide soluble complexes (Braudo, Plashchina, & Schwenke, 2001). The formation of biopolymer soluble complexes can potentially lead to superior functional properties (Klassen, Elmer, & Nickerson, 2011; Semenova, 2017). Recently, soluble complexes have been shown to exhibit with enhanced whey protein stability in beverage application (Wagoner, et al., 2017). This method is based on the pH-dependent electrostatic attractive interaction between positive patches on a protein surface and negatively charged polysaccharides as described by other researchers (Jones & McClements, 2011). Depending on the strength of the electrostatic attraction, the biopolymer complexes will remain as one phase system, i.e., soluble complexes, or undergo associative phase separation

becoming complex coacervations. Numerous studies have focused on the formation of complex coacervations between plant protein and polysaccharide such as pea protein–GA, pea protein–alginate, canola protein–carrageenan, lentil protein–GA, soy protein–chitosan, and canola protein isolate–gelatin, etc. (Aryee & Nickerson, 2012; Klemmer, Waldner, Stone, Low, & Nickerson, 2012; Liu, Elmer, Low, & Nickerson, 2010; Stone, Cheung, Chang, & Nickerson, 2013; Yuan, Wan, Yang, & Yin, 2014). However, the formation and application of soluble complexes between plant protein and polysaccharide has not been fully explored. Soluble complexes are formed within a short range of pH values, i.e., between neutral pH and pH value slightly above isoelectric point of protein. The soluble complexes formation pH range will be influenced by protein/polysaccharide type, biopolymer mixing ratio, total biopolymer concentration and environmental parameters such as ionic strength (Schmitt & Turgeon, 2011). Most research focused on the formation of soluble complexes and /or complex coacervates at very low plant protein concentrations–typically below 0.30 %, at which protein concentration is not enough to represent protein fortification food application (Klemmer, et al., 2012; Schmitt, et al., 2011). Meanwhile, the measurement of optical density (OD_{600}) as a function of pH is generally applied for monitoring interaction behavior and complex formation between proteins and polysaccharides at low protein conditions (Aryee, et al., 2012). The optical density will slightly increase during titration from basic to acidic pH by virtue of the soluble complex formation. Accordingly, pH associated with soluble complexes formation will be determined graphically as the intersection point of the two curve tangents (Liu, et al., 2010). However, this method is not applicable for high concentration of binary protein/polysaccharide system since the initial turbidity of binary protein/polysaccharide solution might be out of spectrometer detection range (e.g., $OD_{600} > 1.0$).

Currently, phase behavior and soluble complexes formation between yellow pea protein and polysaccharide system at higher concentrations are not fully investigated. Therefore, understanding phase behavior and the potential factors influencing soluble complexes formation in yellow pea protein–polysaccharide systems is of most importance in developing desirable pea protein fortified beverage. In this study, high methyl pectin (HMP) was selected as polysaccharides because of its widespread application in acidic dairy beverage. HMP is an anionic polysaccharide with degree of esterification above 50 % (Gancz, Alexander, & Corredig, 2005).The pKa of carboxyl moieties in HMP ranges from 2.9 to 3.3. The purpose of this research was to investigate factors that influence PPI–HMP soluble complexes formation (e.g., pH, biopolymer mixing ratio, and pea protein concentration) and evaluate functional properties of biopolymer soluble complexes including solubility, surface charge, flow behavior, and thermal properties. In addition, we also aimed to develop an alternative method, i.e., state diagram, to evaluate high concentration of binary protein–polysaccharide soluble complexes formation. Results gained from this research will provide a better understanding of pea protein soluble complexes formation that can be applied in beverage industry.

Materials and methods

Materials

High methoxyl pectin (HMP) was kindly donated by CP Kelco (Atlanta, Georgia, USA). Raw yellow pea flour containing 19 % protein was purchased from Harvest Innovations (Indianola, Iowa, USA). Other chemicals and reagents used in this work were of analytical grade and purchased from VWR (Chicago, Illinois, USA). All solutions were prepared using ultrapure distilled de-ionized water (DDW, 18.2 MΩ cm, Barnstead Nanopure ultrapure water system, Thermo Scientific, USA).

Preparation of pea protein isolate

Pea protein isolate (PPI) was extracted from yellow pea flour using a method of alkali extraction–isoelectric precipitated (AE–IEP), as described by Stone, Karalash, Tyler, Warkentin, and Nickerson (2015) with some modification. In brief, yellow pea flours (70.0 g) were dispersed in water at a ratio of 1:15 (w/v) and the solution pH was adjusted to 8.5 using 1.0 M NaOH. The solution was stirred using magnetic stirrer at 500 rpm for 1 h at room temperature (21–23 °C) followed by centrifugation at 6000 rpm for 20 min. The supernatant was then collected and filtered using whatman paper. The pH of the supernatant was adjusted to 4.5 (around isoelectric point of PPI) using 1.0 N HCl to precipitate proteins and then centrifuge again at 6000 rpm for 10 min after which the pellet was collected. The pellet was re-suspended in water and the pH was adjusted 7 using 1.0 M NaOH. Powder PPI was obtained by freeze-drying the pellet solution for 48 h (Lyophilizer, SP scientific, Gardiner, New York). All PPI powder from different batches were mixed and stored in a plastic screw capped bottle at room temperature for further study.

Preparation of PPI and HMP stock solution

PPI stock solutions (0.10 and 2.00 wt %) were prepared by dissolving PPI powder in DDW, adjusting pH of PPI solution to 7.0 using 0.1 M NaOH, and stirring at 500 rpm for 2 h at room temperature (around 21–22 °C), followed by mixing using a hand blender (Tissue–Tearor, BioSpec Products Inc., Oklahoma, USA) for 2 min to ensure complete protein hydration. The PPI stock solutions were further filtered using whatman filter paper and stored at refrigerator overnight prior to use. HMP stock solutions (0.10 and 2.00 wt %) were prepared by dispersing pectin in DDW water and stirring at 500 rpm. The solution was heated to 60 °C for 10 min to

promote hydration and then stirring for 2 h at room temperature. The pectin stock solution was adjusted to pH 7 and then store refrigerated (4 °C) overnight prior to use.

PPI–HMP mixture preparation

Two groups of PPI–HMP mixture were prepared to systematically investigate the formation of PPI–HMP soluble complexes as a function of pH, biopolymer mixing ratio and PPI concentration. One group was to represent low PPI with fixed concentration at 0.05 wt % but variable final HMP concentrations from 0.0025 to 0.5 wt % in PPI–HMP biopolymer mixture. In contrast, the high PPI protein concentration group had a fixed PPI concentration of 1.00 wt % mixed with HMP varying from 0.05 to 1.00 wt % in PPI–HMP biopolymer mixture. In general, the PPI–HMP mixtures were prepared by adding different volume of pectin stock solutions into same volume (10 ml) of PPI stock solution to achieve initial PPI–HMP ratio ranging from 1:1 to 20:1. For the turbidimetric titration, the PPI–HMP mixtures with low PPI (0.05 wt %) were prepared by adjusting the pH from 8.0 to 2.0 under magnetic stirring with pH unit reductions using pH titrator (TitroLine 7000, Germany). The phase behavior of PPI–HMP mixture samples were investigated by visual observation of mixtures after adjusting the pH from 7 to 3 pH unit reductions. The appearance of all mixtures was classified to 4 groups: clear solution, cloudy/milky solution, cloudy solution with precipitate, and clear solution with precipitate.

Turbidity measurement

Turbidity of all PPI–HMP mixtures was measured at 600 nm using a UV–visible spectrophotometer (VWR 6300 Double Beam, USA). The samples were contained within plastic sample cuvettes with a path length of 1.0 cm. Distilled water was used as a blank reference.

Particle charge measurement

Particle charge of PPI, pectin, and their mixtures was determined by using a micro-electrophoresis device (Nano–ZS, Malvern Instruments, Worcestershire, UK). The surface charge data was reported as zeta–potential (ζ, mV).

Percent protein solubility

The pH-dependence of percent protein solubility (%PS) of soluble complexes compared to PPI alone was measured according to the method reported by Adebiyi, et al. (2011) with minor modification. Briefly, the protein concentration of the stock 1.00 wt % PPI solution before and after centrifugation was determined using Bradford dye-binding method. The solution was centrifuged (Eppendorf, New York, USA) at 4000 rpm for 10 min and the protein concentration of supernatant was measured. The absorbance of protein–Coomassie brilliant blue G–250 was read at 595 nm. Bovine serum albumin (BSA) was used to make standard curve. The %PS was calculated as: protein concentration of supernatant/protein concentration of initial solution ×100%.

Rheological property

The apparent viscosity of selected soluble complexes were measured using a Discovery Hybrid Rheometer-2 rheometer (TA Instruments Ltd., New Castle, DE, USA) based on the method described by Liu, Shim, Shen, Wang, and Reaney (2017) with some modification. In brief, ~ 2 mL samples were loaded onto the rheometer bottom plate. A 2° cone plate with 40 mm diameter was used and the gap between plates was fixed at 57 μm. Each sample was equilibrated for 1 min before a linear shear rate ramp was applied from 0.1 to 100 s^{-1} at 25 °C. The apparent viscosity of the samples *versus* shear rate was recorded using TA instrument TRIOS software.

Differential scanning calorimetry

The thermal properties of selected soluble complexes and PPI were measured by using differential scanning calorimeter (DSC Q–2000, TA Instruments Ltd., New Castle, DE, USA), according to the method of Shevkani, Singh, Kaur, and Rana (2015) with some modification. Briefly, ~20 mg samples were loaded into an aluminum pan and hermetically sealed. The reference was an empty aluminum pan. The temperature was increased at a rate of 5 °C /min from 30 to 120 °C. Onset temperature (T_0) and denaturation temperature (T_d) of soluble complexes and PPI were analyzed by TA Universal Analysis 2000 software.

Statistical analysis

All measurements were performed at least twice using freshly prepared samples (*i.e.*, new samples were prepared for each series of experiments) and were reported as means and standard deviation.

Results and discussions

Identification of suitable pH conditions for forming PPI–HMP soluble complexes at low PPI concentration

The PPI–HMP soluble complex formation was primarily driven by electrostatic attractive forces arising between two oppositely charged biopolymers. In this event, pH conditions play an important role in soluble complex formation since pH influences the total number of ionizable reactive groups on protein and polysaccharide. Therefore, pH conditions under which PPI–HMP electrostatic complexes could be formed were identified using turbidimetric analysis, a well-established method to identify $pH_{\varphi 1}$for soluble complexes formation at low biopolymer concentrations (Klemmer, et al., 2012; Liu, Low, & Nickerson, 2009). Initially, we measured the optical density (OD_{600}) of individual biopolymer (0.05 wt % PPI, 0.05 wt % HMP) and mixed

(0.05 wt % PPI and 0.05% HMP) biopolymer solutions as a function of pH from 8 to 2 (**Fig. 2-1a**).

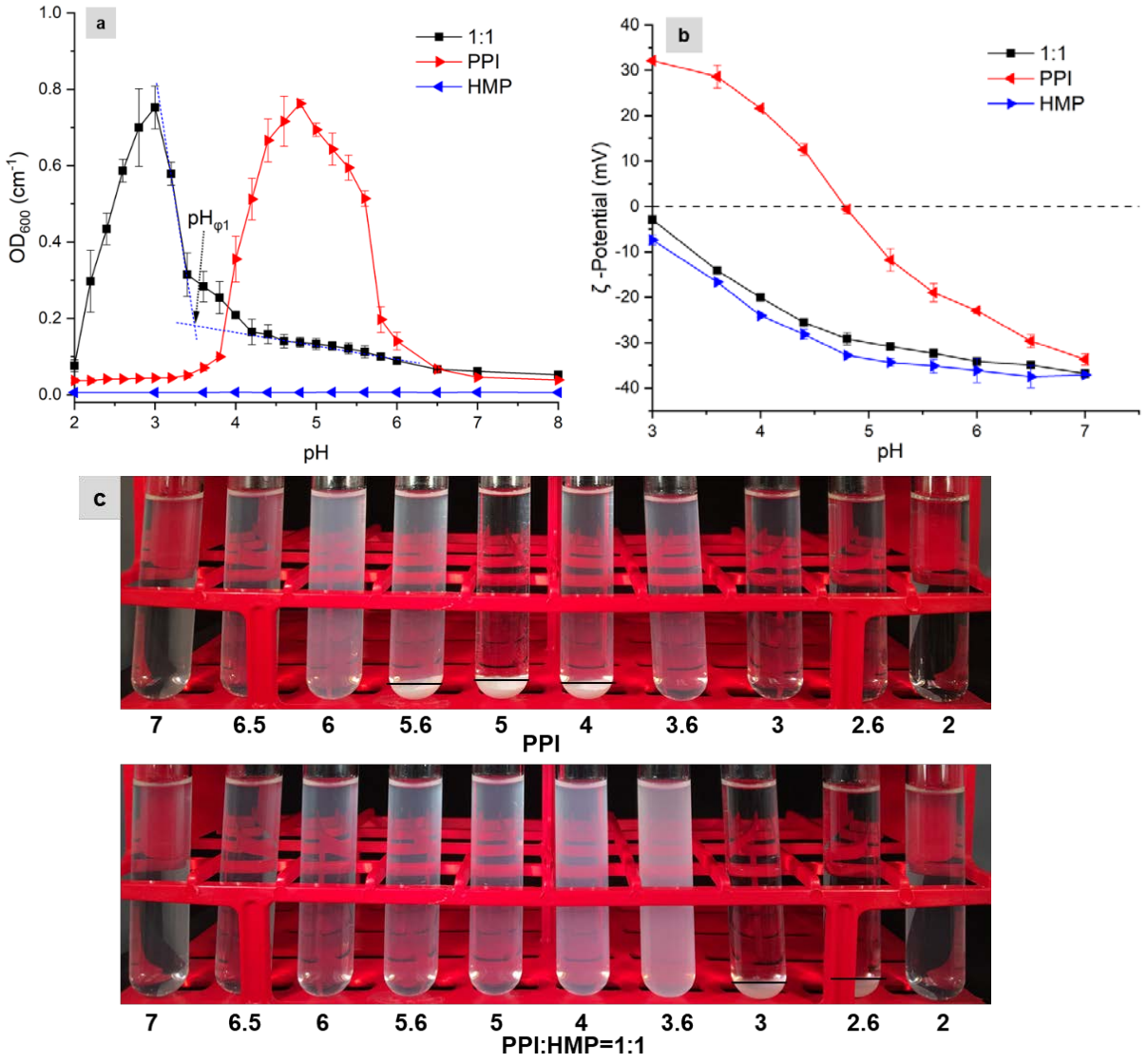

Figure 2-1. (a) Turbidity curves of PPI (0.05 wt %), HMP (0.05 wt%), and mixed (1:1 ratio) PPI–HMP system during acid titration from pH 8–2. $pH_{\varphi 1}$was determined by extending tangent lines on either side of inflection points. (b) Dependence of ζ–potential of PPI (0.05 wt %), HMP (0.05 wt %), and mixed (1:1 ratio) PPI–HMP system on pH. (c) Dependence of PPI and mixed (1:1 ratio) PPI–HMP appearance on pH.

The optical density of HMP solution remained close to zero across the entire pH range tested, which indicated that pectin did not form aggregates to scatter light. Pectin is an anionic biopolymer across most of studied pH range (pKa ≈ 3.5) and so there will be a relatively strong

electrostatic repulsion between the molecules, preventing them from coming into close contact and forming large aggregates. The optical density of PPI solutions remained relatively low under both low pH (2–3.6) and high pH (5.8–7) values. However, it was elevated around intermediate pH values (3.8–5.6) and reached a maximum at ~pH 4.6, indicating extensive protein aggregation around its isoelectric point (Liu, et al., 2010). The optical density of PPI–HMP mixed solutions as a function of pH was considerably different from that of individual PPI solutions, indicating that there was an intermolecular interaction between PPI and HMP (**Fig. 2-1a, c**). The optical density of PPI–HMP mixture remained very low from pH 8 to 6.5, followed by a gradual increase as pH values dropped from 6.5 to 3.6, and finally reached a maximum at ~pH 3.6 under which a homogenous one phase was observed, presumably due to the formation of soluble complexes between negatively charge HMP and patches of positive charges on the surface of PPI molecules. However, precipitation was observed at pH values of 3 to 2.4, which suggests the formation of insoluble complexes (i.e., complex coacervation). This was likely due to strong electrostatic attraction occurring between PPI and HMP was occurred (de Kruif, Weinbreck, & de Vries, 2004). Formation of soluble complexes between protein and polysaccharide have been previously reported for whey protein–pectin, milk proteins–native gums, and β-lactoglobulin–pectin (Azarikia & Abbasi, 2016; Jones, Decker, & McClements, 2009; Wagoner, et al., 2017). In fact, neutralization of negative groups of pectin by positive amino groups of PPI contributes to the formation of two distinct complexes systems, i.e., the homogenous one phase solution referring to as soluble complexes, and the two phase solution referring to as insoluble complexes. The results of optical density measurements on the soluble complexes formation were also supported by ζ–potential (**Fig. 2-1b**) and test tube picture observations (**Fig. 2-1c**). The charge on the individual PPI solution went from negative charge (-

32.8 mV) at pH 7 to positive charge (+32.3 mV) at pH 3, with the point of zero charge being around pH 4.6 (**Fig. 2-1b**). The ζ–potential of the individual HMP solution was negative from pH 7 to pH 3, which can be attributed to the fact that pectin is an anionic biopolymer containing carboxyl functional groups ($pK_a \approx 3.5$). The net ζ–potential in the mixed PPI–HMP system was intermediate between that of the individual PPI and HMP values, and the point of zero charge was appeared when pH was lower than 3. These results suggested that there is an electrostatic binding between anionic carboxyl groups on the pectin and cationic amino groups on the protein surface. We also found that the presence of HMP reduced the aggregation of PPI near its isoelectric point (pH ~4.6), presumably due to its ability to form intermolecular complexes bearing highly negative charge than PPI alone. Based on the above results, we selected $pH_{\varphi 1}$determined from the optical density measurements to indicate the formation of PPI–HMP soluble complexes. The $pH_{\varphi 1}$is defined as the pH value under which the inflexion point in the optical density *versus* pH curve (**Fig. 2-1a**). When the pH is above $pH_{\varphi 1}$, the PPI–HMP soluble complexes with homogenous one phase system is formed, whereas the two-phase insoluble complexes could be formed when passing pHs (3.6).

Identification of PPI–HMP soluble complexes formation as a function of biopolymer mixing ratio at low PPI concentration

The biopolymer ratio is the second critical parameter for controlling the charge balance in mixed systems (Schmitt, et al., 2011). Therefore, the effect of PPI–HMP mixing ratio (1:1–20:1) on soluble complexes formation and the $pH_{\varphi 1}$were investigated at a fixed low PPI concentration (0.05 wt %) by turbidimetric analysis during an acid titration. The $pH_{\varphi 1}$ of each biopolymer mixture was recorded (**Fig. 2-2a**).

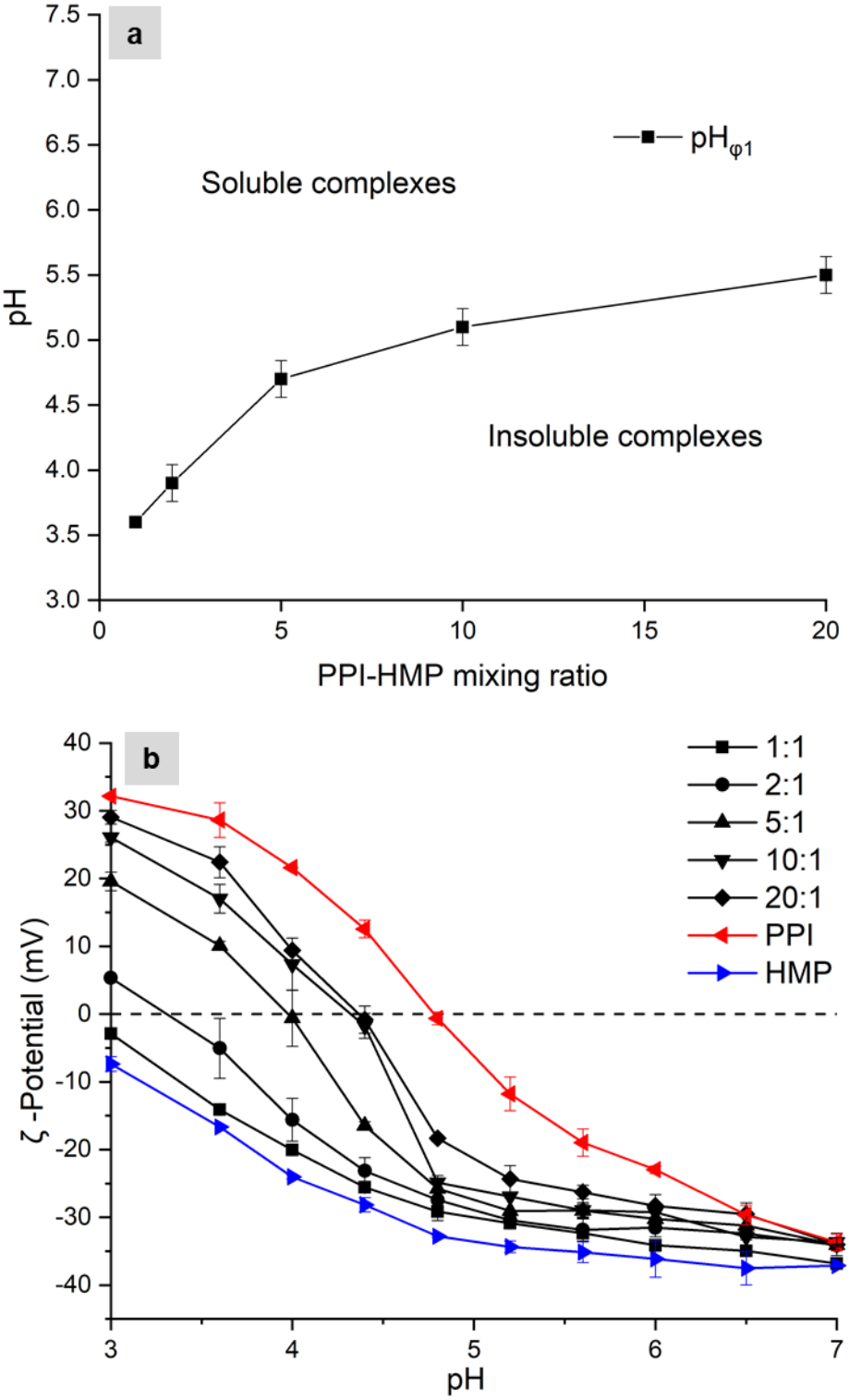

Figure 2-2. (a) $pH_{\varphi 1}$of PPI-HMP mixture at different biopolymer mixing ratio. (b) Dependence of ζ–potential on pH and biopolymer mixing ratio. The PPI concentration was fixed at 0.05 wt%.

As PPI–HMP mixing ratio increased from 1:1 to 20:1 (i.e., HMP concentration decreased), $pH_{\varphi 1}$shifted towards higher pH (**Fig. 2-2a**). For example, the $pH_{\varphi 1}$increased from 3.6 to 5.5 as PPI–HMP mixing ratio increased from 1:1 to 20:1. In other words, higher HMP concentration increased the stability of PPI at lower acidic pH. This phenomenon can be explained by assuming intermolecular complexes formed between HMP and PPI will provide more negative charge on protein surface to prevent protein aggregation at acidic pH. The $pH_{\varphi 1}$ dependence of biopolymer mixing ratio has been previously reported in different biopolymer mixing systems (Liu, et al., 2010; Ru, Wang, Lee, Ding, & Huang, 2012). We also found that the transition $pH_{\varphi 1}$ determined by turbidimetric analysis was close to the value determined using the state diagram (**Fig. 2-3a**).

Additional information about the nature of the PPI–HMP soluble complexes was derived from ζ–potential measurements as a function of pH. The ζ–potential measurements indicated that mixing ratio had a significant impact on the formation and properties of the PPI–HMP complexes (**Fig. 2-2b**). In the absence of HMP, the charge on the PPI became less negative as the pH decreased, as would be expected when the pH moves close its isoelectric point. The ζ–potentials of the soluble complex systems were less negative than that of pectin alone and more negative than protein alone. At all pH values, the ζ–potential became more negative as the PPI–HMP mixing ratio was decreased. This effect can be explained by the fact that the protein has more positive charges on its surface at low pH (Cooper, Dubin, Kayitmazer, & Turksen, 2005; Weinbreck, Nieuwenhuijse, Robijn, & de Kruif, 2004), and therefore more pectin molecules can bind to the exposed cationic amino acid groups.

Identification of PPI–HMP soluble complexes formation as a function of protein concentration

Identification of the $pH_{\varphi 1}$ for low concentration of biopolymer mixture is easy to achieve by using turbidimetric analysis during acid titration (Liu, et al., 2010; Ru, et al., 2012). Nevertheless, it is difficult to determine the $pH_{\varphi 1}$ associated with the formation of soluble complexes of higher biopolymer concentrations, simply because of the high initial optical density of biopolymer mixture (e.g., **Fig. 2-3c**). Meanwhile, proteins and polysaccharides are present together in many protein fortified food systems with relatively high protein concentration to meet protein fortification claim. Recently, a state diagram was employed to represent the phase behavior of protein–polysaccharide mixtures at relatively high biopolymer concentrations (Chun, et al., 2014; Dai, Jiang, Shah, & Corke, 2017). The purpose of these series of experiments was to identify $pH_{\varphi 1}$ of PPI–HMP mixture using a state diagram (Agbenorhevi, Kontogiorgos, & Kasapis, 2013). The effect of PPI–HMP mixing ratio (1:1–20:1), pH (3–7), and PPI concentrations (0.05 and 1.00 wt %) on phase behavior were investigated. The state diagram of PPI–HMP mixtures after standing at ambient temperature for 24 hours is shown in **Fig. 2-3**.

In state diagrams of PPI–HMP mixtures, a border line was drawn to divide the mixtures to one phase soluble complexes region (composition above the line) and two-phase insoluble complexes region (composition below the line). In general, one phase region increased as PPI–HMP mixing ratio decreased. At fixed lower PPI concentration (0.05 wt %), border line exhibited a linear relationship between the mixing ratio and pH. The pH value associated with one phase region shifted toward acidic condition as PPI–HMP mixing ratio decreased (**Fig. 2-3a**). When it came to the fixed higher PPI concentration (1.00 wt %), phase behavior of PPI–HMP mixtures was distinctive as can been seen in state diagram (**Fig. 2-3b**). As observed, the linear border line

disappeared. Furthermore, few phase separations were observed around neutral pH values (e.g., 6.5 and 7).

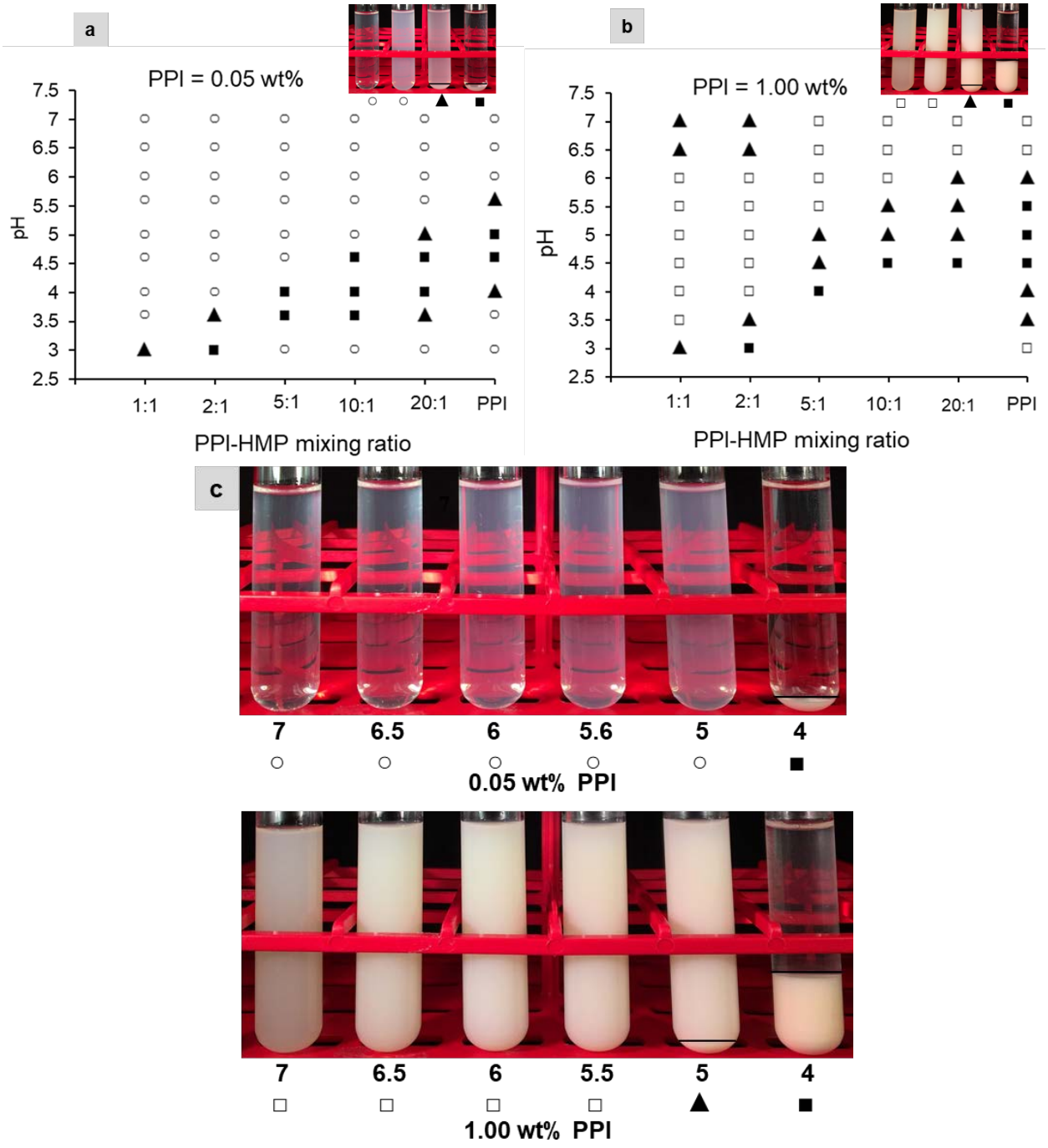

Figure 2-3. State diagram of PPI–HMP mixture in the presence of 0.05 wt% of PPI (a) and 1.00 wt% of PPI (b). (c) The appearance of PPI–HMP mixture (ratio 5:1) as function of pH. ○ represents translucent/transparent solution; □ represents cloudy/milky solution; ▲ represents precipitation and cloudy solution; ■ represents precipitation and clear solution.

According to Agbenorhevi, et al. (2013), biopolymer phase separation observed in higher total biopolymer concentration mixture due to thermodynamic incompatibility could also occur in PPI–HMP mixture. The state diagram clearly showed that one phase region expanded drastically as the PPI–HMP mixing ratio decreased from 5:1 to 2:1 (**Fig. 2-3b**). For instance, when the mixing ratio was 5:1 (HMP concentration was 0.20 wt %), the $pH_{\varphi 1}$ was 5; while in the system of PPI–HMP mixing ratio was 2:1, $pH_{\varphi 1}$ initiated at 3.5. The results clearly showed that HMP concentrations had substantial effects on protein aggregates at lower pH conditions. This indicated that electrostatic binding of anionic carboxyl groups on HMP to cationic amino groups on PPI surface gave rise to the formation of soluble complexes that had sufficient negative charge to repel each other; thus, preventing the aggregation of PPI. At intermediate HMP concentration (0.10–0.20 wt %), soluble complexes can be formed at pH 6 and 5.5, and further decrease the pH led to the phase separation (**Fig. 2-3b**). The cationic amino groups on PPI surface increased dramatically as pH continuous decreased, resulting in charge neutralization with anionic carboxyl groups of pectin binding on the pea protein surface. In consequence, phase separation caused by a nucleation and growth process appeared.

The precipitation of PPI–HMP mixtures was observed as pH decreased, which can be interpreted as a clear signature of insufficient negative groups of HMP which lacking the efficiency to prevent aggregation of protein particles (**Fig. 2-4**). Similarly, Azarikia, et al. (2016) reported that the increment of pectin concentration caused the formation of soluble complexes with β-lactoglobulin and the precipitation of protein was inhibited accordingly. In this study, by decreasing the mixing ratio from 20:1 to 1:1, the negative charge became dominant in the mixture and precipitation prevented at pH above 3.5. The amount of HMP (1.00 wt %) at 1:1 mixing ratio is not only adequate to neutralize the positive charge of PPI at acidic pH, but also

sufficient to hinder approaching PPI through electrostatic repulsion due to prevalence of negative charges in the system.

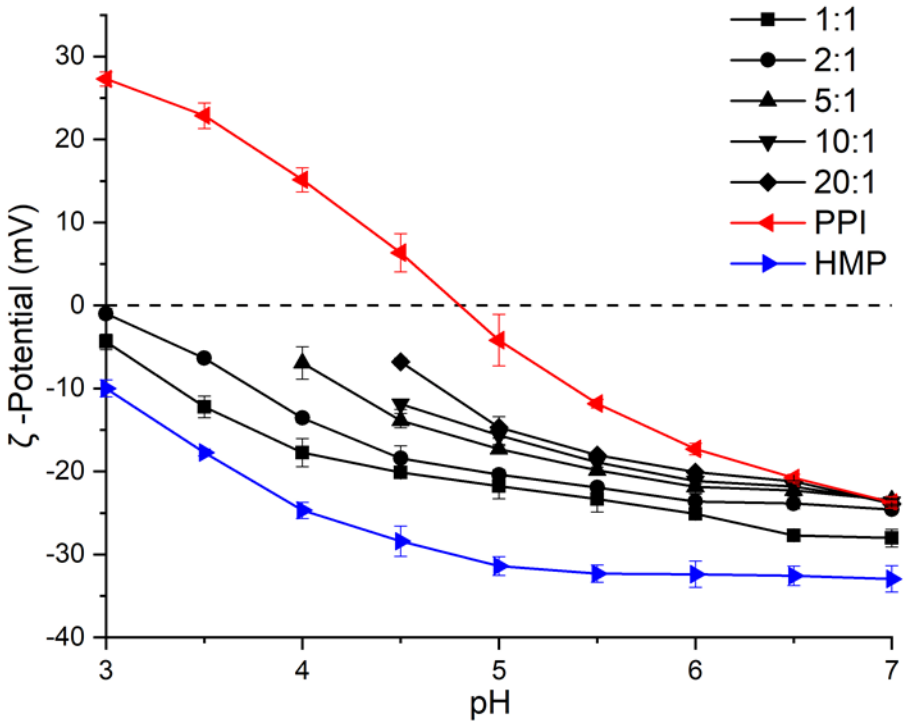

Figure 2-4. Dependence of ζ–potential on pH and biopolymer mixing ratio. The PPI concentration was fixed at 1 wt%.

pH-dependent protein percent solubility (PS) profiles

Solubility is an important prerequisite for a protein to be used as an effective functional ingredient in high moisture food applications, e.g., emulsions, foams and protein fortified beverage. pH-dependent solubility profile of PPI and PPI–HMP soluble complexes was established (**Fig. 2-5)**.

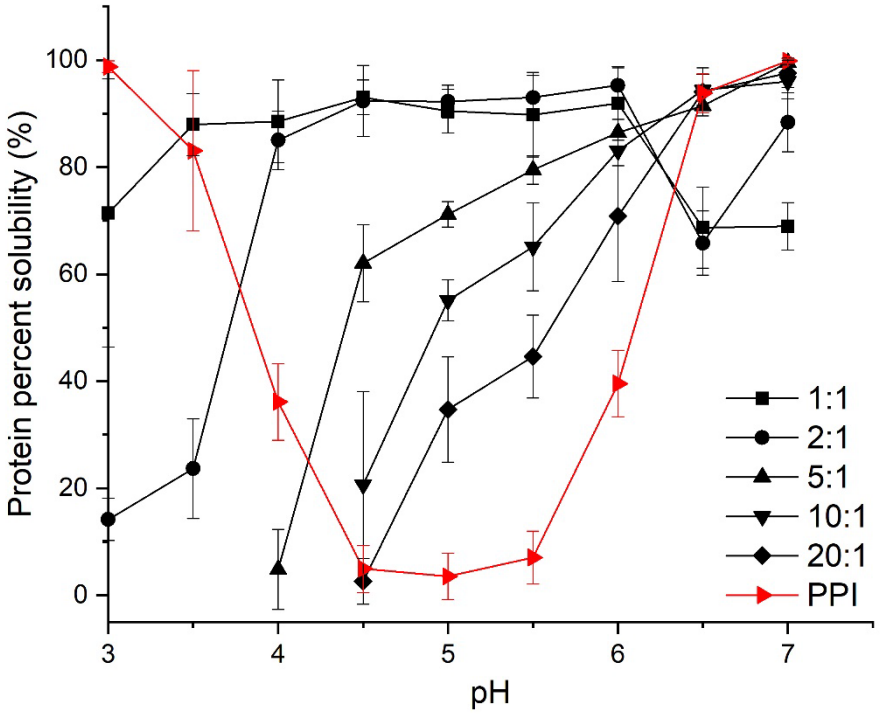

Figure 2-5. Percent protein solubility as function of pH and biopolymer ratio. The PPI concentration was fixed at 1 wt%.

All the samples shared a similar trend in pH-dependent PS profile. The PS of PPI profile showed a decreasing PS with decreasing pH from 7 until it reached minimum solubility (3.54 %) at pH 5 (around the isoelectric point of PPI), followed by an increase in solubility with continuing decrease of pH. Similar pH-dependent PS profiles of pea proteins have been reported for commercial or native PPI (Liang & Tang, 2013). The effect of PPI–HMP mixing ratio (1:1–20:1) on pH-dependent PS profile were also investigated. In general, presence of HMP shifted the pH of minimum PS towards more acidic pH values. For example, the pH of minimum PS was shifted from 4.5 to 4 as the biopolymer mixing ratio decreased from 20:1 to 5:1. Depending on HMP concentrations, PS of PPI–HMP mixtures increased in an expanded pH range compared to PPI alone, which can be explained by the formation of soluble complexes between PPI and HMP rendering more negative surface charge. The change of PPI solubility at acidic environment through the strategies of using polysaccharide is well documented in the literature

(Liu, et al., 2010; Molina Ortiz, Puppo, & Wagner, 2004; Wagoner, et al., 2017). Molina Ortiz, et al. (2004) reported that the presence of carrageenan caused pH range of minimum solubility to shift towards more acidic pH values in soy protein–carrageenan system. Interesting, we also noticed that PS of PPI–HMP mixtures were lower than that of PPI as mixing ratio increased up to 2:1 around neutral pH. For example, the PS of PPI–HMP (2:1) mixture and PPI alone were 65.81 and 93.8 %, respectively at pH 7.0, which agreed with phase separation observed in the state diagram (**Fig. 2-3b**). Such phenomena suggests the existence of thermodynamic incompatibility between PPI and HMP at higher biopolymer concentrations (Ye, 2008).

Flow behavior of PPI–HMP mixture

It is well known that the viscosity of biopolymer mixture is influenced by polysaccharide type (e.g., molecular weight, branching and compositions), concentrations, as well as structure of protein–polysaccharide complexes (Bai, et al., 2017). Previously, researchers have reported that the apparent viscosity increased as the formation of complexes in the protein–polysaccharide systems (Lizarraga, Piante Vicin, González, Rubiolo, & Santiago, 2006). However, opposite results have also been reported and apparent viscosity of the protein–polysaccharide mixture systems can decrease due to electrostatic interactions (Liu, et al., 2012). In order to understand the effect of pH and PPI–HMP mixtures on the viscosity of system, the apparent viscosity was recorded at shear rate from 0.1 to 100 s^{-1} (**Fig. 2-6**).

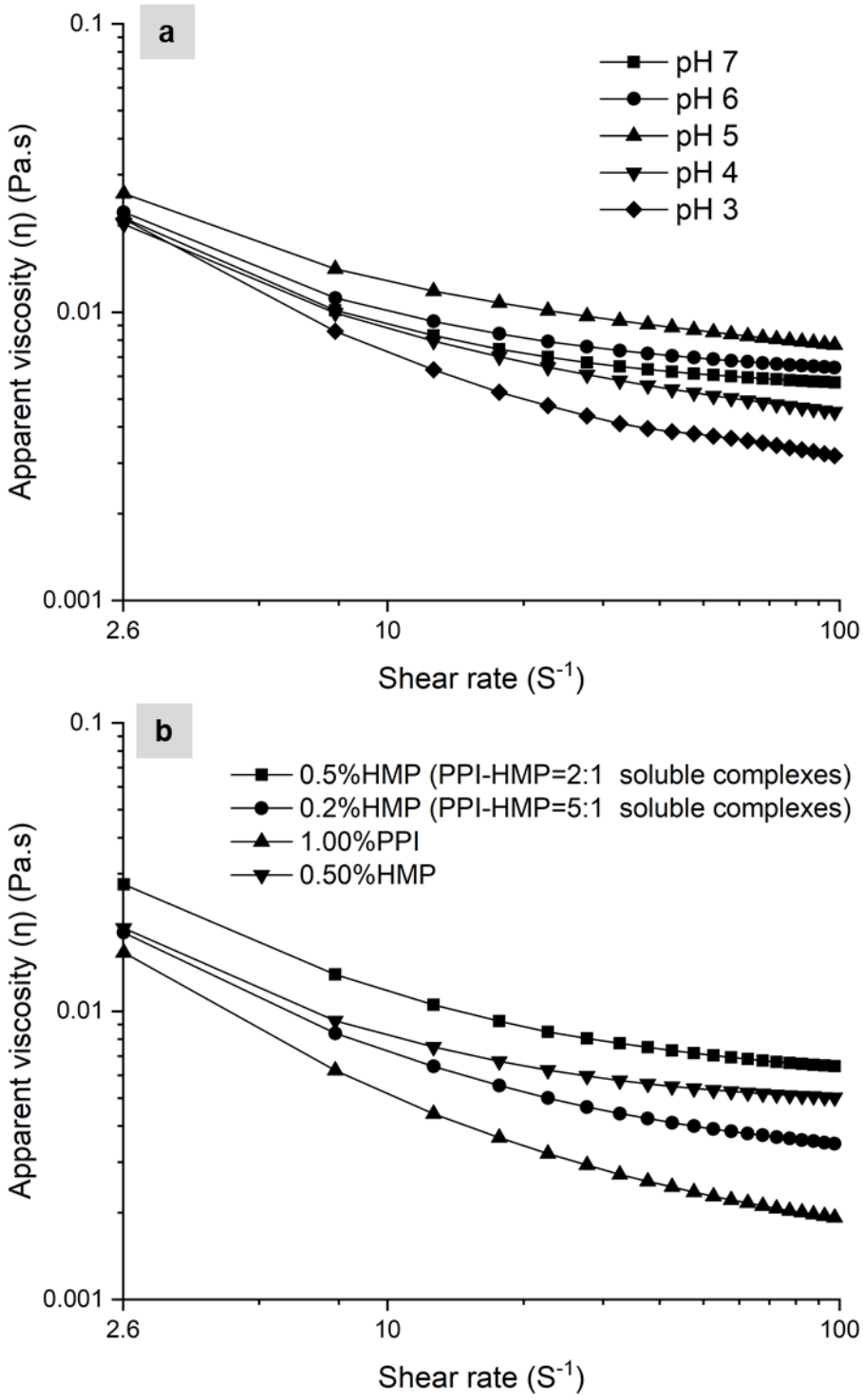

Figure 2-6. (a) Apparent viscosity versus applied shear rate of mixed PPI–HMP system (ratio 2:1) at different pH; (b) Apparent viscosity versus applied shear rate of PPI–HMP soluble complex mixtures, PPI and HMP solution at pH 6.

The apparent viscosity of all samples was reduced as shear rate increased from 0.1 to 100 s^{-1}, indicating a shear thinning behavior. This is likely due to the breakdown of network

surrounding the particles or weak linkages between molecules (Azarikia, et al., 2016), or rearrangement of soluble complexes structure under applied shear rate (Liu, et al., 2017). In case of the PPI–HMP mixture (2:1), the apparent viscosity of PPI–HMP is pH dependent (**Fig. 2-6a**). The relatively high apparent viscosity was observed at pH 5 and 6, indicating the presence of strong negative charges that causing electrostatic repulsion between complexes particles that increase the resistance against flow. Consequently, both ζ–potential and viscosity measurements confirmed the presence of soluble complexes formation in PPI–HMP mixture. Interesting, apparent viscosity of PPI–HMP at pH 5 was higher in comparison to pH 6, while ζ–potential of sample at pH 6 (-23.62 mV) was higher than that of pH 5 (-20.38 mV). Presumably, the side branches of modified HMP molecular by binding PPI molecules at pH 5 was longer than that of pH 6. Thus, PPI–HMP mixture at pH 5 can provide more steric repulsion instead of electrostatic repulsion. In addition, the apparent viscosity of PPI–HMP mixture at pH 7 was slightly lower than that of pH 5 and 6 due to lower amount of soluble materials in colloidal system. As previously explained, there is a phase separation around neutral pH due to thermal incompatibility. This result indicated that hydrogen bonding between the neighboring HMP molecules also enhances viscosity. Meanwhile, apparent viscosity of soluble complexes with different concentration of HMP compare to samples without PPI or HMP was also studied (**Fig. 2-6b**). In general, apparent viscosity of soluble complexes is higher than that of protein or polysaccharide alone. Similar results in protein–polysaccharide complexes have been reported including WPI–pectin soluble complexes (Wagoner, et al., 2017), canola protein–pectin complexes (Stone, et al., 2013), and WPI–flaxseed gum complexes (Mao, Roos, & Miao, 2014). At 2:1 ratio, apparent viscosity was greater than that of 5:1 PPI–HMP mixing ratio. This is likely

because the increase of HMP concentration leads to higher inter- and intramolecular interactions and overlapping of polysaccharide chains (Azarikia, et al., 2016).

Thermal property of PPI–HMP soluble complexes

Thermal property of globular proteins is one of the most important parameters to indicate their heat-induced aggregation and/or gelation behaviors. A higher denaturation temperature (T_d) is usually associated with higher thermal stability for a globular protein (Ladjal-Ettoumi, Boudries, Chibane, & Romero, 2016). Thermal stability of PPI, selected PPI–HMP soluble complexes at pH 6 using T_d as indicator were evaluated by DSC. The onset denaturation temperature (T_{onset}), peak denaturation temperature (T_d) determined from these thermograms are presented in **Table 2-1**.

Table 2-1. Thermal property of PPI–HMP soluble complexes.

	T_{onset}	T_d
PPI	80.03 ± 1.48^{a}	85.12 ± 1.55^{A}
Soluble complexes	82.40 ± 1.79^{b}	87.00 ± 1.31^{B}

† The values with different superscript letters within a column are significantly different ($p<0.05$).

All thermograms showed one endothermic peak (data not shown). The T_d of PPI was registered at 85.12 °C, which was very close to the result reported by Ladjal-Ettoumi, et al. (2016). It has been reported that complexation between protein and polysaccharide (e.g., soluble complexes and complex coacervation) increases the protein thermal stability (Huang, Sun, Xiao, & Yang, 2012; Wagoner, et al., 2017). This phenomenon was also observed in our PPI–HMP complexes. The denaturation temperature of PPI-HMP compared to PPI alone was slightly higher (87 to 85 ℃, respectively, **Table 2-1**), indicating the formation of a new network structure with enhanced thermal stability.

Conclusions

The effect of pH (3–7), PPI–HMP biopolymer mixing ratio (1:1 to 20:1) and PPI concentration (0.05 and 1.00 wt %) on the formation of soluble complexes between PPI and HMP were investigated. The pH of soluble complexes formation shifted towards higher pH as PPI–HMP mixing ratio increased from 1:1 to 20:1 and as PPI concentration increased from 0.05 % to 1.00 wt%. ζ–potential results indicated that at pH values close to the isoelectric point of PPI, the addition of HMP increased surface charge of PPI, resulting in the enhanced solubility. At higher PPI system (1.00 wt %), at biopolymer mixing ratio between 1:1 and 2:1, phase separation was observed at neutral pH as the result of biopolymer thermal incompatibility.

The results also supported that PPI–HMP soluble complexes expanded PPI pH dependent solubility profile towards more acidic pH values as PPI–HMP ratio decreased. PPI–HMP soluble complexes displayed a shear thinning flow behavior. The viscosity of soluble complexes was slightly higher than that of HMP or PPI alone. The viscosity and ζ–potential results indicated that PPI–HMP soluble complex was formed through the electrostatic interaction between the amine groups ($-NH_4^+$) of PPI and the carboxyl groups of HMP ($–COO^–$) and hydrogen bonding in PPI–HMP interaction. Thermal denaturation temperature of PPI was slightly increased through the formation of PPI–HMP soluble complexes. Findings from this study suggest that PPI–HMP soluble complexes improve the functional attributes of PPI at acidic environment.

References

Adebiyi, A. P., & Aluko, R. E. (2011). Functional properties of protein fractions obtained from commercial yellow field pea (*Pisum sativum* L.) seed protein isolate. *Food Chemistry*, *128*(4), 902-908.

Agbenorhevi, J. K., Kontogiorgos, V., & Kasapis, S. (2013). Phase behaviour of oat β-glucan/sodium caseinate mixtures varying in molecular weight. *Food Chemistry, 138*(1), 630-637.

Aryee, F. N. A., & Nickerson, M. T. (2012). Formation of electrostatic complexes involving mixtures of lentil protein isolates and gum arabic polysaccharides. *Food Research International, 48*(2), 520-527.

Azarikia, F., & Abbasi, S. (2016). Mechanism of soluble complex formation of milk proteins with native gums (*tragacanth and Persian gum*). *Food Hydrocolloids, 59*, 35-44.

Bai, L., Liu, F., Xu, X., Huan, S., Gu, J., & McClements, D. J. (2017). Impact of polysaccharide molecular characteristics on viscosity enhancement and depletion flocculation. *Journal of Food Engineering, 207*, 35-45.

Beck, S. M., Knoerzer, K., Sellahewa, J., Emin, M. A., & Arcot, J. (2017). Effect of different heat-treatment times and applied shear on secondary structure, molecular weight distribution, solubility and rheological properties of pea protein isolate as investigated by capillary rheometry. *Journal of Food Engineering, 208*, 66-76.

Ben-Harb, S., Panouillé, M., Huc-Mathis, D., Moulin, G., Saint-Eve, A., Irlinger, F., Bonnarme, P., Michon, C., & Souchon, I. (2018). The rheological and microstructural properties of pea, milk, mixed pea/milk gels and gelled emulsions designed by thermal, acid, and enzyme treatments. *Food Hydrocolloids, 77*, 75-84.

Boye, J., Zare, F., & Pletch, A. (2010). Pulse proteins: Processing, characterization, functional properties and applications in food and feed. *Food Research International, 43*(2), 414-431.

Braudo, E. E., Plashchina, I. G., & Schwenke, K. D. (2001). Plant protein interactions with polysaccharides and their influence on legume protein functionality A Review. *Food / Nahrung, 45*(6), 382-384.

Chun, J. Y., Hong, G. P., Surassmo, S., Weiss, J., Min, S. G., & Choi, M. J. (2014). Study of the phase separation behaviour of native or preheated WPI with polysaccharides. *Polymer, 55*(16), 4379-4384.

Cooper, C. L., Dubin, P. L., Kayitmazer, A. B., & Turksen, S. (2005). Polyelectrolyte–protein complexes. *Current Opinion in Colloid & Interface Science, 10*(1), 52-78.

Dahl, W. J., Foster, L. M., & Tyler, R. T. (2012). Review of the health benefits of peas (*Pisum sativum* L.). *British Journal of Nutrition, 108*(S1), S3-S10.

Dai, S., Jiang, F., Shah, N. P., & Corke, H. (2017). Stability and phase behavior of konjac glucomannan-milk systems. *Food Hydrocolloids, 73*, 30-40.

de Kruif, C. G., Weinbreck, F., & de Vries, R. (2004). Complex coacervation of proteins and anionic polysaccharides. *Current Opinion in Colloid & Interface Science, 9*(5), 340-349.

Dijkink, B. H., & Langelaan, H. C. (2002). Milling properties of peas in relation to texture analysis. Part I. Effect of moisture content. *Journal of Food Engineering, 51*(2), 99-104.

Freitas, R. L., Ferreira, R. B., & Teixeira, A. R. (2000). Use of a single method in the extraction of the seed storage globulins from several legume species. Application to analyse structural comparisons within the major classes of globulins. *International Journal of Food Sciences and Nutrition, 51*(5), 341-352.

Gancz, K., Alexander, M., & Corredig, M. (2005). Interactions of high methoxyl pectin with whey proteins at oil/water interfaces at acid pH. *Journal of Agricultural and Food Chemistry, 53*(6), 2236-2241.

Havemeier, S., Erickson, J., & Slavin, J. (2017). Dietary guidance for pulses: the challenge and opportunity to be part of both the vegetable and protein food groups. *Annals of the New York Academy of Sciences, 1392*(1), 58-66.

Huang, G. Q., Sun, Y. T., Xiao, J. X., & Yang, J. (2012). Complex coacervation of soybean protein isolate and chitosan. *Food Chemistry, 135*(2), 534-539.

Jones, O. G., Decker, E. A., & McClements, D. J. (2009). Formation of biopolymer particles by thermal treatment of β-lactoglobulin–pectin complexes. *Food Hydrocolloids, 23*(5), 1312-1321.

Jones, O. G., & McClements, D. J. (2011). Recent progress in biopolymer nanoparticle and microparticle formation by heat-treating electrostatic protein-polysaccharide complexes. *Advances in Colloid and Interface Science, 167*(1-2), 49-62.

Klassen, D. R., Elmer, C. M., & Nickerson, M. T. (2011). Associative phase separation involving canola protein isolate with both sulphated and carboxylated polysaccharides. *Food Chemistry, 126*(3), 1094-1101.

Klemmer, K. J., Waldner, L., Stone, A., Low, N. H., & Nickerson, M. T. (2012). Complex coacervation of pea protein isolate and alginate polysaccharides. *Food Chemistry*, *130*(3), 710-715.

Ladjal-Ettoumi, Y., Boudries, H., Chibane, M., & Romero, A. (2016). Pea, chickpea and lentil protein isolates: physicochemical characterization and emulsifying propertiesu. *Food Biophysics, 11*(1), 43-51.

Lam, R. S. H., & Nickerson, M. T. (2013). Food proteins: A review on their emulsifying properties using a structure-function approach. *Food Chemistry, 141*(2), 975-984.

Liang, H. N., & Tang, C. H. (2013). pH-dependent emulsifying properties of pea (*Pisum sativum* L.) proteins. *Food Hydrocolloids, 33*(2), 309-319.

Liu, J., Shim, Y. Y., Shen, J. H., Wang, Y., & Reaney, M. J. T. (2017). Whey protein isolate and flaxseed *(Linum usitatissimum* L.) gum electrostatic coacervates: Turbidity and rheology. *Food Hydrocolloids, 64*, 18-27.

Liu, L., Zhao, Q., Liu, T., Long, Z., Kong, J., & Zhao, M. (2012). Sodium caseinate/xanthan gum interactions in aqueous solution: Effect on protein adsorption at the oil–water interface. *Food Hydrocolloids, 27*(2), 339-346.

Liu, S., Elmer, C., Low, N. H., & Nickerson, M. T. (2010). Effect of pH on the functional behaviour of pea protein isolate-gum Arabic complexes. *Food Research International, 43*(2), 489-495.

Liu, S. H., Low, N. H., & Nickerson, M. T. (2009). Effect of pH, salt, and biopolymer ratio on the formation of pea protein isolate-gum arabic complexes. *Journal of Agricultural and Food Chemistry, 57*(4), 1521-1526.

Lizarraga, M. S., Piante Vicin, D. D., González, R., Rubiolo, A., & Santiago, L. G. (2006). Rheological behaviour of whey protein concentrate and λ-carrageenan aqueous mixtures. *Food Hydrocolloids, 20*(5), 740-748.

Mao, L., Roos, Y. H., & Miao, S. (2014). Study on the rheological properties and volatile release of cold-set emulsion-filled protein gels. *Journal of Agricultural and Food Chemistry, 62*(47), 11420-11428.

McCarty, M. F. (1999). Vegan proteins may reduce risk of cancer, obesity, and cardiovascular disease by promoting increased glucagon activity. *Medical Hypotheses, 53*(6), 459-485.

Molina Ortiz, S. E., Puppo, M. C., & Wagner, J. R. (2004). Relationship between structural changes and functional properties of soy protein isolates–carrageenan systems. *Food Hydrocolloids, 18*(6), 1045-1053.

Nosworthy, M. G., Tulbek, M. C., & House, J. D. (2017). Does the concentration, isolation, or deflavoring of pea, lentil, and faba bean protein alter protein quality? *Cereal Foods World, 62*(4), 139-142.

Ru, Q. M., Wang, Y. W., Lee, J., Ding, Y. T., & Huang, Q. R. (2012). Turbidity and rheological properties of bovine serum albumin/pectin coacervates: Effect of salt concentration and initial protein/polysaccharide ratio. *Carbohydrate Polymers, 88*(3), 838-846.

Schmitt, C., & Turgeon, S. L. (2011). Protein/polysaccharide complexes and coacervates in food systems. *Advances in Colloid and Interface Science, 167*(1-2), 63-70.

Semenova, M. (2017). Protein–polysaccharide associative interactions in the design of tailor-made colloidal particles. *Current Opinion in Colloid & Interface Science, 28*, 15-21.

Shevkani, K., Singh, N., Kaur, A., & Rana, J. C. (2015). Structural and functional characterization of kidney bean and field pea protein isolates: A comparative study. *Food Hydrocolloids, 43*, 679-689.

Stone, A. K., Cheung, L., Chang, C., & Nickerson, M. T. (2013). Formation and functionality of soluble and insoluble electrostatic complexes within mixtures of canola protein isolate and (*kappa-*, *iota-* and *lambda*-type) carrageenan. *Food Research International, 54*(1), 195-202.

Stone, A. K., Karalash, A., Tyler, R. T., Warkentin, T. D., & Nickerson, M. T. (2015). Functional attributes of pea protein isolates prepared using different extraction methods and cultivars. *Food Research International, 76*, 31-38.

Taherian, A. R., Mondor, M., Labranche, J., Drolet, H., Ippersiel, D., & Lamarche, F. (2011). Comparative study of functional properties of commercial and membrane processed yellow pea protein isolates. *Food Research International, 44*(8), 2505-2514.

Wagoner, T. B., & Foegeding, E. A. (2017). Whey protein–pectin soluble complexes for beverage applications. *Food Hydrocolloids, 63*, 130-138.

Weinbreck, F., Nieuwenhuijse, H., Robijn, G. W., & de Kruif, C. G. (2004). Complexation of whey proteins with carrageenan. *Journal of Agricultural and Food Chemistry, 52*(11), 3550-3555.

Ye, A. Q. (2008). Complexation between milk proteins and polysaccharides via electrostatic interaction: principles and applications - a review. *International Journal of Food Science and Technology, 43*(3), 406-415.

Yuan, Y., Wan, Z.-L., Yang, X.-Q., & Yin, S.-W. (2014). Associative interactions between chitosan and soy protein fractions: Effects of pH, mixing ratio, heat treatment and ionic strength. *Food Research International, 55*, 207-214.

CHAPTER 3. PHASE BEHAVIOR, THERMODYNAMIC AND MICROSTRUCTURE OF CONCENTRATED PEA PROTEIN ISOLATE–PECTIN MIXTURE: EFFECT OF PH, BIOPOLYMER RATIO AND PECTIN CHARGE DENSITY

Abstract

The impact of pH, PPI–pectin mixing ratio and pectin charge density on phase behavior (co-solubility, soluble complex and complex coacervates) of concentrated biopolymer mixture was investigated using state diagram and ζ–potential measurement. The microstructure, thermodynamic behavior, and non-covalent bonding of PPI to pectin were further explored by confocal laser scanning microscopy (CLSM), isothermal titration calorimetry (ITC), and Fourier transform infrared spectroscopy (FTIR). In general, the pH for soluble complex and complex coacervate formation shifted towards higher pH as PPI–pectin mixing ratio increased. LMP is favorable for complex coacervate over a wider pH range compared with HMP, likely due to its higher overall charge density. The CLSM images revealed that larger aggregates were formed in PPI–LMP coacervates. Both ITC and FTIR analyses indicated that soluble complex and complex coacervates were formed through the electrostatic interaction and hydrogen bonding between PPI and pectin.

Introduction

The interactions between protein and polysaccharide to form complexes have a number of applications including structure control, texture and mouthfeel of foods, stabilization of emulsions and foam, and as a microencapsulation wall material for protecting and delivering bioactive compounds (e.g., vitamins, colorants, probiotics, antioxidants, and oil components) (Moschakis & Biliaderis, 2017; Wijaya, Patel, Setiowati, & Van der Meeren, 2017). In a mixed biopolymer (protein and polysaccharide) system, either a one-phase or two-phase complexing

system can occur depending on the biopolymer characteristics (e.g., type, charge density and molecular weight), biopolymer concentration, and mixing ratio. In a one-phase regime, protein and polysaccharide can exist either as co-solubility or as soluble complexes. In contrast, the biopolymer mixture separates into two distinct phases that have different biopolymer compositions in a two-phase regime. For example, complex coacervation involves electrostatic attraction between protein and polysaccharide with opposite electrical charges, which results in phase separation into solvent-rich and biopolymer-rich phases. In fact, there is a disparity on the definition of complex coacervation. Some researchers defined the insoluble complexes (phase separation) as a consequence of complex coacervation phenomenon (Liu, et al., 2010; Schmitt, Sanchez, Desobry-Banon, & Hardy, 1998); while others described the liquid–liquid phase separation as coacervation, whereas the liquid–solid phase separation was considered as precipitation (Comert, Malanowski, Azarikia, & Dubin, 2016). As summarized by Moschakis (Moschakis, et al., 2017), the transition from liquid–liquid to liquid–solid phase separation is critically dependent on equilibration time and systems (e.g., protein and polysaccharide type and biopolymer concentrations), and the distinction between coacervates and precipitates is not clearly defined. In addition, it is difficult to determine by means of analytical tools. Therefore, the term of coacervation is widely used in both types of phase behaviors (coacervation and precipitation) in many studies. In this work, phase separation of equilibrium binary mixtures was considered as complex coacervation.

The turbidity measurement has been applied to identify boundary pH of aforementioned phase behaviors based on optical properties at the mesoscale using low biopolymer concentrations (Wagoner, Vardhanabhuti, & Foegeding, 2016). Three critical phase transition pH values (pHs) (pH_c, $pH_{\varphi 1}$, $pH_{\varphi 2}$, defined on the basis of changes in turbidity curve slope) were

identified from turbidity curves during titration from basic to acidic pH, corresponding to four different phase behaviors (i.e., pH > pH_c, co-solubility; pH_c~ $pH_{\varphi 1}$, soluble complexes; $pH_{\varphi 1}$~ $pH_{\varphi 2}$, complex coacervates; pH < $pH_{\varphi 2}$, dissolution of complexes) (Li, Zhang, Zhao, Ding, & Lin, 2018; Moschakis, et al., 2017). The soluble complexes and complex coacervates (insoluble complexes) could be differentiated in terms of particle size and density of binary mixture, and thus it could be separated on the basis of gravitational force (centrifugation speed). Between $pH_{\varphi 1}$ and $pH_{\varphi 2}$, a maximum optical density is generally observed and defined as the pH_{opt} at which maximum amount of coacervates is produced. The "maximum amount of coacervates" represents the maximum yield of dried coacervate phase which is typically calculated by *Coacervate yield (%) = (weight of dried coacervates/total biopolymer weight) × 100* (Huang, Du, Xiao, & Wang, 2017). This pH_{opt}, a particular important factor in the application area for microencapsulation, can be alternatively determined by surface charge measurement since it has been widely reported that the maximum turbidity was reached when the net zeta–potential value was zero (Eghbal, et al., 2016; Hasanvand & Rafe, 2018). By further decreasing pH from $pH_{\phi 1}$ to pH_{opt}, the electrostatic attractive forces became stronger and the maximum electrostatic interaction were reached at pH_{opt}. As such, more complex coacervate particles were formed which would lead to the maximum turbidity value at pH_{opt}.

Recently, there is growing interest in the consumption of pulse proteins, such as yellow pea (*Pisum sativum L.*) protein isolate (PPI), as a preferable alternative to animal proteins due to the low cost, more sustainable source of proteins with a lower carbon footprint, and manufacturers can use allergen-free and gluten-free labeling claims (Adebiyi & Aluko, 2011; Havemeier, Erickson, & Slavin, 2017). Globulins and albumins are the two major protein classes, accounting for nearly 70–80% and 10–20% of the total PPI, respectively (Zha, Dong,

Rao, & Chen, 2019). Globulins can be subdivided into mainly legumin (hexameric protein, 300–400 kDa, 11S) and vicilin (trimeric protein, 150–170 kDa, 7S), with minor amounts of convicilin proteins (composed of three ~70 kDa sub-units, 7S) (Lam, Can Karaca, Tyler, & Nickerson, 2018). With regard to polysaccharide, pectin is a typical food-grade anionic polysaccharide which has been widely used to interact with protein to improve their functionality (Ru, Wang, Lee, Ding, & Huang, 2012). Previous studies have demonstrated that the interactions between protein and polysaccharides are highly determined by the charge density of the polysaccharides (Ding, Huang, Cai, & Wang, 2019; Xiong, et al., 2017). In general, the charge density of pectin can be characterized by two parameters: the degree of esterification (DE) of the carboxylic acid groups in galacturonan which determines the overall charge density of the pectin molecule, and the degree of blockiness (DB) that represents the distribution pattern of un-esterified blocks of galacturonic acid (GalA) along the pectin backbone and gives an indication to local charge density of pectin molecules (Ru, et al., 2012; Xu, et al., 2018). Based on DE, pectin can be categorized as low methoxyl (DE < 50%) pectin (LMP) with high overall charge density, and high methoxyl (DE ≥ 50%) pectin (HMP) with low overall charge density (Xu, et al., 2018).

In the past few years, pea protein–polysaccharide interactions have been extensively reviewed (Wijaya, et al., 2017). However, research on phase behaviors and their functionality of pea protein–polysaccharide complexes have mainly focused on their interactions at low biopolymer concentrations (typically below 0.3 wt%) (Aryee & Nickerson, 2012; Rocha, Souza, Magalhaes, Andrade, & Goncalves, 2014). In terms of application areas of encapsulation, fat-mimetics, and texture modifiers, it generally requires higher protein–polysaccharide concentration (Klemmer, Waldner, Stone, Low, & Nickerson, 2012; Stenger, Zeeb, Hinrichs, & Weiss, 2017). It is therefore of the utmost importance to understand the phase behaviors, as well

as thermodynamic and microstructure of pea protein–polysaccharide at higher biopolymer concentrations. One challenge to successfully investigate the phase behavior and identify pHs of concentrated biopolymer system is the high initial turbidity, which invalidates the common turbidimetric method (OD_{600nm}). Additionally, our recent study has shown that the phase transition pHs were shifted on the basis of the biopolymer concentrations (Lan, Chen, & Rao, 2018). As such, the development of an alternative method to identify the phase transition pH values at concentrated biopolymer systems is of great consequence for the commercial viability of pea protein–polysaccharide complexes.

Interactions between PPI and pectin with different charge density in concentrated biopolymer systems have yet to be reported. Therefore, the current study was undertaken to (i) develop a state diagram in conjunction with surface charge measurement to identify critical boundary pH range for the regimes of co-solubility, soluble complexes and complex coacervates at high biopolymer concentration; (ii) investigate the factors (i.e. pH, biopolymer mixing ratio, and charge density of pectin) that influence the phase behaviors of PPI–pectin; and (iii) elucidate the thermodynamics and microstructure of PPI–pectin in different regimes using confocal laser scanning microscopy (CLSM), isothermal titration calorimetry (ITC), and Fourier transform infrared spectroscopy (FTIR). We hypothesized that the differences in overall charge density of pectin (LMP and HMP) would influence the formation of PPI–pectin complexes. Results gained from this research will provide guidance on designing high concentration pea protein fortified food systems.

Materials and methods

Materials

Yellow pea flour was purchased from Harvest Innovations (Indianola, Iowa, USA). As stated by the manufacturer, the yellow pea flour is manufactured from organic food quality yellow peas and contains 20.55% protein, 7.10% moisture, 2.08% lipid, 2.68% ash, and 67.59% carbohydrate. Freeze dried PPI was extracted as previously reported without any modification (Lan, et al., 2018), and composed of 79.50% protein (%N × 6.25, wet basis), 5.28% moisture, 0.77 % lipid, 4.61% crude ash, and 9.84% carbohydrate (by difference from 100%) (AOAC methods (2016)). High methoxyl pectin (HMP) (GENU® pectin type YM–100–L, Lot # LI 62026, 110 kDa of Mw) and low methoxyl pectin (LMP) (GENU® pectin type LM–12 CG, Lot # GR74485, 76 kDa of Mw) were kindly donated by CP Kelco (Atlanta, Georgia, USA) and used without further purification. Rhodamine B was purchased from Sigma–Aldrich Co. (Steinheim, Germany). Sodium hydroxide (NaOH), hydrochloric acid (HCl), other chemicals and reagents used in this work were of analytical grade and purchased from VWR (Chicago, Illinois, USA). Ultrapure water (UPW) was used for the preparation of all solutions (18.2 MΩ·cm, Barnstead GenPure Pro water purification system, Thermo Fisher Scientific Inc., USA). All concentrations were expressed in weight percentage (wt%).

Characterization of pectins

Determination of degree of esterification (DE)

The DE of pectin was determined by the titrimetric method of Food Chemical Codex and Singthong, Cui, Ningsanond, and Goff (2004) with a slight modification. Briefly, pectin powder (0.5 g) was moistened with 2 mL ethanol, dissolved in 100 mL UPW, and stirred magnetically for 5 h at room temperature to completely dissolve pectin. Then, 5 drops of phenolphthalein (0.5

g in 100 mL ethanol) were added to pectin dispersion, followed by titration using 0.5 M NaOH until pink color appeared, and the volume of initial NaOH was recorded as V_1. Subsequently, 10 mL of 0.5 M NaOH was added into the mixture, and the resultant mixture solution was shaken vigorously and allowed to stand for 30 min at room temperature to de-esterify pectin. Afterwards, 10 mL of 0.5 N HCl was added, and the solution was shaken until the pink color disappeared. Eventually, 5 drops of phenolphthalein were added into the solution, and it was further titrated with 0.5 M NaOH to give a pink color that kept stable throughout rough mixing, and the volume of latter NaOH was recorded as V_2. The DE was calculated using equation: DE (%) = $V_2/(V_1+V_2) \times 100\%$.

Determination of galacturonic acid (GalA)

The content of GalA was determined using a colorimetric method described by Yoo, Fishman, Hotchkiss, and Lee (2006) with some modifications. Simply, 0.4 mL of pectin solution (100 μg/mL) was vigorously mixed with 40 μL of ammonium sulfamate (4 mol/L) and 2.5 mL of sodium tetraborate (0.075 mol/L in concentrated sulfuric acid). The mixture was kept in an ice bath during mixing, followed by heating in a boiling water bath for 15 min, and then rapidly cooled to the room temperature by placing it in an ice bath. Then, 80 μL of 3-phenylphenol (0.15 g/100 mL in 0.1 M NaOH) was added into the mixture to develop a pink color in 5 min. After that, the absorbance was recorded at 525 nm using an UV spectrophotometer (UV–Vis 1800, Shimadzu). A standard curve was made based on galacturonic acid at different concentrations (10, 25, 50, 75 and 100 μg/mL). The GalA concentration obtained from abovementioned standard curve was divided by concentration of the pectin solution (100 μg/mL) to calculate GalA content (%) in pectin.

Preparation of PPI and pectin stock solutions

The PPI stock solution (2.00 wt%) was prepared by dissolving PPI in UPW with mechanical stirrer at 1000 rpm for 0.5 h. The solution was then adjusted to pH 9.5 and stirred for 2 h to promote hydration, followed by adjusting the pH to 7.0 and stirring overnight (8–12 h) at room temperature. The 0.1–2.0 M NaOH or HCl was applied in aforementioned pH adjustments. The HMP and LMP stock solutions (2.00 wt%) were initially prepared by dispersing pectin in UPW using mechanical stirring at 500 rpm overnight at room temperature, respectively. Subsequently, HMP and LMP stock solutions were adjusted to pH 7.0 using 0.1–2.0 M NaOH. Sodium azide (0.02 wt%) was added into all stock solutions to prevent microbial growth. Finally, all stock solutions were centrifuged at 5,520×*g* for 15 min (Beckman J2–HS, Beckman Coulter Inc., Indianapolis, IN, USA), and suction filtered through a Whatman #1 filter paper to remove any insoluble matters.

Preparation of PPI–pectin mixtures

PPI–pectin mixtures were prepared by mixing PPI and pectin stock solutions at various weight ratio of PPI to pectin (HMP or LMP) (1:1, 2:1, 5:1, 10:1, and 20:1). The concentration of PPI was fixed at 1.00 wt% and the concentration of pectin varied from 0.05 to 1.00 wt% throughout mixing ratio of 1:1 to 20:1. The pH value of individual mixture (PPI–HMP or PPI–LMP) was adjusted from 8 to 2 with 0.5 decrement by adding HCl (0.1–2.0 N). The use of various concentrations of HCl was to minimize dilution effects and conductivity changes to mixture solution. The PPI and pectin solutions were used as control samples. The mixtures and controls were left to stand quiescent for 24 h at 4 °C. After 24 h of standing, the state diagram of PPI–pectin mixtures was constructed in accordance to visual observation described in our recent work (Lan, et al., 2018). The phase separation was classified into five groups and labeled with

five symbols, namely, (○) translucent solution, (□) turbid solution, (▲) precipitation & cloudy solution, (■) precipitation & clear solution, and (●) precipitation & clear solution with higher volume of precipitation than ■.

Surface charge analysis

Surface charge of 1.00 wt% of single biopolymer solutions (PPI, HMP and LMP), and mixed PPI–pectin solutions was measured as a function of pH (8.0–2.0) and mixing ratio (PPI to pectin at 1:1–20:1) using a Zetasizer Nano–ZS 90 (Malvern Instruments, Worcestershire, UK). The result was reported as zeta–potential (ζ, mV), representing sum of the individual surface charge of different functional groups in the biopolymer mixed solutions or individual biopolymer solution.

Confocal laser scanning microscopy (CLSM)

The CLSM images of mixtures (PPI–HMP or PPI–LMP) at selected pH conditions (pH 8, 7, 6, 5.5 and 3.5) were recorded at room temperature using a LSM 700 confocal laser scanning microscope (Carl Zeiss Microscopy Ltd., Jena, Germany) following a previously reported method (Chen, Li, Ding, & Suo, 2012) with some modifications. Briefly, 2 mL of sample solution and 20 µL of Rhodamine B (0.05 g in 100 mL ethanol) were transferred to a test tube and vortexed for 2 min. Afterwards, 200 µL of stained mixture was placed on a micro-plate well (µ-Plate 96 well, ibidi USA, Inc., Wisconsin), and then observed under microscope. The spectra of Rhodamine B-labeled proteins were observed using excitation wavelength of 555 nm and emission wavelength of 630 nm. Images (1024 × 1024 pixels) were acquired using pre-installed image processing software.

Isothermal titration calorimetry (ITC)

The ITC measurement was performed following the method of Bastos, de Carvalho, and Garcia-Rojas (2018) with some modifications. The titration conditions, such as biopolymer concentration and titration volume, were optimized in our preliminary experiments. Solutions of PPI (48.31 μM, 10 mg/mL), HMP (7.58 μM, 0.83 mg/mL) and LMP (10.97 μM, 0.83 mg/mL) were prepared by dispersing the powder samples in citrate–phosphate buffer at designated pH (pH 6, 5.5 and 3.5) and stirring mechanically at 500 rpm overnight (8–12 h) at room temperature to ensure complete hydration. Subsequently, the solutions were filtered through syringe filters (5 μm) to avoid the pump blocking and degassed for 20 min under vacuum (ITC degassing apparatus, TA instruments, New Castle, USA). The solutions of pectin (HMP and LMP), PPI and buffer were placed in reaction cell, syringe, and reference cell, respectively. The PPI solution was injected through 18 successive 2.5 μL injections, with an interval of 200 s and stirring speed of 350 rpm. The volume of first injection was 1 μL and it was not collected into result. The dilution heat arising from blank titration was determined by titrating PPI solution into the buffer and was subtracted from raw data to determine corrected enthalpy changes. Thermograms were recorded and data were analyzed using NanoAnalyze software (TA instruments, New Castle, USA).

Fourier transform infrared spectroscopy (FTIR)

The dried powder of soluble complex was collected by freezing liquid sample in slushy nitrogen (-210 °C), and then lyophilized for 48 h (laboratory scale lyophilizer, SP scientific, Gardiner, New York, USA). The dried powder of complex coacervates was obtained by centrifugation (Eppendorf, New York, USA) at 3,220×*g* for 15 min, and the collected precipitate was lyophilized for 48 h. FTIR spectra of dried soluble complexes, complex coacervates, and controls (PPI, HMP, and LMP powder) were recorded using a FTIR spectrophotometer (Varian,

CA, USA), equipped with an attenuated total reflectance accessory (Pike Miracle, Pike Technologies, Madison, WI, USA), Globar (MIR) source, KBr beam separator, and MCT detector. The samples were scanned in the absorbance mode from 4000 to 400 cm^{-1} by accumulating 32 scans with a resolution of 4 cm^{-1}. The background was collected before each measurement. Samples were measured in triplicate and reported as means.

Statistical analysis

The experimental treatments with three replicates were arranged based on completely randomized design (CRD). All measurements were repeated at least twice using freshly prepared samples and values were expressed as means ± SD. Significant differences between means ($p < 0.05$) were performed using t-test, one-way analysis of variance (ANOVA) and F-protected LSD by SAS software (Version 9.3, SAS Institute Inc., NC, USA).

Results and discussion

Characterization of pectin

The DE and GalA contents of two commercial pectins were measured and presented in **Table 3-1**. The DE (81%) of HMP was over two-fold higher than that of LMP (35%); while the GalA content of HMP (37%) was lower than that of LMP (54%). Similar trend was also found in previous report that 72% DE of HMP contains 28% GalA, and 42% DE of LMP with 58% GalA (Pillai, et al., 2019). The DE and GalA values of two pectin indicate that LMP has significantly higher overall charge density than that of HMP, since less amount of carboxylic acid groups in GalA residues were methyl esterified.

Table 3-1. The degree of esterification (DE) and galacturonic acid (GalA) content of pectin.

Pectin	DE (%)	GalA content (%)
HMP	81.4 ± 1.6[a]	37.6 ± 5.2[a]
LMP	35.2 ± 0.6[b]	53.9 ± 4.1[b]

[†] The values with different superscript letters within a column are significantly different ($p < 0.05$).

Effect of pH, mixing ratio and pectin type on phase behaviors of PPI–pectin mixture

The phase behavior of PPI–pectin mixtures as a function of pH, PPI–pectin mixing ratio, and pectin type were recorded and constructed as a state diagram. In total, 5 distinguishable phase behaviors and appearances were illustrated in state diagram stand quiescent for 24 h (**Fig. 3-1**). The changes of pectin solution as a function of pH was not included in the state diagram due to their translucent appearance across the entire measured pH range.

An example of PPI–HMP mixtures that was prepared at a total biopolymer concentrations (C_{total}) of 1.20 wt% showed a cloudy appearance with undetectable turbidity value in the pH range of 6.5–4.5. This is the major reason that the classic turbidimetric method is inappropriate to identify the boundary pH range of co-solubility, soluble complexes and complex coacervates at a concentrated binary biopolymer system. At neutral pH, PPI–HMP mixtures had significantly different phase behaviors depending on the total biopolymer concentrations. For instance, at C_{total} > 1.50 wt %, phase separations were observed in the mixing ratios of 1:1 and 2:1 at pH 7 (**Fig. 3-1a**) due to the thermal incompatibility (Kontogiorgos, Tosh, & Wood, 2009). In contrast, the mixtures remained translucent in remaining mixing ratios (5:1, 10:1, and 20:1) at the same pH conditions, indicating the co-solubility of PPI and HMP (Liu, Shim, Wang, & Reaney, 2015; Zhang, et al., 2018).

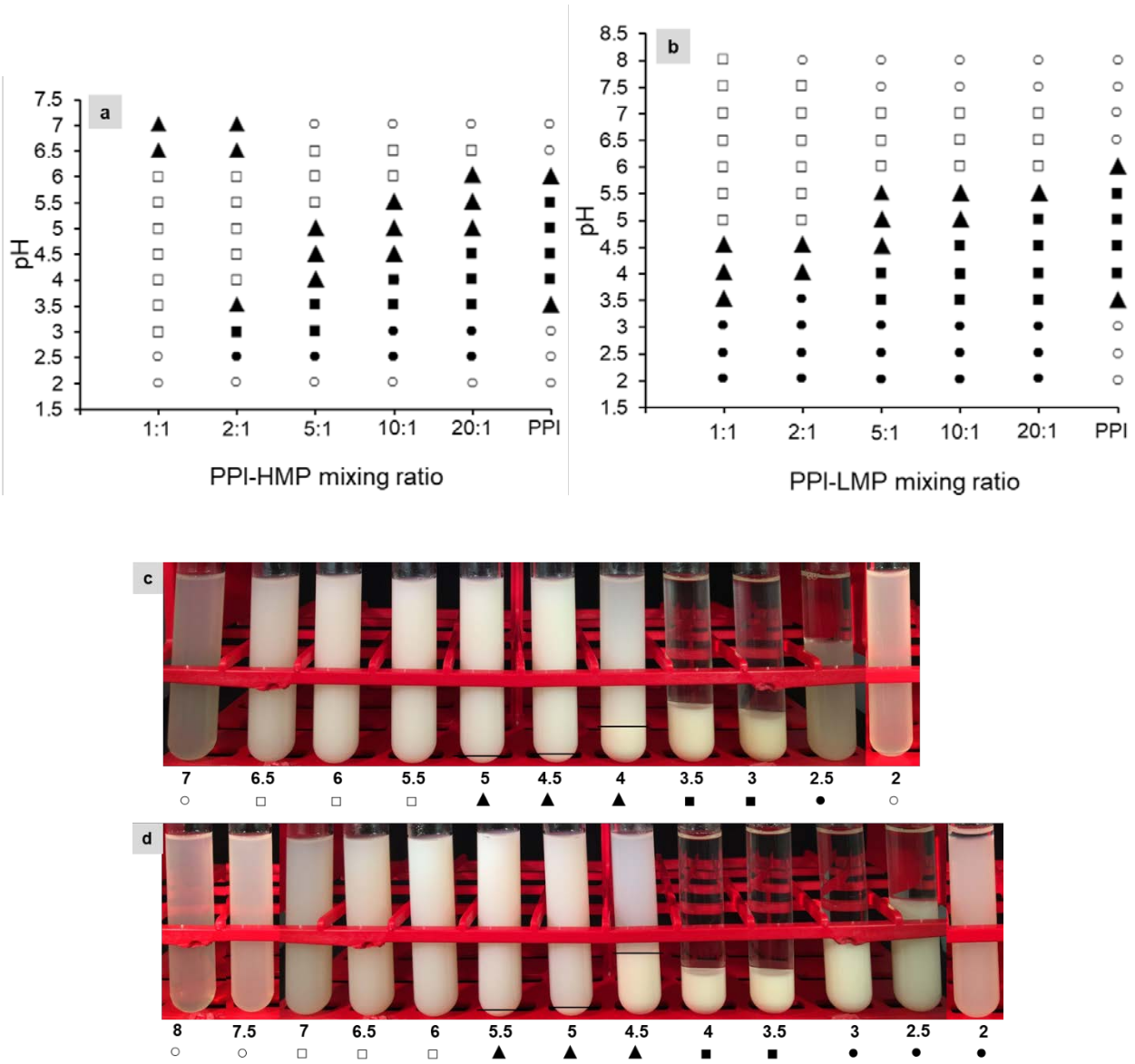

Figure 3-1. State diagram of PPI–pectin mixture as function of pH and mixing ratio (a) HMP; (b) LMP. The appearance of PPI–pectin mixture (ratio 5:1) as function of pH (c) HMP, and (d) LMP. The PPI concentration was fixed at 1 wt%. The appearance was observed after 24 h standing. ○ represents translucent solution; □ represents turbid solution; ▲ represents precipitation & cloudy solution; ■ represents precipitation & clear solution; ● represents precipitation & clear solution that has higher volume of precipitation than ■.

Interestingly, thermal incompatibility phenomena were not observed in PPI–LMP system. Besides, their co-solubility was observed at slightly higher pH conditions (pH 7.5–8) (**Fig. 3-1b**). The thermal incompatibility between proteins and polysaccharides occurs when the soluble complex and/or co-solubility is inhibited by limiting their electrostatic interaction and hydrogen

bonding. Furthermore, thermal incompatibility is sensitive to salt concentrations, temperature, pH, and DE of polysaccharides (Tolstoguzov, 1991). At C_{total} > 1.50 wt %, the observed co-solubility of LMP with PPI is probably due to higher amount of carboxyl group ($–COO^-$) that enhances ionic–dipole moment with aqueous phase. As the pH was adjusted to acidic conditions, the turbid solutions without precipitation (□), representing soluble complexes, were observed within a wide pH range (i.e., 6–3) at PPI and HMP ratio 1:1 or a narrower range (pH 6.5–6) at a ratio of 10:1 (**Fig. 3-1a**) in PPI–HMP solutions. However, turbid solutions without precipitation appeared in pH range of 8–5 at ratio 1:1 and pH 7–6 at 10:1(**Fig. 3-1b**) in PPI–LMP solutions. This suggests the weaker electrostatic interactions between PPI and both pectins under these pH conditions. The further decrease in pH triggered the progressive formation of insoluble complexes with different phase behaviors, as can be seen at pH 5–2.5 in PPI–HMP (**Fig. 3-1c**) or pH 5.5–2 in PPI–LMP at the same ratio of 5:1 of PPI and pectin, respectively **(Fig. 3-1d**).

In addition, aggregation or self-association of pea protein particles also increased steadily as the pH decreased, especially at pH where electroneutrality occurred, such as pH 5 (Lan, et al., 2018). In this work, precipitates with three types of phase behaviors (▲, ■, and ● in **Fig. 3-1**) were all considered as complex coacervates according to a prodigious amount of literature on the definition of complex coacervates (Ach, et al., 2015; Moschakis, et al., 2017). It is generally accepted that the occurrence of complex coacervates starts from protein–polysaccharide interaction ($pH_{\varphi 1}$), and then transits to the end of the plateau ($pH_{\varphi 2}$), generally concomitant to the appearance of spurious precipitates that can be easily identified by classic turbidimetric method at lower biopolymer concentrations (Moschakis, et al., 2017). The pH values at which a phase transits from ▲ to ● in the current study correspond to the $pH_{\varphi 1}$ and $pH_{\varphi 2}$, respectively, at a low biopolymer concentration system. In addition, the phase behavior of precipitation & clear

solution (■) in the state diagram was comparable to that of complex coacervates identified under pH_{opt}. However, the maximum electrostatic interaction pH (pH_{opt}) cannot be determined by state diagram. When environmental pH dropped to the most acidic condition (pH 2), some of complex coacervates in PPI–HMP system completely vanished and became co-soluble again (**Fig. 3-1a**), which could be attributed to the lowest ζ–potential absolute value of HMP at pH 2 (**Fig. 3-3a**).

For mixing ratio, the pHs generally shifted to higher pH values as the PPI–pectin mixing ratio increased from 1:1 to 20:1 (**Fig. 3-1**). For example, the boundary pH ranges for complex coacervates in PPI–HMP system (filled shape in **Fig. 3-1a**) expanded from a small range of pH 3.5–2.5 (at ratio of 2:1) to a large range of pH 6–2.5 (at ratio of 20:1). This suggests that the combination of higher concentration of protein with lower concentration of pectin promotes the formation of complex coacervates. When compared to a low PPI concentration system (i.e. 0.05 wt% of PPI) (Lan, et al., 2018), the pH ranges for soluble complex formation at a concentrated protein condition (i.e. 1.00 wt% of PPI) tended to be narrower, whereas the pH ranges for complex coacervate became broader (**Fig. 3-1**). This indicates that the higher protein concentration was favorable to form complex coacervate rather than soluble complexes.

It is worth noting that the pHs of PPI–pectin system varies depending on both DE and GalA contents of pectin. For better illustration, the effect of DE on pHs in PPI to pectin mixing ratio of 5:1 was presented in **Fig. 3-2**. As DE decreased from 81% (HMP) to 35% (LMP), the critical pH values for the initiation of soluble complexes (pH_c) and complex coacervates ($pH_{\varphi 1}$) increased from pH 6.5 to 7, and 5 to 5.5, respectively. In contrast, the dissolution pH for complex coacervates ($pH_{\varphi 2}$) decreased with DE of pectin decreased. In other words, LMP showed earlier initial electrostatic interaction (higher pH_c and $pH_{\varphi 1}$) and lower dissolution pH for coacervates ($pH_{\varphi 2}$) than that of HMP, indicating LMP contains more charges to stabilize the coacervates over

a wider pH range compared with HMP (Warnakulasuriya, Pillai, Stone, & Nickerson, 2018). Interestingly, the maximum electrostatic interaction pH (pH_{opt}) was independent with DE of pectin at PPI to pectin mixing ratio of 5:1. Similar impact of charge density on complex coacervates have been reported in pea protein–pectin (Warnakulasuriya, et al., 2018) and OVA–carboxymethylcellulose (Xiong, et al., 2017) systems with low total biopolymer concentrations (0.05–0.1 wt%).

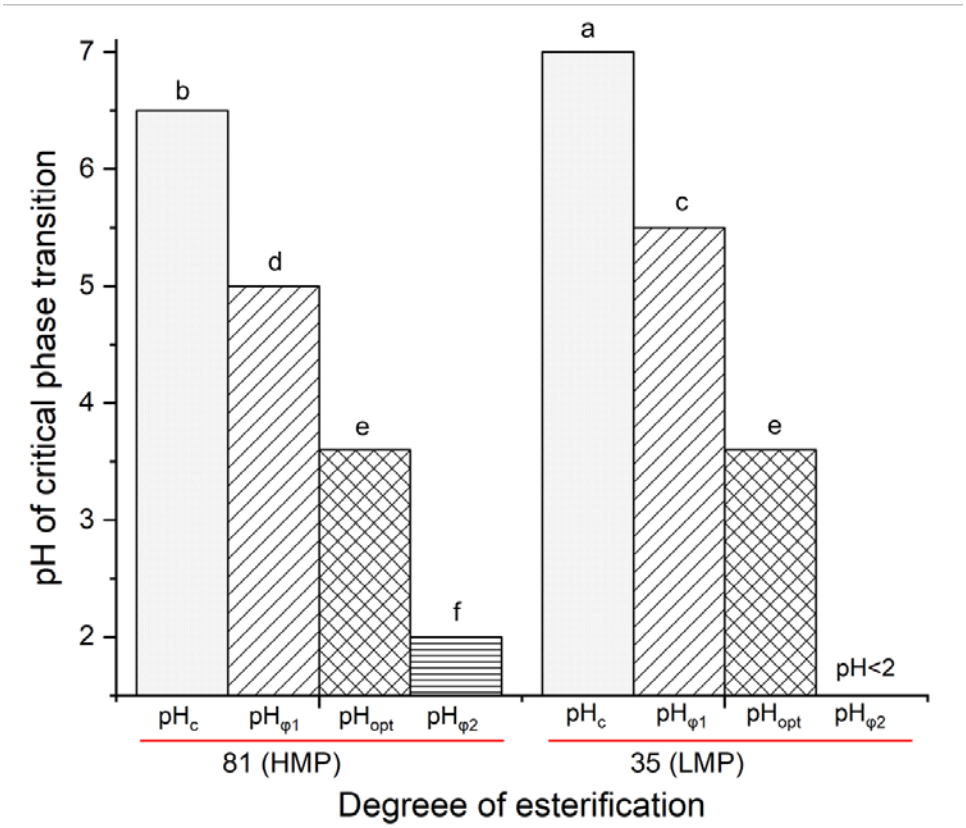

Figure 3-2. The effect of degree of esterification (DE) on pHs values associated with co-solubility, soluble complex and complex coacervate of PPI–pectin mixture. Four pHs (pH_c, $pH_{\varphi1}$, pH_{opt} and $pH_{\varphi2}$) of phase transition were included. The PPI–pectin mixing ratio was fixed at 5:1, and PPI concentration was fixed at 1 wt%. The measurements were repeated three times. The bars with different letters are significantly different ($p< 0.05$).

Additional information about the phase behaviors of PPI–pectin deriving from ζ–potential measurements as functions of pH (8–2) and mixing ratios (1:1–20:1) are shown in **Fig. 3-3**. PPI–pectin mixtures displayed intermediate ζ–potentials between the two individual

biopolymer solution and surface charge of mixtures gradually increased from negative to positive values as the environmental pH decreased from neutral to acidic conditions (**Fig. 3-3a&b**). When pH declined from 8 to 6, ζ–potentials of all studied mixtures had no significant changes and stayed more negative than -20 mV (PPI–HMP) or -25 mV (PPI–LMP). Both ζ–potential and state diagram results indicate that soluble complexes were formed when the net charge was relatively high. Starting from pH 5 (close to the IEP of PPI), ζ–potentials of mixtures increased rapidly and went from highly negative charge to positive charge upon the further decrease of pH.

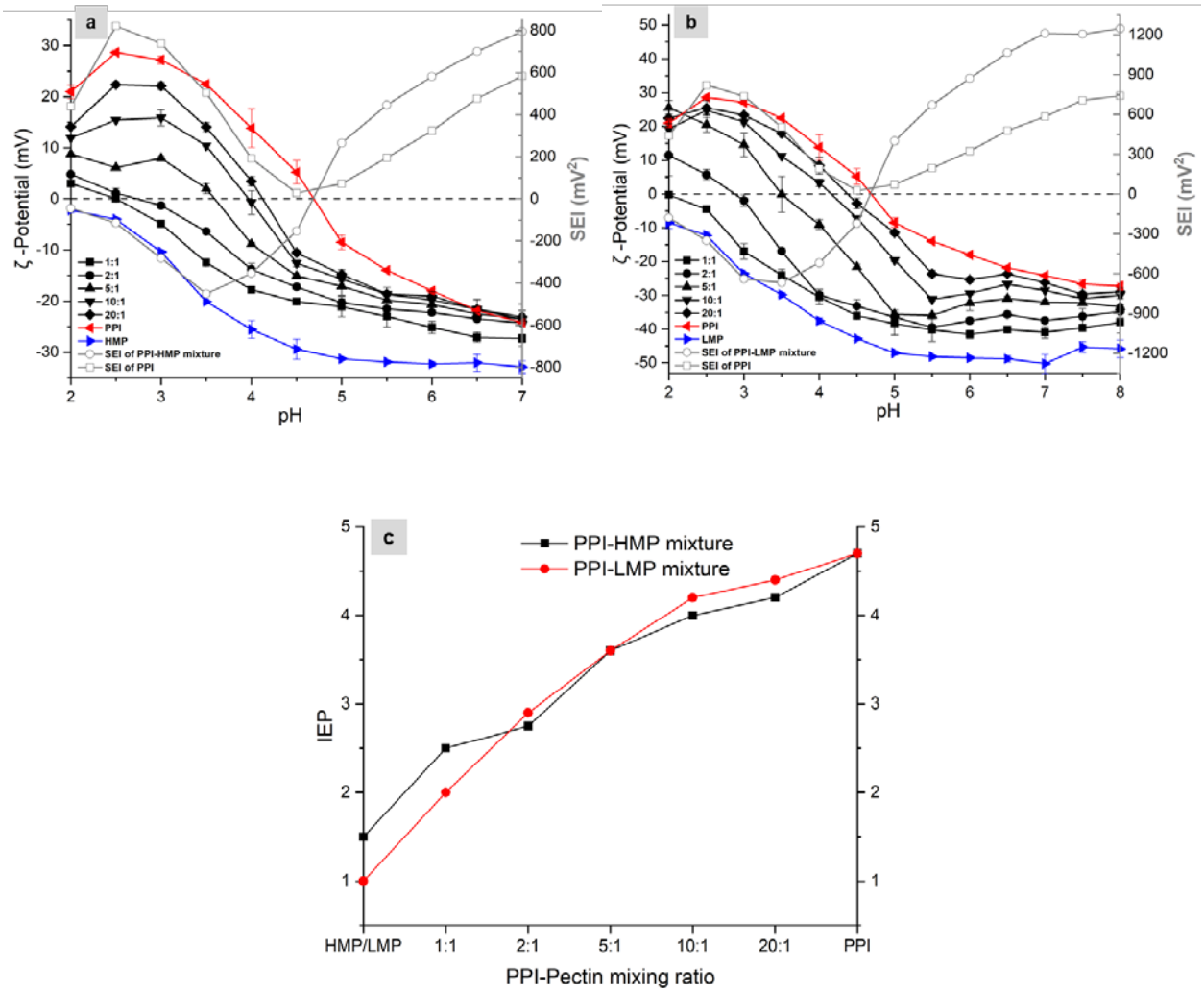

Figure 3-3. Dependence of Zeta (ζ)–potential on pH and biopolymer mixing ratio (a) HMP; (b) LMP. The strength of electrostatic interaction (SEI) of PPI to PPI, PPI to HMP, and PPI to LMP was presented in grey color. (c) Plot of isoelectric point (IEP) as function of PPI–pectin mixing ratio. The PPI concentration was fixed at 1.0 wt%.

In order to elucidate the type of interaction force (attractive *vs.* repulsive) and the magnitude as a function of pH, the strength of electrostatic interaction (SEI) of PPI–pectin at a mixing ratio 5:1 was determined (**Fig. 3-3a&b)**. The SEI of the mixture was calculated as the multiplication of ζ–potential values of individual biopolymer at each pH (Chang, Gupta, Timilsena, & Adhikari, 2016; Espinosa-Andrews, et al., 2013; Timilsena, Wang, Adhikari, & Adhikari, 2016; Yuan, Wan, Yang, & Yin, 2014). Similarly, the SEI of PPI was calculated as square of ζ–potential value of PPI at each pH (**Fig. 3-3a&b**). The positive SEI values correspond to an overall repulsive force while negative values indicate an attractive force between biopolymer molecules. As seen from **Fig. 3-3a&b**, SEI of PPI–pectin mixtures showed that the system was dominated by the overall repulsive forces at pH above IEP of PPI, and by attractive forces below the IEP of PPI. The highest attractive force appeared at pH 3.5 for PPI–HMP and pH 3–3.5 for PPI–LMP. This helps mostly to explain the co-solubility and soluble complexes occurring in a pH range with relatively strong repulsive forces between two biopolymers. It also aids to justify that dense and maximum coacervates were produced at the highest overall attractive forces between two biopolymers (**Fig. 3-3a&b**).

Since the state diagram developed in this study cannot be directly applied to determine pH_{opt} for maximum complex coacervates yield, pH_{opt} can be alternatively determined when the ζ–potential of biopolymer mixtures approach zero (IEP) (Anema & de Kruif, 2014). The influence of biopolymer mixing ratio and pectin type on IEP can be observed by plotting these two factors (**Fig. 3-3c)**. As mixing ratio increased, IEP values shifted towards higher pH values. For instance, IEP switched from ~3.5 at a mixing ratio of 5:1 to ~4.2 (close to IEP of PPI) at 20:1, which coincides with state diagram results (**Fig. 3-2b**). Similar trend was also documented in pea protein–HMP system at low biopolymer concentrations (Pillai, et al., 2019). With regard

to pectin type, its influence on IEP of PPI was dose dependent. The presence of high concentration LMP in binary PPI–pectin system (PPI: LMP = 1:1) shifted IEP of PPI towards the lower pH as compared with HMP. This is due to the greater number of carboxyl group on the LMP chain, allowing for more reactive sites of LMP to form complexation with PPI.

Microstructural insights into phase behaviors of PPI–pectin mixture

In order to better understand the microstructural properties of PPI–pectin under different phase regime, a PPI to pectin mixing ratio of 5:1 was selected to prepare co-solubility, soluble complexes and complex coacervates. Based on the result of state diagram and ζ–potential, PPI–HMP solutions prepared at pH 7, 5.5, and 3.5 while PPI–LMP solutions at pH 8, 6, and 3.5 were the representative of co-solubility, soluble complexes, and complex coacervates, respectively. The microstructures of PPI–pectin at three different pH values were characterized using CLSM (**Fig. 3-4)**. The red color indicating the PPI network was stained by rhodamine B.

Around neutral pH conditions, PPI (**Fig. 3-4a**), PPI–HMP (**Fig. 3-4d**), and PPI–LMP (**Fig. 3-4g**) showed homogeneous distribution of tiny particles without any difference. These images confirm that PPI was co-soluble with pectin with negligible electrostatic interactions, which was consistent with state diagram and ζ–potential results (**Fig. 3-1&2**). As the pH decreased to the regime of soluble complex, homogeneous and relatively larger particles were observed (**Fig. 3-4e&h**), corresponding to turbid appearance in state diagram (**Fig. 3-1c&d**). Similar microstructure was previously reported in soluble complexes of soybean protein–chitosan (Yuan, et al., 2014). As the pH dropped to the regime of complex coacervates (e.g., pH 3.5), dense and large aggregates appeared in both PPI–pectin mixtures (**Fig. 3-4f&i**). This increased size of complexes could be attributed to strong attractive interactions between two oppositely charged biopolymers (evidenced by the highest SEI at pH 3.5 in **Fig. 3-2**) (Yuan, et

al., 2014). Similar CLSM images of complex coacervates were also reported in mixture systems of whey protein–beet pectin (Chen, et al., 2012) and soybean protein–chitosan (Yuan, et al., 2014). The effect of pectin charge density on microstructure of soluble complexes was invisible both in PPI–HMP and PPI–LMP (**Fig. 3-4e&h**) since weak electrostatic interactions were involved. By contrast, the microstructure of PPI–LMP complex coacervates displayed remarkable difference compared with PPI–HMP complex coacervates in the sense that LMP led to the formation of larger aggregates than that of HMP.

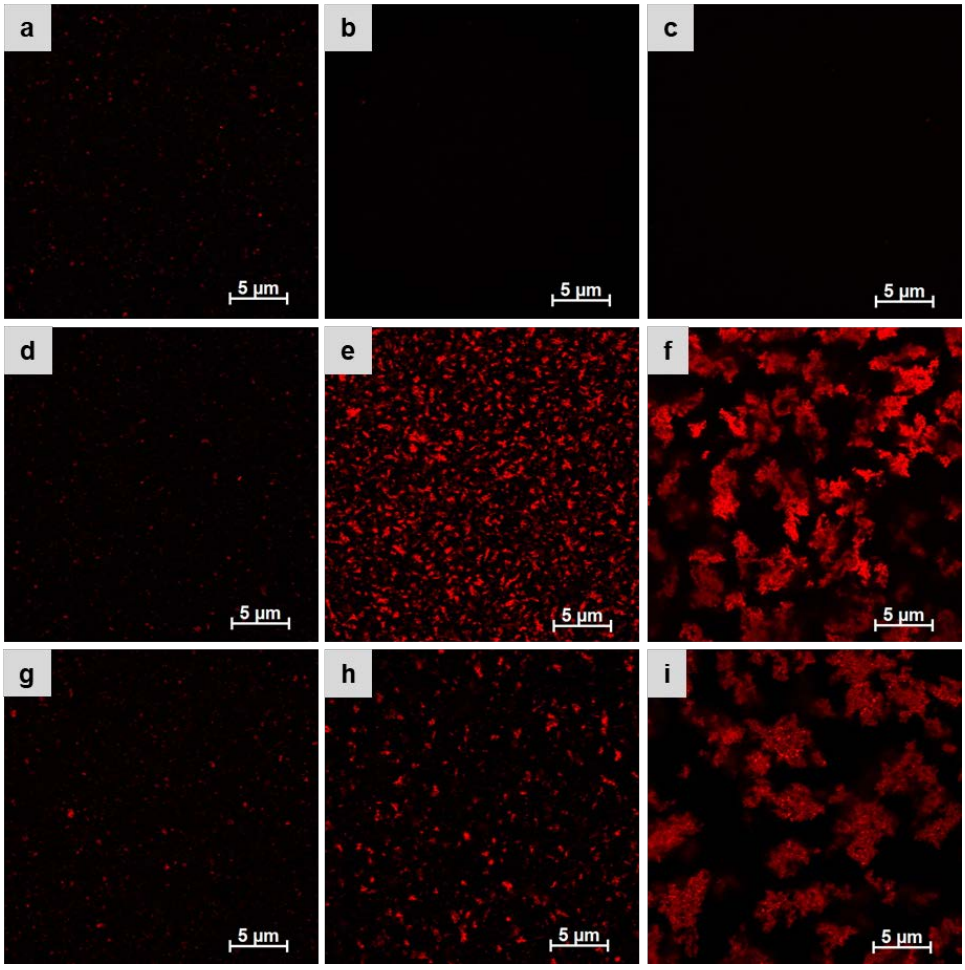

Figure 3-4. Confocal images of PPI (a), HMP (b), and LMP (c) dispersions at pH 7; PPI–HMP mixtures at pH 7 (d), pH 5.5 (e), and pH 3.5 (f); PPI–LMP mixtures at pH 8 (g), pH 6 (h), and pH 3.5 (i). The PPI–pectin mixing ratio was fixed at 5:1, and PPI concentration was fixed at 1 wt%. Red color represents the protein phase in the CLSM image. Bar represents 5 µm.

Thermodynamic insights into phase behaviors of PPI–pectin complexes

Isothermal titration calorimetry (ITC) was applied to reveal molecular recognition by titrating PPI with HMP and LMP at selected pH. In our study, we aimed to reveal molecular recognition by titrating PPI with HMP and LMP at selected pH values to represent the formation of soluble complexes and complex coacervates. The typical thermogram of heat rate *vs.* time profile was presented on the top panel of **Fig. 3-5**. In our study, the binding parameters for soluble complexes were not calculated since an extremely low enthalpy change was registered (**Fig. 3-5a&b**).The binding isotherm for complex coacervation (bottom panel in **Fig. 3-5c&d**) was fitted from thermogram using "one independent binding site model" (Xiong, et al., 2016).

In general, both pH and pectin type exerted significant impact on the intensity of interactions between PPI–pectin. As expected, quite low enthalpy change (ΔH = -10 ~ 10 kJ/mol) was shown in PPI–HMP at pH 5.5 and PPI–LMP at pH 6 (**Fig. 3-5a&b**) due to weak electrostatic interaction between two biopolymers. Similar phenomenon was previously reported in the titration of Persian gum to chickpea protein solution at pH 5 (Mousazadeh, et al., 2018). On the contrary, the exothermic titration profiles and regular peak decrease were presented in PPI–HMP and PPI–LMP mixture at pH 3.5 (**Fig. 3-5c&d**) because of the nonspecific electrostatic interactions between pectin chains and PPI molecules (Hadian, et al., 2016; Li, et al., 2018). These interactions were reduced and reached a binding saturation after mole ratio of PPI–HMP and PPI–LMP approached to 4:1 and 7:1, respectively (**Fig. 3-5c&d**). In general, the binding saturation ratio between PPI and pectin complexation is strongly dependent on pH, as indicated in previous reports (Dong, et al., 2015; Xiong, et al., 2016). This is because the environmental pH will not only impact the solubility of PPI, but also influence the conformational change PPI as well as the net surface charges of both PPI and pectin. Similar

exothermic sequences were also found in interactions of sodium caseinate–LMP (Wang, Dumas, & Gharsallaoui, 2019) and soy proteins–GA (Dong, et al., 2015). It is widely accepted in literatures to determine binding saturation ratios of protein–polysaccharide, protein–polyelectrolytes, and protein–protein systems by using binding isotherm (Li, et al., 2018; Wang, et al., 2019; Xiong, et al., 2016).

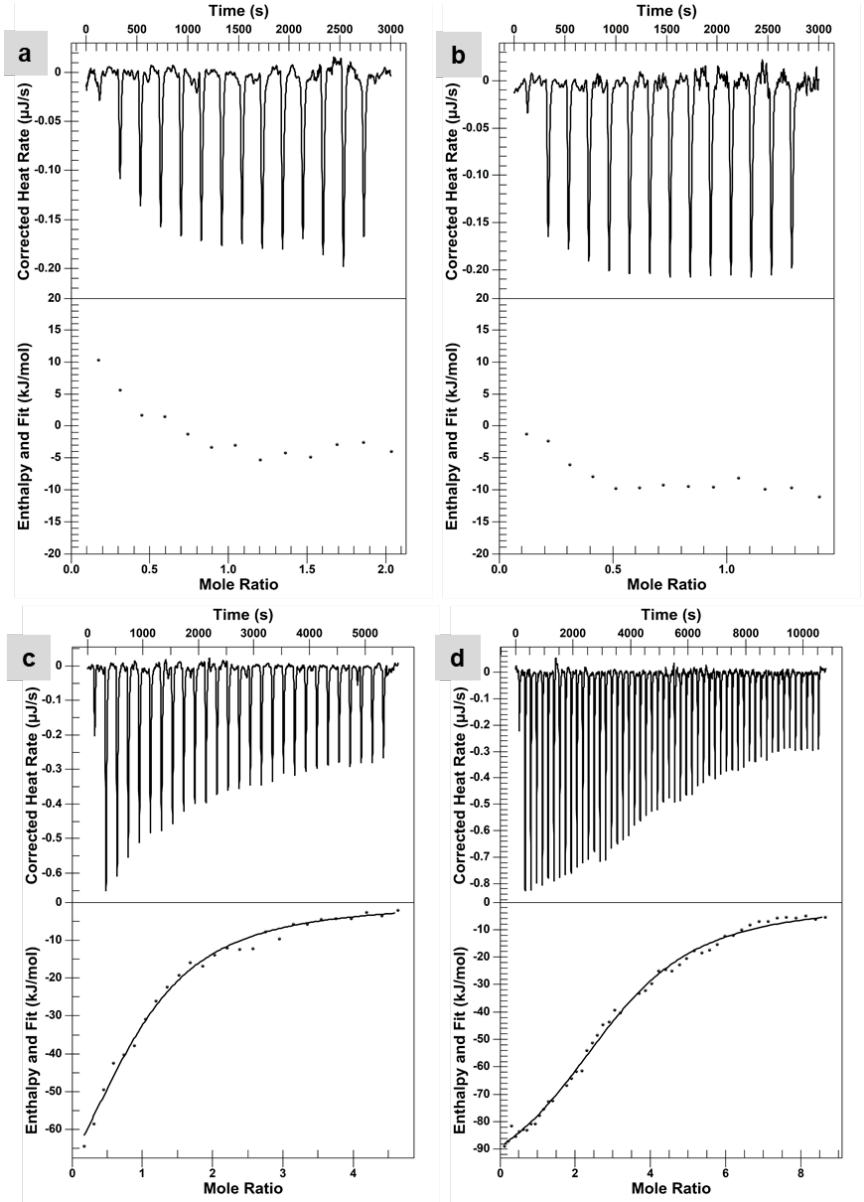

Figure 3-5. Thermogram (top panel) and binding isotherm (bottom panel) corresponding to the titration of PPI dispersion with HMP at pH 5.5 (a), LMP at pH 6 (b), HMP at pH 3.5 (c), and LMP at pH 3.5 (d) at 25 °C. The concentration of PPI, HMP, LMP in citrate–phosphate buffer was 48.31, 7.58 and 10.97 µM, respectively.

The thermodynamic parameters of PPI–pectin at pH 3.5 were calculated on the basis of binding isotherm as follows: binding affinity stoichiometry (*n*), binding affinity constant (K_a), reaction enthalpy (ΔH, kJ/mol), change of entropy ($T\Delta S$), and change of Gibbs free energy (ΔG) (**Table 3-2**). Both interaction of PPI–HMP and PPI–LMP had binding constant with the order of 10^5 M^{-1}, manifesting strong molecular interactions between PPI and pectin. The similar negative values of ΔG (~-30 kJ/mol) indicated a spontaneous nature of the interaction between PPI and pectin. Both ΔH and $T\Delta S$ values were negative without differences, suggesting that the complexation process between the protein and pectin was enthalpically favorable. The molecular forces, including hydrogen bonding, electrostatic interactions, and hydrophobic interactions were involved in interactions (Bastos, et al., 2018; Sperber, Cohen Stuart, Schols, Voragen, & Norde, 2010). The binding affinity stoichiometry (*n*) resulting from PPI–LMP at pH 3.5 was 3.74, specifying that approximate 4 PPI molecules were bound to one LMP molecule. This value was much higher than that of PPI–HMP system (0.99). This again elucidates that LMP had greater negative charged reactive sites than HMP to interact with amine groups of PPI, which was in agreement with pectin characterization results that LMP carries higher overall charge density than HMP.

Table 3-2. Thermodymic parameters of binding between PPI and pectins at 25 °C in citrate–phosphate buffer (pH 3.5).

Pectin	*n*	K_a (M^{-1}) ×10^5	ΔH (kJ/mol)	$T\Delta S$ (kJ/mol)	ΔG (kJ/mol)
HMP	0.99±0.30[a]	4.84±0.04[a]	-100±0[a]	-67.56±0.20[a]	-32.44±0.20[a]
LMP	3.74±0.39[b]	1.97±0.01[a]	-100±0[a]	-69.79±0.18[a]	-30.22±0.18[a]

† The parameters of *n*, K_a, ΔH, $T\Delta S$ and ΔG represent binding stoichiometry, binding affinity constant, reaction enthalpy, change of entropy and Gibbs free energy change, respectively. *T* is the absolute temperature.
‡ The values with different superscript letters within a column are significantly different (p< 0.05).

FTIR characterization of PPI–pectin complexes

FTIR analysis was applied to further examine the influence of pH and pectin type on non-covalent bonding (i.e. electrostatic interactions and hydrogen bonding) between functional groups of PPI and pectin. Again, the PPI to pectin mixing ratio of 5:1 was selected to conduct these experiments.

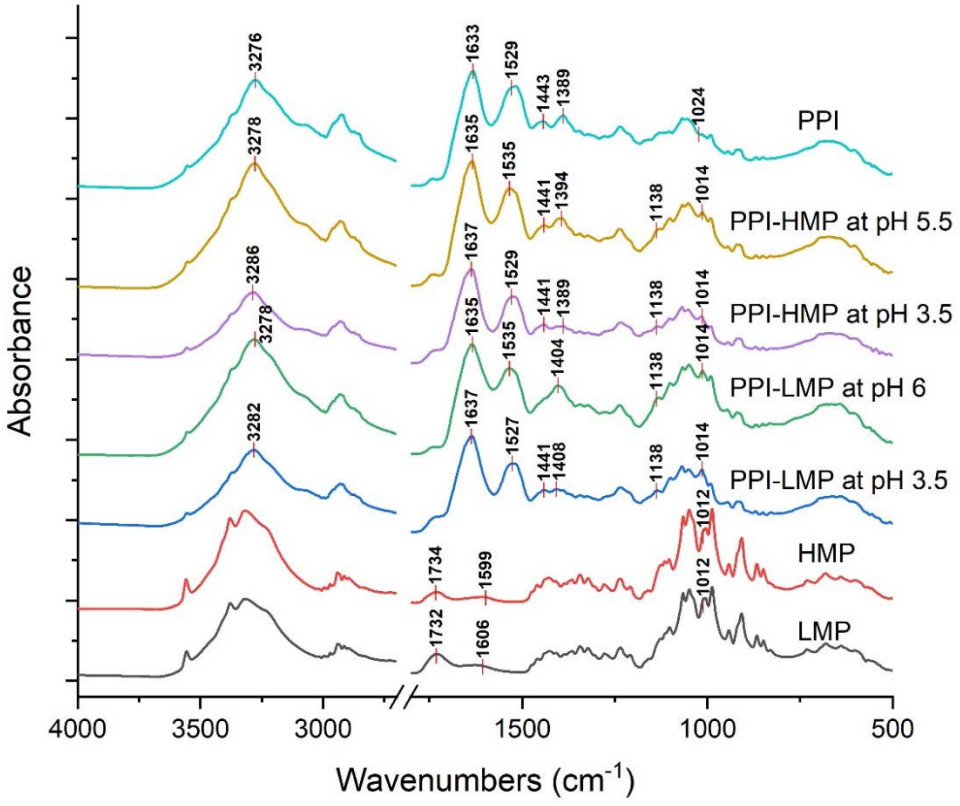

Figure 3-6. FTIR spectra of PPI, HMP, LMP, PPI–HMP and PPI–LMP complexes prepared at selected pH conditions. The PPI–pectin mixing ratio was fixed at 5:1, and PPI concentration was fixed at 1 wt%.

As seen from **Fig. 3-6**, the spectrum of PPI exhibited absorption band of O–H contraction vibration at 3276 cm^{-1}, C=O, N–H and C–N stretching/bending at 1633, 1529, 1389 cm^{-1} (features of amide I, II and III, respectively), which was consistent to a previous report (Lan, Xu, Ohm, Chen, & Rao, 2019). Both HMP and LMP had similar FTIR spectra. For example, bands of C–O–C stretching vibration at 1012 cm^{-1}, and broad and strong O–H stretching at 3600–2800

cm^{-1} due to the inter- and intra-molecular hydrogen bonding of GalA backbone (Albano & Nicoletti, 2018; Singthong, et al., 2004). In addition, the absorption band of carbonyl groups (C=O) from esterified carboxylic acid groups ($COOCH_3$) of GalA and the asymmetric stretching vibration of ionized carboxylic acid groups ($–COO^-$) (non-esterified) were presented at around 1732 and 1599 cm^{-1}, respectively (**Fig. 3-6**) (Singthong, et al., 2004). The absorbance intensity or band area for each of these two functional groups did not show significant differences between HMP and LMP due to overall low absorbance in our study.

Overall, the spectra of PPI–pectin mixtures were dominated by pea protein due to the high PPI to pectin mixing ratio (5:1) and showed some difference from each individual biopolymer (**Fig. 3-6**). For example, all PPI–pectin mixtures presented a new peak (1138 cm^{-1}), a broad band (around 1020–1080 cm^{-1}) in "fingerprint region", which could be a superposition of pea protein and pectin spectra. The significant change of PPI–pectin mixtures spectra could be found in the carbonyl–amide region. For instance, all mixtures exhibited shift in peaks of O–H, amide I, II, and III towards higher wavenumbers in comparison with PPI. These changes indicate that both soluble complexes and complex coacervates formed through the electrostatic interaction between the amino groups of pea protein ($–NH_3^+$) and carboxylic acid groups of the pectin ($–COO^-$) (Souza & Garcia-Rojas, 2017; You, Liu, & Zhao, 2018). Furthermore, these changes also suggest that an increase of hydrogen bonding in the complexes could existed due to the presence of pectin (Li, et al., 2018). Only showed slightly different peak shifts were observed between soluble complexes and complex coacervates (**Fig. 3-6**). Compared to PPI, soluble complexes had smaller peak shifts for amide I (around 2 *vs.* 4 cm^{-1}) and O–H (around 2 *vs.* 10 cm^{-1}). In contrast, larger peak shift in amide II (around 6 *vs.* 10 cm^{-1}) towards higher wavenumbers than that of complex coacervates. The results again support that there were weaker

electrostatic interactions in soluble complexes than that in complex coacervates (Li, et al., 2018). Similarly, pectin type also imposes a slight impact on their intermolecular interactions based on the spectra of PPI–pectin mixtures. In respect to soluble complexes, the difference between HMP and LMP mainly occurred in the amide III region, where two peaks of PPI–HMP (1441 and 1394 cm^{-1}) merged into one broader peak of 1404 cm^{-1} in PPI–LMP. More peak differences (peak around 3286, 1529 and 1389 cm^{-1}) were observed in complex coacervates between PPI–HMP and PPI–LMP. These results indicate that the overall intermolecular interaction may be affected by environmental pH conditions and as well biopolymer type.

Conclusions

The effect of pH (2–8), PPI–pectin mixing ratio (1:1 to 20:1) and pectin type (HMP, LMP) on phase behavior of concentrated PPI–pectin system was studied. This work indicates that the pHs of co-solubility, soluble complex and complex coacervate could be identified using the combination of state diagram and ζ–potential measurement. The pH_{opt}, a pH condition to maximize the formation of complex coacervates, could be recognized at the net charge neutrality of the mixed biopolymer solutions. In general, the pH of soluble complexes, complex coacervates formation shifted towards higher pH as PPI–pectin mixing ratio increased from 1:1 to 20:1. With regard to DE of pectin, LMP showed earlier initial electrostatic interaction (higher pH_c and $pH_{\varphi 1}$) and lower dissolution pH for coacervates ($pH_{\varphi 2}$) than that of HMP, due to higher overall charge density of LMP. Particularly, the CLSM images revealed that larger aggregates were formed in PPI–LMP coacervates than in PPI–HMP coacervates. Both ITC and FTIR analyses indicated that the complexation including soluble complex and complex coacervates were formed through the electrostatic interaction between the nonspecific amine groups of PPI (NH_3^+) and the carboxyl groups of pectin ($–COO^-$) and hydrogen bonding was also involved in

PPI–pectin interaction. The study provides guidelines for understanding phase behaviors and structures in a concentrated biopolymer system and supports our hypothesis that the differences in overall charge density of pectin (LMP and HMP) would influence the formation of PPI–pectin complexes.

References

Ach, D., Briançon, S., Dugas, V., Pelletier, J., Broze, G., & Chevalier, Y. (2015). Influence of main whey protein components on the mechanism of complex coacervation with acacia gum. *Colloids and Surfaces A: Physicochemical and Engineering Aspects, 481*, 367-374.

Adebiyi, A. P., & Aluko, R. E. (2011). Functional properties of protein fractions obtained from commercial yellow field pea (*Pisum sativum* L.) seed protein isolate. *Food Chemistry, 128*(4), 902-908.

Albano, K. M., & Nicoletti, V. R. (2018). Ultrasound impact on whey protein concentrate-pectin complexes and in the O/W emulsions with low oil soybean content stabilization. *Ultrasonics Sonochemistry, 41*, 562-571.

Anema, S. G., & de Kruif, C. G. (2014). Complex coacervates of lactotransferrin and beta-lactoglobulin. *Journal of Colloid and Interface Science, 430*, 214-220.

Aryee, F. N. A., & Nickerson, M. T. (2012). Formation of electrostatic complexes involving mixtures of lentil protein isolates and gum arabic polysaccharides. *Food Research International, 48*(2), 520-527.

Bastos, L. P. H., de Carvalho, C. W. P., & Garcia-Rojas, E. E. (2018). Formation and characterization of the complex coacervates obtained between lactoferrin and sodium alginate. *International Journal of Biological Macromolecules, 120*, 332-338.

Chang, P. G., Gupta, R., Timilsena, Y. P., & Adhikari, B. (2016). Optimisation of the complex coacervation between canola protein isolate and chitosan. *Journal of Food Engineering, 191*, 58-66.

Chen, B. C., Li, H. J., Ding, Y. P., & Suo, H. Y. (2012). Formation and microstructural characterization of whey protein isolate/beet pectin coacervations by laccase catalyzed cross-linking. *Lwt-Food Science and Technology, 47*(1), 31-38.

Comert, F., Malanowski, A. J., Azarikia, F., & Dubin, P. L. (2016). Coacervation and precipitation in polysaccharide-protein systems. *Soft Matter, 12*(18), 4154-4161.

Ding, L., Huang, Y., Cai, X., & Wang, S. (2019). Impact of pH, ionic strength and chitosan charge density on chitosan/casein complexation and phase behavior. *Carbohydrate Polymers, 208*, 133-141.

Dong, D., Li, X. F., Hua, Y. F., Chen, Y. M., Kong, X. Z., Zhang, C. M., & Wang, Q. (2015). Mutual titration of soy proteins and gum arabic and the complexing behavior studied by isothermal titration calorimetry, turbidity and ternary phase boundaries. *Food Hydrocolloids, 46*, 28-36.

Eghbal, N., Yarmand, M. S., Mousavi, M., Degraeve, P., Oulahal, N., & Gharsallaoui, A. (2016). Complex coacervation for the development of composite edible films based on LM pectin and sodium caseinate. *Carbohydrate Polymers, 151*, 947-956.

Espinosa-Andrews, H., Enríquez-Ramírez, K. E., García-Márquez, E., Ramírez-Santiago, C., Lobato-Calleros, C., & Vernon-Carter, J. (2013). Interrelationship between the zeta potential and viscoelastic properties in coacervates complexes. *Carbohydrate Polymers, 95*(1), 161-166.

Hadian, M., Hosseini, S. M. H., Farahnaky, A., Mesbahi, G. R., Yousefi, G. H., & Saboury, A. A. (2016). Isothermal titration calorimetric and spectroscopic studies of β-lactoglobulin-water-soluble fraction of *Persian* gum interaction in aqueous solution. *Food Hydrocolloids, 55*, 108-118.

Hasanvand, E., & Rafe, A. (2018). Rheological and structural properties of rice bran protein-flaxseed (*Linum usitatissimum* L.) gum complex coacervates. *Food Hydrocolloids, 83*, 296-307.

Havemeier, S., Erickson, J., & Slavin, J. (2017). Dietary guidance for pulses: the challenge and opportunity to be part of both the vegetable and protein food groups. *Annals of the New York Academy of Sciences, 1392*(1), 58-66.

Huang, G. Q., Du, Y. L., Xiao, J. X., & Wang, G. Y. (2017). Effect of coacervation conditions on the viscoelastic properties of N,O-carboxymethyl chitosan - gum arabic coacervates. *Food Chemistry, 228*, 236-242.

Klemmer, K. J., Waldner, L., Stone, A., Low, N. H., & Nickerson, M. T. (2012). Complex coacervation of pea protein isolate and alginate polysaccharides. *Food Chemistry, 130*(3), 710-715.

Kontogiorgos, V., Tosh, S. M., & Wood, P. J. (2009). Phase behaviour of high molecular weight oat β-glucan/whey protein isolate binary mixtures. *Food Hydrocolloids, 23*(3), 949-956.

Lam, A. C. Y., Can Karaca, A., Tyler, R. T., & Nickerson, M. T. (2018). Pea protein isolates: Structure, extraction, and functionality. *Food Reviews International, 34*(2), 126-147.

Lan, Y., Chen, B., & Rao, J. (2018). Pea protein isolate–high methoxyl pectin soluble complexes for improving pea protein functionality: Effect of pH, biopolymer ratio and concentrations. *Food Hydrocolloids, 80*, 245-253.

Lan, Y., Xu, M., Ohm, J.-B., Chen, B., & Rao, J. (2019). Solid dispersion-based spray-drying improves solubility and mitigates beany flavour of pea protein isolate. *Food Chemistry, 278*, 665-673.

Li, Y., Zhang, X., Zhao, Y., Ding, J., & Lin, S. (2018). Investigation on complex coacervation between fish skin gelatin from cold-water fish and gum arabic: Phase behavior, thermodynamic, and structural properties. *Food Research International, 107*, 596-604.

Liu, J., Shim, Y. Y., Wang, Y., & Reaney, M. J. T. (2015). Intermolecular interaction and complex coacervation between bovine serum albumin and gum from whole flaxseed *(Linum usitatissimum L.*). *Food Hydrocolloids, 49*, 95-103.

Liu, S. H., Cao, Y. L., Ghosh, S., Rousseau, D., Low, N. H., & Nickerson, M. T. (2010). Intermolecular interactions during complex coacervation of pea protein isolate and gum arabic. *Journal of Agricultural and Food Chemistry, 58*(1), 552-556.

Moschakis, T., & Biliaderis, C. G. (2017). Biopolymer-based coacervates: Structures, functionality and applications in food products. *Current Opinion in Colloid & Interface Science, 28*, 96-109.

Mousazadeh, M., Mousavi, M., Askari, G., Kiani, H., Adt, I., & Gharsallaoui, A. (2018). Thermodynamic and physiochemical insights into chickpea protein-*Persian* gum interactions and environmental effects. *International Journal of Biological Macromolecules, 119*, 1052-1058.

Pillai, P. K. S., Stone, A. K., Guo, Q., Guo, Q., Wang, Q., & Nickerson, M. T. (2019). Effect of alkaline de-esterified pectin on the complex coacervation with pea protein isolate under different mixing conditions. *Food Chemistry, 284*, 227-235.

Rocha, C. M. R., Souza, H. K. S., Magalhaes, N. F., Andrade, C. T., & Goncalves, M. P. (2014). Rheological and structural characterization of agar/whey proteins insoluble complexes. *Carbohydrate Polymers, 110*, 345-353.

Ru, Q. M., Wang, Y. W., Lee, J., Ding, Y. T., & Huang, Q. R. (2012). Turbidity and rheological properties of bovine serum albumin/pectin coacervates: Effect of salt concentration and initial protein/polysaccharide ratio. *Carbohydrate Polymers, 88*(3), 838-846.

Schmitt, C., Sanchez, C., Desobry-Banon, S., & Hardy, J. (1998). Structure and technofunctional properties of protein-polysaccharide complexes: A review. *Critical Reviews in Food Science and Nutrition, 38*(8), 689-753.

Singthong, J., Cui, S. W., Ningsanond, S., & Goff, H. D. (2004). Structural characterization, degree of esterification and some gelling properties of Krueo Ma Noy (*Cissampelos pareira*) pectin. *Carbohydrate Polymers, 58*(4), 391-400.

Souza, C. J. F., & Garcia-Rojas, E. E. (2017). Interpolymeric complexing between egg white proteins and xanthan gum: Effect of salt and protein/polysaccharide ratio. *Food Hydrocolloids, 66*, 268-275.

Sperber, B. L., Cohen Stuart, M. A., Schols, H. A., Voragen, A. G., & Norde, W. (2010). Overall charge and local charge density of pectin determines the enthalpic and entropic contributions to complexation with β-lactoglobulin. *Biomacromolecules, 11*(12), 3578-3583.

Stenger, C., Zeeb, B., Hinrichs, J., & Weiss, J. (2017). Formation of concentrated biopolymer particles composed of oppositely charged WPI and pectin for food applications. *Journal of Dispersion Science and Technology, 38*(9), 1258-1265.

Timilsena, Y. P., Wang, B., Adhikari, R., & Adhikari, B. (2016). Preparation and characterization of chia seed protein isolate-chia seed gum complex coacervates. *Food Hydrocolloids, 52*, 554-563.

Tolstoguzov, V. B. (1991). Functional properties of food proteins and role of protein-polysaccharide interaction. *Food Hydrocolloids, 4*(6), 429-468.

Wagoner, T., Vardhanabhuti, B., & Foegeding, E. A. (2016). Designing whey protein-polysaccharide particles for colloidal stability. In M. P. Doyle & T. R. Klaenhammer (Eds.), *Annual Review of Food Science and Technology* (Vol. 7, pp. 93-116). Palo Alto: Annual Reviews.

Wang, J., Dumas, E., & Gharsallaoui, A. (2019). Low methoxyl pectin / sodium caseinate complexing behavior studied by isothermal titration calorimetry. *Food Hydrocolloids, 88*, 163-169.

Warnakulasuriya, S., Pillai, P. K. S., Stone, A. K., & Nickerson, M. T. (2018). Effect of the degree of esterification and blockiness on the complex coacervation of pea protein isolate and commercial pectic polysaccharides. *Food Chemistry, 264*, 180-188.

Wijaya, W., Patel, A. R., Setiowati, A. D., & Van der Meeren, P. (2017). Functional colloids from proteins and polysaccharides for food applications. *Trends in Food Science & Technology, 68*, 56-69.

Xiong, W. F., Ren, C., Jin, W. P., Tian, J., Wang, Y. T., Shah, B. R., Li, J., & Li, B. (2016). Ovalbumin-chitosan complex coacervation: Phase behavior, thermodynamic and rheological properties. *Food Hydrocolloids, 61*, 895-902.

Xiong, W. F., Ren, C., Tian, M., Yang, X. J., Li, J., & Li, B. (2017). Complex coacervation of ovalbumin-carboxymethylcellulose assessed by isothermal titration calorimeter and

rheology: Effect of ionic strength and charge density of polysaccharide. *Food Hydrocolloids, 73*, 41-50.

Xu, A. Y., Melton, L. D., Ryan, T. M., Mata, J. P., Rekas, A., Williams, M. A. K., & McGillivray, D. J. (2018). Effects of polysaccharide charge pattern on the microstructures of beta-lactoglobulin-pectin complex coacervates, studied by SAXS and SANS. *Food Hydrocolloids, 77*, 952-963.

Yoo, S.-H., Fishman, M. L., Hotchkiss, A. T., & Lee, H. G. (2006). Viscometric behavior of high-methoxy and low-methoxy pectin solutions. *Food Hydrocolloids, 20*(1), 62-67.

You, G., Liu, X. L., & Zhao, M. M. (2018). Preparation and characterization of *hsian-tsao* gum and chitosan complex coacervates. *Food Hydrocolloids, 74*, 255-266.

Yuan, Y., Wan, Z.-L., Yang, X.-Q., & Yin, S.-W. (2014). Associative interactions between chitosan and soy protein fractions: Effects of pH, mixing ratio, heat treatment and ionic strength. *Food Research International, 55*, 207-214.

Zha, F., Dong, S., Rao, J., & Chen, B. (2019). Pea protein isolate-gum arabic Maillard conjugates improves physical and oxidative stability of oil-in-water emulsions. *Food Chemistry, 285*, 130-138.

Zhang, T., Xu, X., Li, Z., Wang, Y., Xue, Y., & Xue, C. (2018). Interactions and phase behaviors in mixed solutions of kappa-carrageenan and myofibrillar protein extracted from *Alaska Pollock* surimi. *Food Research International, 105*, 821-827.

CHAPTER 4. PHASE BEHAVIOR AND COMPLEX COACERVATION OF CONCENTRATED PEA PROTEIN ISOLATE–BEET PECTIN SOLUTION

Abstract

The objective of this study was to develop an alternative method named state diagram to identify boundary formation pH for complex coacervates obtained from concentrated solutions (2 wt%) of pea protein isolate (PPI) and sugar beet pectin (SBP). The effects of pH (7–2) and PPI–SBP mixing ratios (1:1–20:1) on coacervates formation were investigated by state diagram, zeta–potential, rheological, and phase composition analysis. Isothermal titration calorimetry, scanning electron microscopy, and Fourier transform infrared spectroscopy were employed to elucidate thermodynamic behaviors, non-covalent bonding of coacervates, and microstructure of coacervates. We demonstrate that state diagram can explicitly identify the three critical phase transition pH values (pHs) ($pH_{\varphi 1}$, pH_{opt}, and $pH_{\varphi 2}$) at which recognizable transitions take place in concentrated colloids solutions. The mixing ratio dependent of $pH_{\varphi 1}$ increased to pH 5.5 as PPI–SBP mixing ratio increased to 20:1. The pH_{opt} was recognized at the net charge neutrality or the highest storage modulus of the mixed colloids solutions.

Introduction

Complex coacervation is a phase separation of a macromolecular solution and composed of two oppositely charged biopolymers (e.g., protein–polysaccharide, polyelectrolyte–protein, protein–protein) based on the physicochemical mechanism of associative separation (Adal, et al., 2017; Gomez-Mascaraque, Llavata-Cabrero, Martinez-Sanz, Fabra, & Lopez-Rubio, 2018). In terms of the protein–polysaccharide system, complex coacervation primarily occurs as a result of attractive electrostatic interactions of charged groups between globular proteins and polysaccharides (Wagoner, Vardhanabhuti, & Foegeding, 2016). The strength of such interactions

is typically predominantly determined by the parameters relating to the modulation of electrostatic interactions, including environmental pH, biopolymer ratio, total biopolymer concentration, ionic strength, temperature, and polysaccharides chemical/molecular compositions (e.g., molecular weight, chain branching, charge density and distribution, etc.) (Kayitmazer, Koksal, & Iyilik, 2015; Kizilay, et al., 2014; Priftis & Tirrell, 2012; Samanta & Ganesan, 2018). Protein–polysaccharide complex coacervates have great potential applications in the food and pharmaceutical industry, such as encapsulation of bioactive compounds (Gomez-Mascaraque, et al., 2018), fat replacers (Krzeminski, Prell, Busch-Stockfisch, Weiss, & Hinrichs, 2014), films fabrication (Silva, Fonseca, Amado, & Mauro, 2018), stabilization of emulsions (Rodriguez, Binks, & Sekine, 2018), and protein purification (Li, Hua, Chen, Kong, & Zhang, 2016)

Many studies have investigated the phase behavior and the possible mechanism of complex coacervates formation in protein–polysaccharide system at low biopolymer concentrations (typically below 0.3 wt%) (Aryee & Nickerson, 2012; Liu, Shim, Shen, Wang, & Reaney, 2017; Liu, et al., 2010). At a lower biopolymer concentration, the turbidimetric analysis has long been applied to identify boundary pH range for phase behaviors/transitions based on the optical properties of biopolymer mixtures at the mesoscale regime (Wagoner, et al., 2016). When adjusting the pH of a mixed biopolymer solution from neutral to acidic pH, four different pH regions can be divided with regarding to their interactions by using three critical phase transition pH values (pHs) (pH_c, $pH_{\varphi1}$, $pH_{\varphi2}$), corresponding to four different phase behaviors of biopolymer mixtures ($pH > pH_c$, co-soluble; $pH_c \sim pH_{\varphi1}$, soluble complexes; $pH_{\varphi1} \sim pH_{\varphi2}$, complex coacervates; $pH < pH_{\varphi2}$, dissolution of complexes) (Li, Zhang, Zhao, Ding, & Lin, 2018). Between $pH_{\varphi1}$ and $pH_{\varphi2}$, a highest turbidity of biopolymer mixture is observed, which is

defined as the pH (pH_{opt}), corresponding to the maximum amount of coacervates yield is produced at pH_{opt}.

Recently, zeta–potential values have been proposed as an alternative means to determine the phase transition conditions for the formation of complex coacervation at lower biopolymer concentrations. It should be noted that the application of protein–polysaccharide complex coacervates generally requires higher biopolymer concentration in the area of encapsulation, fat-mimetics, and texture modifiers (Klemmer, Waldner, Stone, Low, & Nickerson, 2012; Stenger, Zeeb, Hinrichs, & Weiss, 2017). According to literature reports, researchers have identified the critical formation pH_{opt} using abovementioned turbidimetric method at lower biopolymer concentration. This critical pH_{opt} was then directly applied to prepare complex coacervates with higher biopolymer concentrations under the assumption that pH_{opt} is independent of biopolymer concentration (Stone, Teymurova, Chang, Cheung, & Nickerson, 2015). Our recent study has shown that the phase transition pHs were shifted on account of varying biopolymer concentrations (Lan, Chen, & Rao, 2018). Meanwhile the turbidimetric method is not applicable to identify pHs for high concentration of binary protein/polysaccharide system, since the initial turbidity of system is so high. As such, an alternative technique should be developed to properly identify critical $pH_{\varphi 1}$ and/or pH_{opt} in higher concentration biopolymer systems at which the maximum complexes coacervates are formed (Hosseini, et al., 2013; Ye, Flanagan, & Singh, 2006).

Recently, there is growing interest in the utilization of plant proteins, particularly yellow PPI in food application due to health benefits, cheaper price, allergen and gluten-free claim that can be made. The major two fractions of PPI are globulin and albumin, accounting for nearly 70–80% and 10–20% of the total pea protein, respectively (Zha, Dong, Rao, & Chen, 2019). The

most important globulins are legumin (11S, S = Svedberg Unit), vicilin (7S) and convicilin (7–8S) (Lam, Can Karaca, Tyler, & Nickerson, 2018). To the best of our knowledge, there is no study on fabricating complex coacervation between PPI and other polysaccharides in concentrated biopolymer systems. It is a challenge and of most importance to be able to precisely identify the pH range for formation of complex coacervates in order to understand their phase transition, structural aspects, and functional properties in concentrated biopolymer systems.

In this study, we assembled coacervates-based biopolymer particles using in-house prepared PPI and anionic polysaccharide SBP. The main purpose of this study was to investigate factors (i.e. pH and biopolymer mixing ratios) that influence the phase behavior of PPI–SBP complex coacervates at concentrated solution (2.0 wt%), and to evaluate the structural properties of these coacervates. We also aimed to develop an alternative method, state diagram, to identify boundary formation pH for complex coacervates under high biopolymer concentration. In addition, isothermal titration calorimetry (ITC), Fourier transform infrared spectroscopy (FTIR), and scanning electron microscopy (SEM) were employed to gain structural insights of how subtle pH differences could potentially impact the formation and properties of PPI–SBP complexes coacervates.

Materials and methods

Materials

Yellow pea flour was manufactured from organic yellow pea seeds and was purchased from Harvest Innovations (Indianola, Iowa, USA). Freeze dried PPI was extracted from yellow pea flour using alkali extraction-isoelectric precipitated method, as stated in our previous report without any modifications (Lan, et al., 2018). The triplicated proximate analyses on final PPI powder were carried out according to AOAC methods (2016): 79.50% protein (%N × 6.25, wet

basis), 5.28% moisture, 0.77 % lipid, 4.61% crude ash, and 9.84% carbohydrate (by difference from 100%). Sugar beet pectin (SBP) (Betapec RU301, Lot # 11710767, 45 kDa of Mw, 55% of degree of esterification (DE), 65% of galacturonic acid, as reported by the manufacturer) was kindly donated by Herbstreith & Fox KG (Neuenbürg, Germany) and used without further purification. Analytical grade of sodium hydroxide (NaOH), hydrochloric acid (HCl), and other chemicals and reagents were procured from VWR (Chicago, Illinois, USA). All solutions were prepared using ultrapure water and the concentrations were as weight percentage (wt%) (18.2MΩ·cm, Barnstead GenPure Pro water purification system, Thermo Fisher Scientific Inc., USA).

Fabrication of complex coacervates

Preparation of PPI and SBP stock solutions

PPI stock solution (2.00 wt%) was prepared by dissolving powdered PPI in water and magnetically stirred at 1000 rpm for 0.5 h at 25 °C. Subsequently, the pH of solutions was increased to pH 9.5 with 0.1–2 M NaOH and stirred for 2 h to promote hydration, followed by adjusting pH back to pH 7 using 0.1–2 M HCl and stirred for another 12 h to ensure complete dissolution. SBP stock solution (2.00 wt%) was initially prepared by dispersing SBP in water and stirring mechanically at 500 rpm for 12 h at 25 °C. The SBP solution was then adjusted to pH 7 using 0.1–2 M NaOH. Finally, both stock solutions were centrifuged at 5520×*g* for 15 min (Beckman J2-HS, Beckman Coulter Inc., Indianapolis, IN, USA), and suction filtered through a Whatman #1 filter paper to remove any insoluble matters. Sodium azide (0.02 wt%) was added to both stock solutions to prevent microbial growth.

Preparation of PPI–SBP mixture

Fixed PPI solution (1.00 wt%) was mixed with SBP solution with concentration varying from 0.05 to 1.00 wt% to achieve the initial PPI–SBP ratio ranging from 1:1 to 20:1. The pH values of mixture were then adjusted from 7 to 2 with 0.5 decrement by the addition of HCl with various concentrations (0.1, 0.3, 0.6, 0.9, 2.0 M). The utilization of HCl at various concentrations was to minimize dilution effects as well as conductivity change in mixture solution, as stated by Liu et al (Liu, Low, & Nickerson, 2009). The single PPI and SBP solutions were used as controls. The aqueous mixtures and controls were left to stand static for 24 h at 4 °C to allow phase equilibrium.

Construction of state diagram

After standing static for 24 h at 4 °C, the state diagram of PPI–SBP mixtures was constructed based on visual observation according to the method described in our recent work (Lan, et al., 2018). Five different symbols were applied to distinguish different phase behaviors of the observed phase separations in the test tubes, namely, ○, □, ▲, ■, ● to represent translucent solution, turbid solution, precipitation & cloudy solution, precipitation & clear solution, and precipitation & clear solution with higher volume of precipitation than ■, respectively.

Surface charge analysis

Surface charges of single biopolymer solutions (PPI or SBP, 1.00 wt%) and PPI–SBP mixtures were measured using a Zetasizer Nano–ZS 90 (Malvern Instruments, Worcestershire, UK), and reported as zeta–potential (ζ, mV).

Viscoelastic properties of complex coacervates

PPI–SBP coacervates were firstly centrifuged at 3220×g for 15 min, and the dynamic viscoelastic properties of precipitates collected after centrifugation were evaluated using a Discovery Hybrid Rheometer-2 rheometer (TA Instruments Ltd., New Castle, DE, USA) described by Liu et al (Liu, et al., 2017) with some modifications. Briefly, coacervates obtained at different mixing ratios (1:1 to 20:1) and pH conditions (pH 4.5–2.5) were placed on the bottom plate and a solvent trap cover was applied to prevent evaporation during the measurement. All rheological tests were carried out at 25 °C (regulated by a circulating water bath of Peltier system), using a cone plate geometry (2°, 40 mm diameter) and a fixed gap (57 μm) between two plates. Samples were equilibrated for 2 min before each measurement.

Two types of oscillatory analyses, strain sweep and frequency sweep, were conducted to determine viscoelastic behavior of coacervates. Strain sweep was firstly performed to determine the linear viscoelastic region (LVR), where dynamic G′ and G″ are independent of strain amplitude. Each strain sweep test was performed at a constant frequency of 1 Hz and the strain varying from 0.01 to 100%. Based on LVR, constant strain amplitude of 0.1% was applied for subsequent frequency sweep measurements over an angular frequency range of 0.1–100 rad/s. Data analysis was performed with TA TRIOS software (TA Instruments Ltd., New Castle, DE, USA).

Quantification of PPI in coacervate phase

All samples were centrifuged (Eppendorf, New York, USA) at 3220×g for 15 min, and the supernatant was recovered to analyze the protein content in accordance to the methods described by Rocha et al. (Rocha, Souza, Magalhaes, Andrade, & Goncalves, 2014) and Warnakulasuriya et al. (Warnakulasuriya, Pillai, Stone, & Nickerson, 2018) with some

modifications. Briefly, the percentage of PPI in the supernatant was calculated as: (PPI concentration of supernatant / PPI concentration of non-centrifuged solution) × 100%. The PPI concentration was measured using the Bradford dye-binding method as described in our previous report (Lan, et al., 2018). The PPI in the coacervate phase was calculated as 100% – percentage of PPI in the supernatant.

Isothermal titration calorimetry (ITC)

The ITC measurement was performed following the method reported by Bastos et al. (Bastos, de Carvalho, & Garcia-Rojas, 2018) with some modifications. Briefly, the thermodynamic parameters of PPI–SBP interaction at pH 3.5 were investigated using Nano ITC (TA instruments, New Castle, USA) at 25 °C. The titration conditions, including biopolymer concentration and titration volume, were optimized based on our preliminary experimental results. Solutions of PPI (48.31 μM, 10 mg/mL) and SBP (7.41 μM, 0.33 mg/mL) were prepared by dispersing each of them in citrate–phosphate buffer solution (pH 3.5) and mechanical stirring at 500 rpm for 12 h at 25 °C to ensure complete hydration. Prior to use, the solution was filtered through a 0.45 μm syringe filter to avoid the pump blocking and degassed for 20 min under vacuum using an ITC degassing apparatus (TA instruments, New Castle, USA). The pH 3.5 buffer was used to eliminate a pH mismatch between a titrant (a syringe solution) and a titrand (a cell solution), which composed of 7 mM citric acid and 5 mM dibasic sodium phosphate.

SBP, PPI, and buffer solutions were placed in 190 μL of reaction cell, 50 μL of syringe, and reference cell, respectively. The PPI solution was added through 18 successive 2.5 μL injections, with an interval of 200 s between injection, while the first injection was 1 μL and did not collect into result. The stirring speed was set at 350 rpm during titration. The dilution heat

from the blank titration was determined by titrating PPI solution into the buffer, then subtracted from raw data to determine the corrected enthalpy changes.

Thermograms were recorded by NanoAnalyze software (TA instruments, New Castle, USA). The binding isotherms were obtained by integrating isotherm peaks and subtracting the dilution heat from blank. The binding isotherms were presented as enthalpy changes *vs* PPI–SBP mole ratios. Thermodynamic parameters including binding stoichiometry (n), binding affinity constant (K_a), reaction enthalpy (Δ_H) and change of entropy ($T\Delta S$) were calculated by iterative curve fitting of the binding isotherms. The Gibbs free energy change (ΔG) was calculated from the equation ($\Delta G = \Delta H - T\Delta S$), where T is the absolute temperature.

Scanning electron microscopy (SEM)

A small volume of coacervates was centrifuged at 3220×g for 15 min and collected precipitate was frozen in slushy nitrogen (–210 °C), and then lyophilized, according to a method developed by Phadungath (Phadungath, 2005) with slight modifications. The dried coacervates were fractured manually and fragments were attached to cylindrical aluminum mounts with colloidal–silver paste (Structure Probe Inc., West Chester PA, USA) oriented to view the fractured surface. The powdered control samples (PPI and SBP) were attached to adhesive carbon tab on cylindrical aluminum mounts, and the excess was blown off with a stream of nitrogen gas. All samples were then sputter coated with gold (Cressington 108auto, Ted Pella, Redding, CA, USA) to make them electrically conductive and finally examined in a scanning electron microscope (JEOL Model JSM–6490LV, Peabody, MA, USA) using an accelerating voltage of 15 kV. Micrographs (5000×) were presented as a representative of each sample.

Fourier transform infrared spectroscopy (FTIR)

The dried powder of coacervates was obtained by centrifugation (Eppendorf, New York, USA) at 3220×*g* for 15 min, and the collected precipitate was lyophilized for 48 h (laboratory scale lyophilizer, SP scientific, Gardiner, New York, USA). FTIR spectra of dried coacervates and controls (PPI and SBP powder) were recorded according to our previous published paper without any modification (Lan, Xu, Ohm, Chen, & Rao, 2019).

Statistical analysis

A completely randomized design (CRD) with two replicates was applied to arrange all experimental variants. All measurements were performed three times and data was expressed as mean ± SD. One-way analysis of variance (ANOVA) and F-protected LSD by SAS software (Version 9.3, SAS Institute Inc., NC, USA) were conducted, and significant difference was defined at $p < 0.05$ by Tukey's test.

Results and discussion

Effect of pH and mixing ratios on complex coacervation formation

State diagram

The first question that should be posed here is the boundary pH range of the complex coacervates at concentrated PPI–SBP solutions. As one can see from **Fig. 4-1b**, An example of PPI–SBP mixtures prepared at a total biopolymer concentration of 1.20 wt% showed a distinct cloudy appearance in pH range of 6.5–4.5 (**Fig. 4-1b**), which represents a solution with undetectable turbidity. This is the major reason that classic turbidimetric method is inappropriate to identify the boundary pH range of complex coacervates, especially the pH with a maximum optical absorbance (pH_{opt}). As such, the phase behaviors of PPI–SBP mixtures after standing at

25 °C for 24 h, as a function of pH and mixing ratios, were observed and constructed as a state diagram in **Fig. 4-1**.

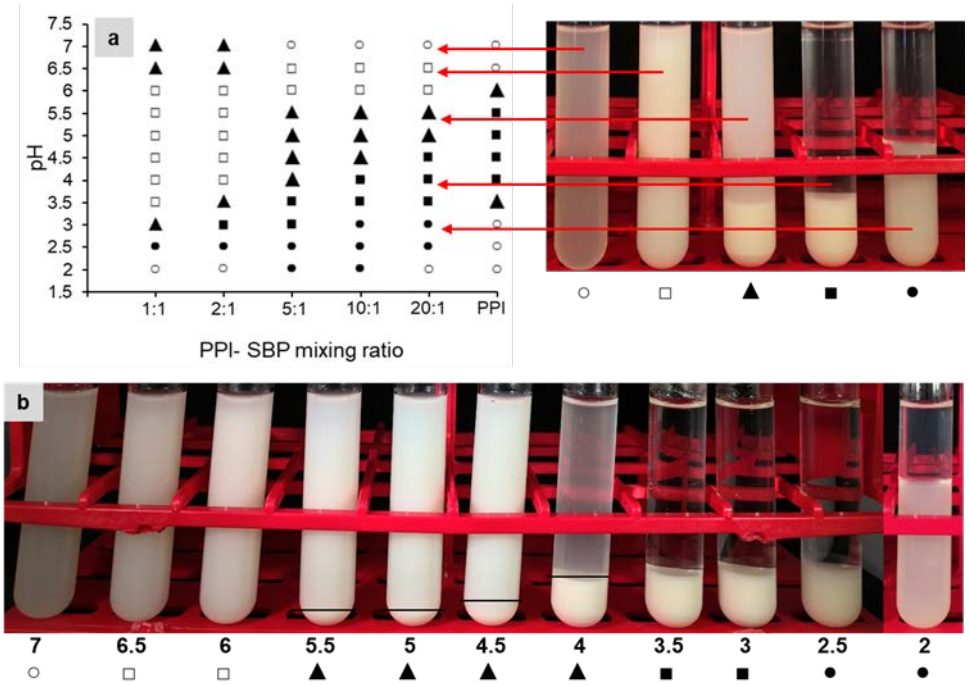

Figure 4-1. (a) State diagram of PPI, and PPI–SBP mixtures at different mixing ratios during acid titration. (b) The appearance of PPI–SBP mixture (5:1 mixing ratio) as function of pH. The PPI concentration was fixed at 1 wt%. The appearance was observed after 24 h standing. ○ represents translucent solution; □ represents turbid solution; ▲ represents precipitation and cloudy solution; ■ represents precipitation and clear solution; ● represents precipitation and clear solution that has higher volume of precipitation than ■.

SBP solutions as a function of pH were not included in this state diagram as they presented a translucent appearance throughout pH 7–2. Five distinguishable phase behaviors and appearances were presented in the state diagram (**Fig. 4-1**). At neutral pH, two phases of PPI–SBP mixtures or one phase of PPI–SBP solutions were observed depending on the total biopolymer concentrations. For example, when the total biopolymer concentration was > 1.50 wt %, PPI and SBP repelled each other in the ratios of 1:1 and 2:1 at pH 7 due to the thermal incompatibility (Kontogiorgos, Tosh, & Wood, 2009). As such, it leads to a phase separation into a PPI-enriched phase and an SBP-enriched phase. In contrast, translucent appearances of one phase solutions were observed in the rest of tested mixing ratios (5:1, 10:1, and 20:1) at the same

pH, indicating the co-solubility of PPI and SBP (Liu, Shim, Wang, & Reaney, 2015; Zhang, et al., 2018). As the pH decreased to acidic conditions, the turbid without precipitation (□), corresponding to the soluble complexes, was observed within a wide pH range (6–4) in ratios of 1:1 and 2:1 or a narrow pH range (6.5–6) in ratios of 5:1–20:1, suggesting the initiation of electrostatic interactions between PPI and SBP. The further decrease in pH caused the formation of insoluble complexes (coacervates or precipitates) that associated with three various phase behaviors (**Fig. 4-1**). According to a prodigious amount of literature on complex coacervation involving oppositely charged protein–polysaccharide, it is generally accepted that the pH regions for complex coacervates starts from $pH_{\varphi 1}$, and then transits to the end of the plateau ($pH_{\varphi 2}$) using turbidimetric method at low biopolymer concentrations (Ach, et al., 2015; Moschakis & Biliaderis, 2017). In this work, precipitates in three phase behaviors (▲, ■, and ● in **Fig. 4-1**) were all defined as coacervates with different structural and functional properties. The pH region of coacervates that was labelled using symbol ranging from ▲ to ● in the current study was similar to $pH_{\varphi 1}$ to $pH_{\varphi 2}$ at low biopolymer concentration system. The phase behavior of precipitation & clear solution (■) in the state diagram was matches the pH_{opt} that was identified at low biopolymer concentration system. When biopolymer mixture pH was further reduced to the most acidic pH 2, complex coacervates completely vanished and translucent appearance of one phase solution were observed again, which could be attributed to the pH is below the pKa value of SBP at pH 2 (**Fig. 4-2a**). There was no association between PPI and SBP at acidic pH 2.

In terms of mixing ratios, the pH region of complex coacervates expanded to that of larger pH regions with the increase of PPI to SBP ratios. For example, boundary pH region 3–2.5 of complex coacervates expanded from pH 3–2.5 to a range of pH 5.5–2.5, when PPI to SBP mixing ratio increased from 1:1 to 20:1 (**Fig. 4-1a**). This also indicated that higher concentration

of protein with lower concentration of sugar beet pectin favors the formation of complex coacervates. Similar phase behaviors and pH–mixing ratio relationship determined via state diagram were also documented in the systems of WPI–GA (Ach, et al., 2015), soybean protein–chitosan (Yuan, Wan, Yang, & Yin, 2014), and milk protein–tragacanth gum (Azarikia & Abbasi, 2016).

ζ–potentials of PPI–SBP mixture as a function of pH

As formation of complex coacervates are driven by electrostatic interactions, the ζ–potential could provide strength of electrostatic interaction (SEI) information regarding the interactions between charged proteins and polysaccharides as well as formation and stability of coacervates. Hence, the ζ–potential of homogeneous PPI, SBP, and PPI–SBP mixture was determined as a function of pH (7–2) and mixing ratios (1:1–20:1) (**Fig. 4-2a**).

The PPI–SBP mixtures displayed intermediate ζ–potentials in between the two individual biopolymers in solution (**Fig. 4-2a**). In general, complex coacervation requires opposite charges while this is not the case for soluble complex formation. An overall positively charged pea protein (< pH 4.7) with a negative charge patch could have electrostatic attraction with a cationic SBP to form complex coacervates. Coacervates start to form as the net charge of the biopolymer mixture approaches zero. Therefore, the isoelectric point (IEP) was used to represent the pH at which the zero-net charge of a biopolymer mixture was achieved **(Fig. 4-2b)**. At low mixing ratios of 1:1 and 2:1, the presence of SBP shifted the IEP of PPI from 4.7 to nearly 2.5 (**Fig. 4-2b**). Mixtures at these two ratios exhibited similar surface charges to that of SBP solution with ζ–potentials remaining negatively over the pH range of 7–2.5 (**Fig. 4-2a**). As the mixing ratio increased, IEP values shifted towards higher pH values, reaching an IEP of 4.2 at a mixing ratio of 20:1, which was close to that of PPI alone (**Fig. 4-2b**).

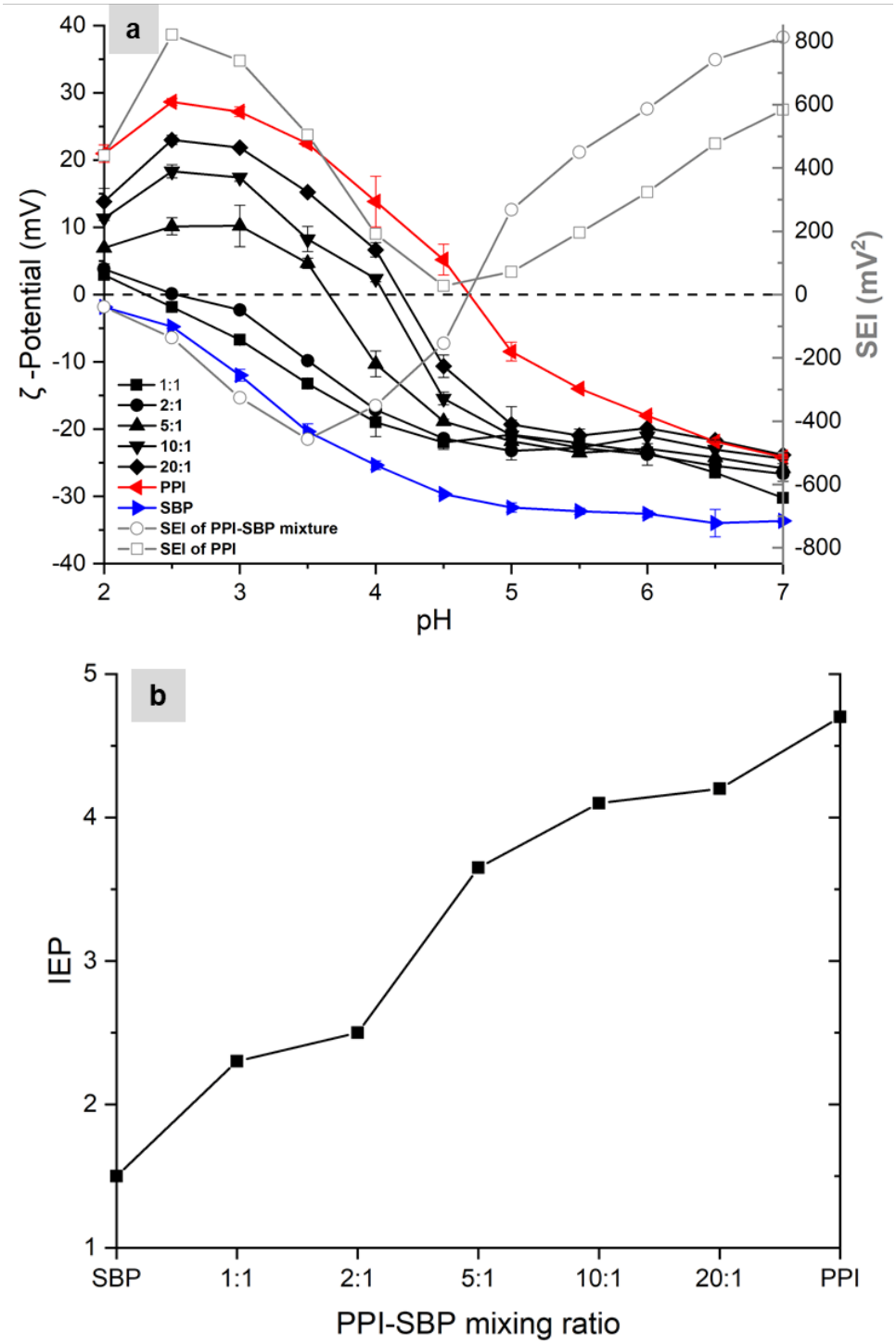

Figure 4-2. (a) Zeta (ζ)–potential changes of PPI, SBP, PPI–SBP mixtures at different mixing ratios and the strength of electrostatic interaction (SEI) of PPI–PPI and PPI–SBP during acid titration. (b) Plot of isoelectric point (IEP) against PPI–SBP mixing ratio (including data points of pure SBP and PPI). The PPI concentration was fixed at 1 wt%.

Similar trend in IEP shift caused by biopolymer interaction was also reported in pea protein–HMP system (Pillai, et al., 2019). The IEP results along with state diagram showed that the overall systems were charge neutral at maximum complexation, which is in agreement with results reported by Skelte et al. on complex coacervates of lactotransferrin and β-lactoglobulin (Anema & de Kruif, 2014). Charge neutralization can be achieved by altering the charge of one or both biopolymer macroions, or changing the mixing ratios within the protein–polysaccharide system (Lan, et al., 2018). Above observations testified that PPI–SBP complex coacervates formation occurred largely via electrostatic interactions between the cationic amino groups of pea protein and anionic carboxyl groups of pectin.

On the basis of ζ–potential, SEI was applied to further elucidate the type (attractive or repulsive) and magnitude of forces during complex coacervation (Chang, Gupta, Timilsena, & Adhikari, 2016; Espinosa-Andrews, et al., 2013; Timilsena, Wang, Adhikari, & Adhikari, 2016; Yuan, et al., 2014). The SEI of PPI–SBP solutions and PPI at different pHs were calculated as the multiplication of ζ–potential values of PPI and SBP or PPI itself at each pH (**Fig. 4-2a**). The positive SEI values indicated that there was an overall repulsive force between biopolymers. In contrast, an attractive force between biopolymers was existed when SEI value was negative. The PPI solutions had an overall repulsive force throughout pH 7–2, with the lowest SEI nearby pH 4.5 (IEP of PPI), and increased SEI as pH was away from IEP (**Fig. 4-2a**). This demonstrates well the phase behaviors of PPI (**Fig. 4-1a)** that the highest precipitation occurred at pH 4.5 due to the lowest repulsive forces. By contrast, SEI of PPI–SBP mixtures indicated that the system was dominated by the overall repulsive forces at pH above IEP of PPI, or by attractive forces below the IEP with a highest attractive force at pH 3.5 (**Fig. 4-2a**). This helps mostly to explain

the phase behavior that dense and maximum coacervates were produced around pH 3–4 in PPI–SBP mixtures at a mixing ratio of 5:1 (**Fig. 4-1a**).

Viscoelastic properties of complex coacervates

Viscoelastic behaviors (storage modulus G′ and loss modulus G″ versus angular frequency) of coacervates provide knowledge about network structure and play important roles in determining their applications as they affect product texture (Liu, et al., 2017). It is commonly reported that G′ is able to indicate strength of electrostatic interaction between protein and polysaccharide, the higher G′ representing greater electrostatic interaction (Espinosa-Andrews, Sandoval-Castilla, Vázquez-Torres, Vernon-Carter, & Lobato-Calleros, 2010; Liu, et al., 2017; Raei, Rafe, & Shahidi, 2018). Therefore, all coacervates presented in state diagram (**Fig. 4-1**) were collected by centrifugation and used in the analysis of viscoelastic properties.

First, the effect of pH on viscoelastic properties was evaluated by preparing coacervates at varied pH (pH 2–4.5), but fixed PPI–SBP mixing ratio of 5:1 (**Fig. 4-3a&b**). Storage modulus G′ of all PPI–SBP coacervates was higher than the loss modulus G″ without a crossover point over the frequency range of 0.01–100 rad/s, implying a highly interconnected gel-like network structure of coacervates (Raei, et al., 2018). Moreover, pH plays a major role in viscoelasticity of coacervates since both dynamic G′ and G″ of coacervates increased as the pH approached 3.5. The highest G′ and G″ were found at coacervates formed at pH 3.5, close to IEP of PPI–SBP system at mixing ratio of 5:1 (**Fig. 4-2a**). This finding indicated that the maximum electrostatic attraction occurred at the pH where PPI–SBP mixture electroneutrality was achieved, and caused the development of strongest entangled gel-like network structures. Similar findings were reported in mixture system of WPI–flaxseed gum (FG) (Liu, et al., 2017) and WPI– HMP (Raei, et al., 2018).

Second, in order to address the impact of mixing ratios on the viscoelasticity of PPI–SBP coacervates, the viscoelasticity of coacervates obtained at studied mixing ratios (1:1–20:1) was tested, and only the samples at a mixing ratio that had the highest G′ and G″ (maximum electrostatic interaction) were presented in **Fig. 4-3c&d**. As one can see, both dynamic moduli (G′ and G″) were relatively higher at mixing ratios of 20:1, 10:1, and 5:1, indicating that complex coacervates with stronger gel-like network structures were more easily formed with higher weight percentage of protein. This can be explained by the fact that higher solid mass of protein can lead to higher viscoelasticity.

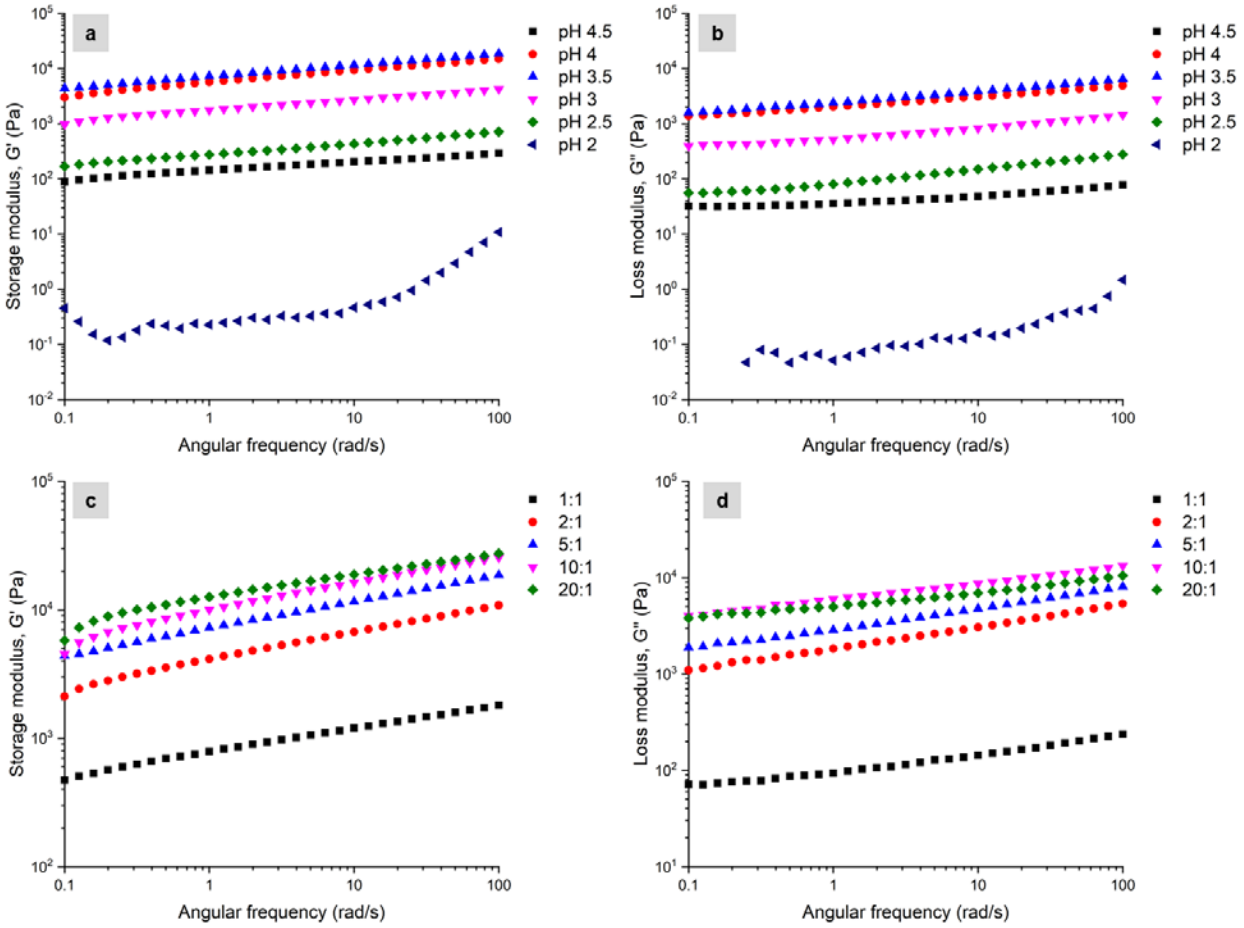

Figure 4-3. The (a) storage modulus G′ and (b) loss modulus G″ versus angular frequency for PPI–SBP coacervates prepared at different pH values (the PPI–SBP mixing ratio was fixed at 5:1). The (c) G′ and (d) G″ of coacervates prepared at different mixing ratios and at the pH that the highest G′ occurred within each mixing ratio. The PPI concentration was fixed at 1 wt%.

PPI content in complex coacervates

Influence of pH and mixing ratio on the content of PPI in coacervates was investigated (**Table 4-1**). Presumably, the percentage of PPI in the coacervates could be considered as the amount of PPI interacting with SBP after equilibrium. The coacervates were collected at the bottom of the tubes, and the protein contents both in the total sample and the supernatant were measured. The PPI content in coacervation phase was calculated from the difference.

Table 4-1. Percentage (%) of PPI in PPI–SBP coacervate phases collected at different mixing ratios during acid titration.

pH	PPI–SBP mixing ratio				
	1:1	2:1	5:1	10:1	20:1
4.5	–	–	57.2±6.6[a]	97.0±0.7[a]	97.6±0.7[a]
4.0	–	–	91.8±0[b]	97.4±0.3[a]	96.8±0.3[a]
3.5	–	65.8±1.0[a]	96.6±0.1[b]	93.3±1.7[a]	85.1±2.0[b]
3.0	33.1±4.0[a]	96.3±0.2[b]	87.5±1.7[b]	75.7±0[b]	67.8±5.6[c]
2.5	58.7±6.8[b]	71.2±2.9[a]	68.6±3.1[a]	56.8±3.2[c]	50.9±1.9[d]
2.0	–	–	57.3±10.1[a]	43.5±2.8[d]	–

[†]The concentration of PPI was fixed at 1 wt%.
[‡]Values are expressed as mean ± standard deviation of at least three different samples.
[§]Values with different superscript letters in the same column are significantly different at $p<0.05$.

For instance, at a mixing ratio of 5:1, the PPI content retained in coacervates was increased firstly to a maximum of 96.6% when the pH decreased from pH 4.5 to 3.5, and then reduced to a lower percentage of 57.3% as the pH further dropped to pH 2. This finding, in conjunction with the observations in state diagram, ζ–potential, and rheological tests, proved that maximum associative interaction between PPI and SBP occurred at pH 3.5 (■). The coacervates collected at pH 3.5 had relative denser texture, smaller pore appearance, maximum SEI, and highest storage modulus at a mixing ration of 5:1. (**Fig. 4-1, 4-2, and 4-3)**.

Additionally, throughout pH 7–2 at a mixing ratio of 1:1, the highest PPI content in coacervates was around 59% and occurred at pH 2.5. As PPI–SBP mixing ratio increased to 2:1, the protein percentage raised abruptly to 96% and occurred at higher pH value (3.0). As mixing

ratio further increased to 20:1, no significant changes in PPI content, except that the occurrence pH continuously shifted towards higher pH was observed. The shift in pH values from pH 2.5 to 4.5 was similar to boundary pH shift as seen in state diagram (**Fig. 4-1**), which again illustrated that the pH for maximum production of coacervates shifted as the increase of PPI–SBP mixing ratio.

Thermodynamic characterization of interactions between PPI and SBP

In order to further understand interactions of PPI–SBP, including binding model and thermodynamics of complex coacervation process, ITC was applied to reveal molecular recognition by titrating PPI with SBP at pH 3.5 and 25 ºC, and to record the released or absorbed heat in a reaction chamber. The typical thermogram of heat rate versus time profile was shown in the top panel of **Fig. 4-4**.

The titration profile was exothermic, and the exothermic peaks decreased regularly to a steady state after 14th injection of SBP with molar ratio of around 1.6, indicating that the binding between PPI and SBP was saturated. The exothermic reaction was mainly attributed to the nonspecific electrostatic neutralization of the opposite charges carried by two biopolymers demonstrating an enthalpic contribution of complex coacervation (Hadian, et al., 2016; Li, et al., 2018). The regular decrease of peaks was associated to a reduction in free PPI remaining in the reaction cell after successive injections, along with a reduction of dilution heat (Li, et al., 2018). Similar exothermic sequences were also found in mixing processes of lactoferrin–sodium alginate (Bastos, et al., 2018), and fish skin gelatin–GA (Li, et al., 2018).

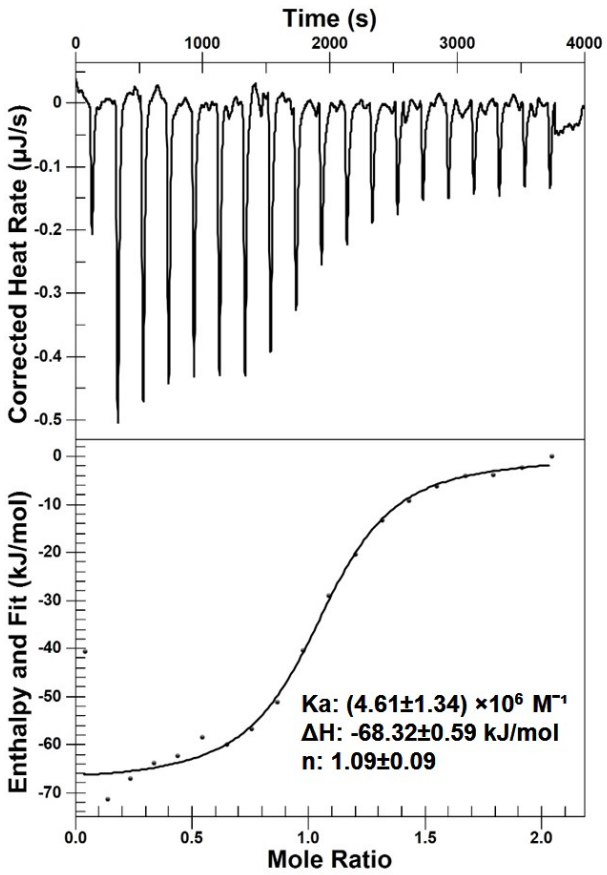

Figure 4-4. Thermogram (top panel) and binding isotherm (bottom panel) corresponding to the titration of PPI (48.31 μM) with SBP (7.41 μM) dispersion in citrate–phosphate buffer (pH 3.5) at 25 °C.

The binding isotherm (bottom panel in **Fig. 4-4**) was fitted from thermogram using "one independent binding site" model since two inflection points were not observed in the binding isotherm (Xiong, et al., 2016). The related thermodynamic parameters were calculated based on binding isotherm and as follows: binding affinity stoichiometry (n = 1.09±0.09), binding affinity constant (K_a = 4.61 ×10^6±1.34 ×10^6 M^{-1}), reaction enthalpy (ΔH = -68.32±0.59 kJ/mol), change of entropy ($T\Delta S$ = -30.34±1.32 kJ/mol), and change of Gibbs free energy (ΔG = -37.98±0.74 kJ/mol). The value of n indicated that 1.1 PPI molecules were bound to one SBP molecule. The binding constant was on the order of 10^6 M^{-1}, indicating strong molecular interactions between PPI and SBP (Bastos, et al., 2018). The negative value of ΔG indicated a spontaneous nature of the interaction between these two biopolymers. Both ΔH and $T\Delta S$ values were negative which

serves as the evidence for the enthalpically favorable and entropically unfavorable of PPI–SBP complexation process. It also implies that hydrogen bonding, electrostatic interactions, and hydrophobic interactions were involved in molecular interactions (Bastos, et al., 2018; Souza, da Costa, Souza, Simas Tosin, & Garcia-Rojas, 2018; Yang, Liu, Zeng, & Chen, 2018).

Morphological characterization of complex coacervates (dense colloids *vs* soft colloids)

Microstructure analysis

As above discussed, PPI–SBP coacervates prepared at pH values of 3.5 (■) and 2.5 (●) with PPI–SBP ratio of 5:1 showed significantly different phase behavior and viscoelasticity. Therefore, the microstructure of these two samples were further characterized using SEM to reveal the interior structure (**Fig. 4-5 a-d**).

PPI collected at its IEP (pH 4.5) presented as clusters with dense three-dimensional networks (**Fig. 4-5a**), similar to morphology of isoelectric point precipitated and freeze-dried milk proteins (Phadungath, 2005). The highly condensed structure could be attributed to aggregation of pea protein particles at pH where electroneutrality occurred. The SBP powders showed a column/ plate-shaped bulky morphology intermingled with small pieces (**Fig. 4-5b**).

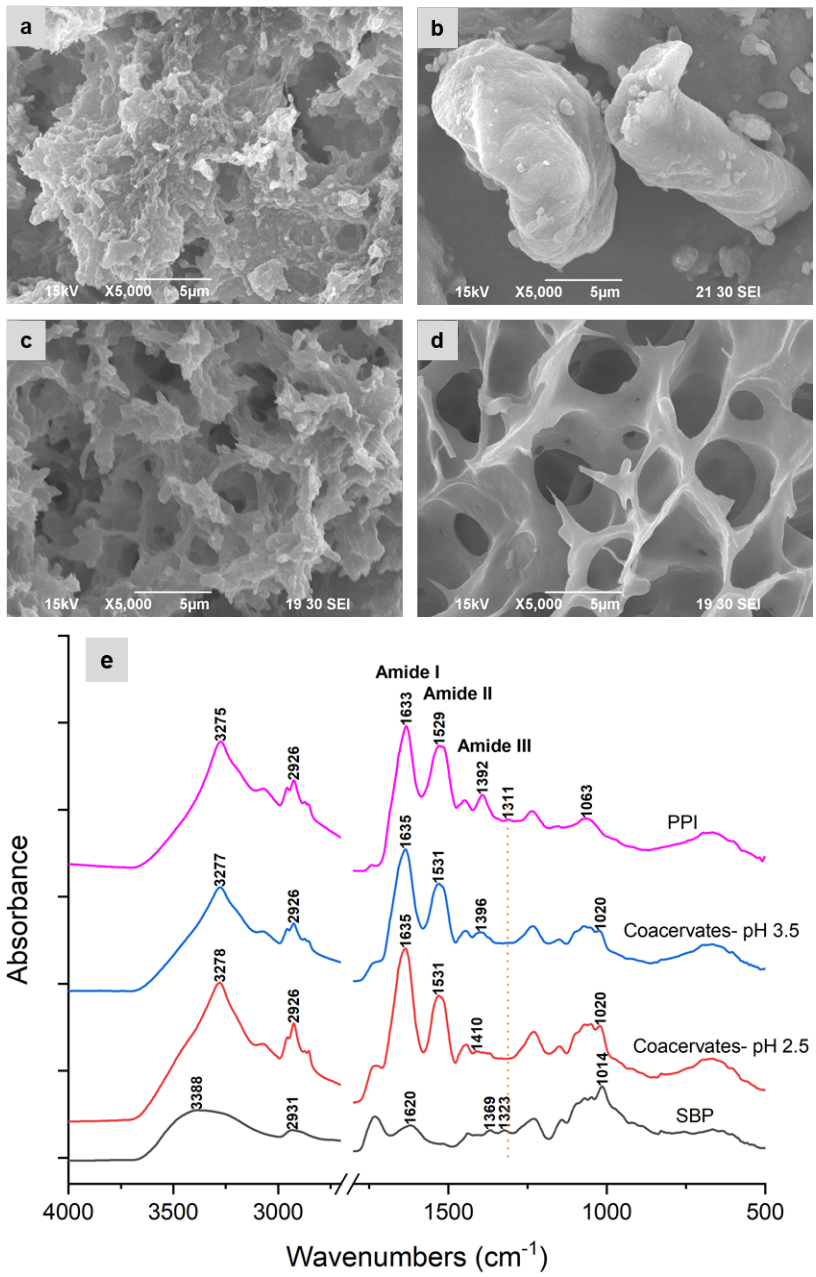

Figure 4-5. SEM micrographs (5000×) of (a) PPI collected at pH 4.5, (b) SBP powder, and PPI–SBP coacervates collected at (c) pH 3.5 and (d) pH 2.5; (e) FTIR spectra of the coacervates prepared at pH 3.5 and 2.5. The PPI–SBP mixing ratio was fixed at 5:1, and PPI concentration was fixed at 1 wt%. Bar in SEM images represents 5 μm.

SEM results showed that the coacervates structures were critically dependent on environmental pH, and their evolution could be described in two stages. To begin with, when pH at 3.5, the neutral aggregates of pea protein and the hydrophobic interaction strengthen the complex coacervates between PPI and SBP. Thus, the network structures of coacervates become

more condensed and much less organized. At a later stage of coacervation when pH at 2.5(●), no neutral aggregates of pea protein are involved. As such the network structures are highly organized with relatively homogeneous large pore size distribution and smooth inner pore surfaces (**Fig. 4-5d**). This interpretation is corroborated by ζ–potentials, state diagram, and viscoelastic measurements that coacervates at pH 3.5 had higher SEI, storage modulus, and denser phase behavior than those at pH 2.5. The relationship between coacervate microstructure and viscoelasticity were similar to previous reports (Anvari, Pan, Yoon, & Chung, 2015; Espinosa-Andrews, et al., 2010; Huang, Du, Xiao, & Wang, 2017). Such findings have led to calls to optimize the application of complex coacervates, particularly in the area of encapsulation since coacervates obtained at pH 2.5 in the current study would have better encapsulation capacity than those prepared at pH 3.5.

FTIR analysis

Furthermore, FTIR analysis was carried in parallel with SEM image to examine the non-covalent bonding (i.e. electrostatic interactions and hydrogen bonding) between functional groups of PPI and SBP at different pH of coacervates (i.e. pH 3.5 and 2.5).

The spectrum of PPI was consistent to our previous report (Lan, et al., 2019), with strong –OH contraction vibration band at 3275 cm^{-1}, C–H stretching at 2926 cm^{-1}, and stretching or bending of C=O, N–H and C–N bonds at 1633, 1529, 1392 cm^{-1} (features of amide I, II and III, respectively), and C–O vibration stretching at 1063 cm^{-1} (**Fig. 4-5e**). The spectrum of SBP exhibited typical absorption bands of polysaccharides at 3388 cm^{-1} (–OH broad band), at 2931 cm^{-1} (C–H stretching vibration), at 1620 cm^{-1} ($–COO^-$ symmetric stretching vibration), and at 1014 cm^{-1} (C–O–C stretching vibration) (**Fig. 4-5e**). These findings were confirmed from

previous reports (Mata, Blázquez, Ballester, González, & Muñoz, 2009; Synytsya, Čopíková, Matějka, & Machovič, 2003).

Overall, the spectra of PPI–SBP complex coacervates were dominated by the pea protein due to higher protein ratio (5:1), but different from each individual biopolymer (**Fig. 4-5e**). For example, a peak of PPI (2926 cm^{-1}) alone also presented in coacervates produced at both pH 3.5 and 2.5, whereas a peak of PPI (1311 cm^{-1}) and two peaks of SBP (1369 and 1323 cm^{-1}) were disappeared in both coacervates, confirming that complex coacervates with a different structure were formed. In addition, the spectra of coacervates changed significantly in the carbonyl-amide region. On one hand, both PPI-SBP coacervates did not show the symmetric $–COO^-$ stretching vibration (1620 cm^{-1}) that occurs in SBP. On the other hand, both coacervates showed shift in peaks of amide I, II, and III towards higher wavenumbers as compared to PPI due to the electrostatic interaction between the amino groups of PPI ($–NH_3^+$) and carboxylic groups of SBP ($–COO^-$). Similar results were also reported in egg white protein–xanthan gum and hsian-tsao gum-chitosan system (Souza & Garcia-Rojas, 2017; You, Liu, & Zhao, 2018).The introduction of SBP could also contribute to an increase in hydrogen bonding of complex coacervates (Li, et al., 2018). This result was in agreement with other studies in complex coacervation of chia seed protein isolate–chia seed gum (Timilsena, et al., 2016) and lactoferrin–sodium alginate (Bastos, et al., 2018). The spectra of PPI–SBP complex coacervates in “fingerprint region” presented a broad band (approximately 1020–1080 cm^{-1}) which was probably attributed to spectra superposition of PPI (peak at 1063 cm^{-1}, C–O stretching) and SBP (peak 1014 cm^{-1}, C–O–C stretching), implying an electrostatic interaction between PPI and SBP during the formation of complex coacervates (Bastos, et al., 2018). Furthermore, environmental pH (pH 3.5 and 2.5) imposed slightly peak shifts on complex coacervates (**Fig. 4-5e**). Compared to PPI, coacervates

formed at pH 3.5 had lower amide III peak shift towards higher wavenumbers than those prepared at pH 2.5 (4 vs. 18 cm^{-1}) while both coacervates had the same C–O–C peak shift towards higher wavenumbers compared to SBP. These results indicated that the overall intermolecular interaction may be affected by environmental pH conditions (Li, et al., 2018).

Conclusions

This work supports the feasibility of state diagram for identifying boundary formation pH region ($pH_{\varphi 1}$ and $pH_{\varphi 2}$) of complex coacervates in protein–polysaccharide system at a relatively high concentration of biopolymers. The boundary pH region identified by state diagram is in line with zeta–potential, rheological, and phase composition measurements. The pH_{opt} can also be identified using both zeta–potential and rheological measurements. In general, $pH_{\varphi 1}$ shifts from 3 to 5.5 as the PPI–SBP mixing ratio increases from 1:1 to 20:1. PPI–SBP complex coacervation is a spontaneous exothermic process and mainly formed through the electrostatic interaction and hydrogen bonding between nonspecific amino groups of PPI and carboxylic groups of SBP. Both SEM and FTIR results show that the coacervates structures critically depend on the pH. Coacervates possess stronger and denser structure with greater storage modulus at the pH_{opt} where electroneutrality is achieved. The smooth inner pore surfaces with homogeneous large pore size distribution of PPI–SBP microstructure could be formed at the late stage of coacervates when the environmental pH is near the $pH_{\varphi 2}$. Of particular note in the findings from the current study is that it is the prerequisite to optimize pH and mixing ratio of protein–polysaccharide complexation for desired microstructure and viscoelastic properties, which can be accomplished using state diagram developed here. Ongoing work will apply these new understandings for the application of PPI–SBP coacervates in the area of microencapsulation.

References

Ach, D., Briançon, S., Dugas, V., Pelletier, J., Broze, G., & Chevalier, Y. (2015). Influence of main whey protein components on the mechanism of complex coacervation with acacia gum. *Colloids and Surfaces A: Physicochemical and Engineering Aspects, 481*, 367-374.

Adal, E., Sadeghpour, A., Connell, S., Rappolt, M., Ibanoglu, E., & Sarkar, A. (2017). Heteroprotein complex formation of bovine lactoferrin and pea protein isolate: A multiscale structural analysis. *Biomacromolecules, 18*(2), 625-635.

Anema, S. G., & de Kruif, C. G. (2014). Complex coacervates of lactotransferrin and beta-lactoglobulin. *Journal of Colloid and Interface Science, 430*, 214-220.

Anvari, M., Pan, C.-H., Yoon, W.-B., & Chung, D. (2015). Characterization of fish gelatin–gum arabic complex coacervates as influenced by phase separation temperature. *International Journal of Biological Macromolecules, 79*, 894-902.

Aryee, F. N. A., & Nickerson, M. T. (2012). Formation of electrostatic complexes involving mixtures of lentil protein isolates and gum arabic polysaccharides. *Food Research International, 48*(2), 520-527.

Azarikia, F., & Abbasi, S. (2016). Mechanism of soluble complex formation of milk proteins with native gums (*tragacanth and Persian gum*). *Food Hydrocolloids, 59*, 35-44.

Bastos, L. P. H., de Carvalho, C. W. P., & Garcia-Rojas, E. E. (2018). Formation and characterization of the complex coacervates obtained between lactoferrin and sodium alginate. *International Journal of Biological Macromolecules, 120*, 332-338.

Chang, P. G., Gupta, R., Timilsena, Y. P., & Adhikari, B. (2016). Optimisation of the complex coacervation between canola protein isolate and chitosan. *Journal of Food Engineering, 191*, 58-66.

Espinosa-Andrews, H., Enríquez-Ramírez, K. E., García-Márquez, E., Ramírez-Santiago, C., Lobato-Calleros, C., & Vernon-Carter, J. (2013). Interrelationship between the zeta potential and viscoelastic properties in coacervates complexes. *Carbohydrate Polymers, 95*(1), 161-166.

Espinosa-Andrews, H., Sandoval-Castilla, O., Vázquez-Torres, H., Vernon-Carter, E. J., & Lobato-Calleros, C. (2010). Determination of the gum arabic–chitosan interactions by Fourier Transform Infrared Spectroscopy and characterization of the microstructure and rheological features of their coacervates. *Carbohydrate Polymers, 79*(3), 541-546.

Gomez-Mascaraque, L. G., Llavata-Cabrero, B., Martinez-Sanz, M., Fabra, M. J., & Lopez-Rubio, A. (2018). Self-assembled gelatin-iota-carrageenan encapsulation structures for intestinal-targeted release applications. *Journal of Colloid and Interface Science, 517*, 113-123.

Hadian, M., Hosseini, S. M. H., Farahnaky, A., Mesbahi, G. R., Yousefi, G. H., & Saboury, A. A. (2016). Isothermal titration calorimetric and spectroscopic studies of β-lactoglobulin-water-soluble fraction of *Persian* gum interaction in aqueous solution. *Food Hydrocolloids, 55*, 108-118.

Hosseini, S. M. H., Emam-Djomeh, Z., Razavi, S. H., Moosavi-Movahedi, A. A., Saboury, A. A., Atri, M. S., & Van der Meeren, P. (2013). β-Lactoglobulin–sodium alginate interaction as affected by polysaccharide depolymerization using high intensity ultrasound. *Food Hydrocolloids*, *32*(2), 235-244.

Huang, G. Q., Du, Y. L., Xiao, J. X., & Wang, G. Y. (2017). Effect of coacervation conditions on the viscoelastic properties of N,O-carboxymethyl chitosan - gum arabic coacervates. *Food Chemistry, 228*, 236-242.

Kayitmazer, A. B., Koksal, A. F., & Iyilik, E. K. (2015). Complex coacervation of hyaluronic acid and chitosan: effects of pH, ionic strength, charge density, chain length and the charge ratio. *Soft Matter, 11*(44), 8605-8612.

Kizilay, E., Seeman, D., Yan, Y. F., Du, X. S., Dubin, P. L., Donato-Capel, L., Bovetto, L., & Schmitt, C. (2014). Structure of bovine beta-lactoglobulin-lactoferrin coacervates. *Soft Matter, 10*(37), 7262-7268.

Klemmer, K. J., Waldner, L., Stone, A., Low, N. H., & Nickerson, M. T. (2012). Complex coacervation of pea protein isolate and alginate polysaccharides. *Food Chemistry, 130*(3), 710-715.

Krzeminski, A., Prell, K. A., Busch-Stockfisch, M., Weiss, J., & Hinrichs, J. (2014). Whey protein–pectin complexes as new texturising elements in fat-reduced yoghurt systems. *International Dairy Journal, 36*(2), 118-127.

Lam, A. C. Y., Can Karaca, A., Tyler, R. T., & Nickerson, M. T. (2018). Pea protein isolates: Structure, extraction, and functionality. *Food Reviews International, 34*(2), 126-147.

Lan, Y., Chen, B., & Rao, J. (2018). Pea protein isolate–high methoxyl pectin soluble complexes for improving pea protein functionality: Effect of pH, biopolymer ratio and concentrations. *Food Hydrocolloids, 80*, 245-253.

Lan, Y., Xu, M., Ohm, J.-B., Chen, B., & Rao, J. (2019). Solid dispersion-based spray-drying improves solubility and mitigates beany flavour of pea protein isolate. *Food Chemistry, 278*, 665-673.

Li, X., Hua, Y., Chen, Y., Kong, X., & Zhang, C. (2016). Protein selectivity controlled by polymer charge density and protein yield: Carboxylated polysaccharides versus sulfated polysaccharides. *Journal of Agricultural and Food Chemistry, 64*(47), 9054-9062.

Li, Y., Zhang, X., Zhao, Y., Ding, J., & Lin, S. (2018). Investigation on complex coacervation between fish skin gelatin from cold-water fish and gum arabic: Phase behavior, thermodynamic, and structural properties. *Food Research International, 107*, 596-604.

Liu, J., Shim, Y. Y., Shen, J. H., Wang, Y., & Reaney, M. J. T. (2017). Whey protein isolate and flaxseed *(Linum usitatissimum* L.) gum electrostatic coacervates: Turbidity and rheology. *Food Hydrocolloids, 64*, 18-27.

Liu, J., Shim, Y. Y., Wang, Y., & Reaney, M. J. T. (2015). Intermolecular interaction and complex coacervation between bovine serum albumin and gum from whole flaxseed *(Linum usitatissimum L.*). *Food Hydrocolloids, 49*, 95-103.

Liu, S. H., Cao, Y. L., Ghosh, S., Rousseau, D., Low, N. H., & Nickerson, M. T. (2010). Intermolecular interactions during complex coacervation of pea protein isolate and gum arabic. *Journal of Agricultural and Food Chemistry, 58*(1), 552-556.

Liu, S. H., Low, N. H., & Nickerson, M. T. (2009). Effect of pH, salt, and biopolymer ratio on the formation of pea protein isolate-gum arabic complexes. *Journal of Agricultural and Food Chemistry, 57*(4), 1521-1526.

Mata, Y. N., Blázquez, M. L., Ballester, A., González, F., & Muñoz, J. A. (2009). Sugar-beet pulp pectin gels as biosorbent for heavy metals: Preparation and determination of biosorption and desorption characteristics. *Chemical Engineering Journal, 150*(2), 289-301.

Moschakis, T., & Biliaderis, C. G. (2017). Biopolymer-based coacervates: Structures, functionality and applications in food products. *Current Opinion in Colloid & Interface Science, 28*, 96-109.

Phadungath, C. (2005). The mechanism and properties of acid-coagulated milk gels. *Songklanakarin Journal of Science and Technology, 27*(2), 433-448.

Pillai, P. K. S., Stone, A. K., Guo, Q., Guo, Q., Wang, Q., & Nickerson, M. T. (2019). Effect of alkaline de-esterified pectin on the complex coacervation with pea protein isolate under different mixing conditions. *Food Chemistry, 284*, 227-235.

Priftis, D., & Tirrell, M. (2012). Phase behaviour and complex coacervation of aqueous polypeptide solutions. *Soft Matter, 8*(36), 9396-9405.

Raei, M., Rafe, A., & Shahidi, F. (2018). Rheological and structural characteristics of whey protein-pectin complex coacervates. *Journal of Food Engineering, 228*, 25-31.

Rocha, C. M. R., Souza, H. K. S., Magalhaes, N. F., Andrade, C. T., & Goncalves, M. P. (2014). Rheological and structural characterization of agar/whey proteins insoluble complexes. *Carbohydrate Polymers, 110*, 345-353.

Rodriguez, A. M. B., Binks, B. P., & Sekine, T. (2018). Emulsion stabilisation by complexes of oppositely charged synthetic polyelectrolytes. *Soft Matter, 14*(2), 239-254.

Samanta, R., & Ganesan, V. (2018). Influence of protein charge patches on the structure of protein-polyelectrolyte complexes. *Soft Matter, 14*(46), 9475-9488.

Silva, K. S., Fonseca, T. M. R., Amado, L. R., & Mauro, M. A. (2018). Physicochemical and microstructural properties of whey protein isolate-based films with addition of pectin. *Food Packaging and Shelf Life, 16*, 122-128.

Souza, C. J. F., da Costa, A. R., Souza, C. F., Simas Tosin, F. F., & Garcia-Rojas, E. E. (2018). Complex coacervation between lysozyme and pectin: Effect of pH, salt, and biopolymer ratio. *International Journal of Biological Macromolecules, 107*, 1253-1260.

Souza, C. J. F., & Garcia-Rojas, E. E. (2017). Interpolymeric complexing between egg white proteins and xanthan gum: Effect of salt and protein/polysaccharide ratio. *Food Hydrocolloids, 66*, 268-275.

Stenger, C., Zeeb, B., Hinrichs, J., & Weiss, J. (2017). Formation of concentrated biopolymer particles composed of oppositely charged WPI and pectin for food applications. *Journal of Dispersion Science and Technology, 38*(9), 1258-1265.

Stone, A. K., Teymurova, A., Chang, C., Cheung, L., & Nickerson, M. T. (2015). Formation and functionality of canola protein isolate with both high- and low-methoxyl pectin under associative conditions. *Food Science and Biotechnology, 24*(4), 1209-1218.

Synytsya, A., Čopíková, J., Matějka, P., & Machovič, V. (2003). Fourier transform Raman and infrared spectroscopy of pectins. *Carbohydrate Polymers, 54*(1), 97-106.

Timilsena, Y. P., Wang, B., Adhikari, R., & Adhikari, B. (2016). Preparation and characterization of chia seed protein isolate-chia seed gum complex coacervates. *Food Hydrocolloids, 52*, 554-563.

Wagoner, T., Vardhanabhuti, B., & Foegeding, E. A. (2016). Designing whey protein-polysaccharide particles for colloidal stability. In M. P. Doyle & T. R. Klaenhammer (Eds.), *Annual Review of Food Science and Technology* (Vol. 7, pp. 93-116). Palo Alto: Annual Reviews.

Warnakulasuriya, S., Pillai, P. K. S., Stone, A. K., & Nickerson, M. T. (2018). Effect of the degree of esterification and blockiness on the complex coacervation of pea protein isolate and commercial pectic polysaccharides. *Food Chemistry, 264*, 180-188.

Xiong, W. F., Ren, C., Jin, W. P., Tian, J., Wang, Y. T., Shah, B. R., Li, J., & Li, B. (2016). Ovalbumin-chitosan complex coacervation: Phase behavior, thermodynamic and rheological properties. *Food Hydrocolloids, 61*, 895-902.

Yang, J., Liu, G., Zeng, H., & Chen, L. (2018). Effects of high pressure homogenization on faba bean protein aggregation in relation to solubility and interfacial properties. *Food Hydrocolloids, 83*, 275-286.

Ye, A. Q., Flanagan, J., & Singh, H. (2006). Formation of stable nanoparticles via electrostatic complexation between sodium caseinate and gum arabic. *Biopolymers, 82*(2), 121-133.

You, G., Liu, X. L., & Zhao, M. M. (2018). Preparation and characterization of *hsian-tsao* gum and chitosan complex coacervates. *Food Hydrocolloids, 74*, 255-266.

Yuan, Y., Wan, Z.-L., Yang, X.-Q., & Yin, S.-W. (2014). Associative interactions between chitosan and soy protein fractions: Effects of pH, mixing ratio, heat treatment and ionic strength. *Food Research International, 55*, 207-214.

Zha, F., Dong, S., Rao, J., & Chen, B. (2019). Pea protein isolate-gum arabic Maillard conjugates improves physical and oxidative stability of oil-in-water emulsions. *Food Chemistry, 285*, 130-138.

Zhang, T., Xu, X., Li, Z., Wang, Y., Xue, Y., & Xue, C. (2018). Interactions and phase behaviors in mixed solutions of kappa-carrageenan and myofibrillar protein extracted from *Alaska Pollock* surimi. *Food Research International, 105*, 821-827.

CHAPTER 5. MICROENCAPSULATION OF HEMPSEED OIL BY PEA PROTEIN ISOLATE–SUGAR BEET PECTIN COMPLEX COACERVATION: INFLUENCE OF COACERVATION PH AND WALL/CORE RATIO

Abstract

The objective of this study was to investigate the impact of coacervation formation pH (3.5 and 2.5) and wall/core ratio (1:1, 2:1 and 4:1) on physicochemical properties of spray-dried hempseed oil (HSO) microcapsules by means of pea protein isolate (PPI)–sugar beet pectin (SBP) complex coacervates. In general, phase behaviors and viscoelastic properties of PPI–SBP coacervates were affected by the wall/core ratio. The microstructure of coacervates were highly dependent on the coacervation formation pH, which greatly impacted the spray drying efficiency (PY), encapsulation efficiency (EE), particle size, oil distributions in microcapsules, and the oxidative stability of HSO. At the pH_{opt} (3.5), PPI–SBP complex coacervates possess stronger and denser structure owing to the greater electrostatic interaction, whereas softer and smooth structure was formed at pH 2.5 as evidenced by rheological properties and FTIR. Because of the distinct microstructure of coacervates formed at different pH values, microcapsules spray-dried from coacervates prepared at pH 2.5 had a remarkable higher PY and EE than that formed at pH 3.5. However, the oxidative stability of HSO microcapsules prepared using the PPI–SBP coacervates fabricated at pH 2.5 was significantly shortened. This is because the weaker electrostatic interaction strength was formed at pH 2.5 between PPI–SBP, resulting in the partially broken PPI–SBP network caused by the spray drying process. As such, some hollow particle and incomplete particle shape was observed in SEM and CLSM image, which promoted the lipid oxidation of encapsulated HSO. In terms of wall/core ratio, the lower wall/core ratio

had lower EE, higher percentage of surface oil on microcapsules, and lower oxidative stability of HSO.

Introduction

Hemp (*Cannabis sativa* L.), has been cultivated as an oil plant in many countries (Liang, Appukuttan Aachary, & Thiyam-Holländer, 2015). In general, hempseeds contain 25–35% oil, more than 75% of which are polyunsaturated fatty acids (PUFA). Fatty acid composition of hempseed oil (HSO) is comprised of 53% of linoleic acid (LA, 18:2 n6), 12% of α-linolenic acid (ALA, 18:3 n3), and 4% of γ-linolenic acid (GLA, 18:3 n3) (Lan, Zha, et al., 2019). The LA to ALA ratio (3:1) of HSO represents the most desirable nutritional profile of lipids for human (Lan, Zha, et al., 2019). As a result, health benefits associated with the consumption of HSO have been well documented such as reducing the risk of cardiovascular and neurodegenerative disease (Lee, et al., 2011). However, PUFA in HSO are highly susceptible to oxidative degradation during food processing, storage, and transportation, and thus causing the loss of its biological functionality. This has imposed a great challenge in incorporation of HSO into functional foods.

Microencapsulation technology through biopolymer-based complex coacervates has proved to be a potential solution to protect labile bioactive compounds, including PUFA enriched healthy oils. The formation of complex coacervates is primarily induced by electrostatic attraction between two oppositely charged biopolymers such as protein and polysaccharide. Depending on the strength of electrostatic interaction, phase separation could occur which results in the formation of solvent-rich and biopolymer-rich phases. Biopolymer enriched phase, generally referred to as complex coacervates, can be used as a wall material to encapsulate bioactive compounds that are sensitive to loss their biological activity during food processing or

storage conditions. Typically, the fabrication of microcapsules through complex coacervation technique encompass multiple steps. In step 1, hydrophobic bioactive compound such as PUFA enriched health oil is mixed with protein–polysaccharide solutions at a proper mass ratio to form oil-in-water (O/W) emulsion. After that, pH adjustment is performed to promote complex coacervation between protein–polysaccharide. As a result, the optimum pH selection plays a crucial role on the functional performance of finished microcapsules as it determines the electrostatic interaction strength between biopolymers. For low biopolymer concentrations, the classic turbidimetric method has been applied to successfully identify the optimum pH for the formation of complex coacervation, including the pH range of complex coacervate formation and the pH condition (pH_{opt}) of maximum coacervates yield (Behrouzain, Razavi, & Joyner, 2020; Chang, Gupta, Timilsena, & Adhikari, 2016). This method, however, is inexpedient to identify these key pH parameters at concentrated biopolymer systems as the initial turbidity is too high to beyond the capacity of a spectrophotometer. This has challenged the application of complex coacervates in the area of microencapsulation where higher protein–polysaccharide mixture concentrations are often required to achieve greater coacervate yield because of wall (e.g., coacervates) to core (e.g., bioactive compounds) ratio effect (Bakry, Huang, Zhai, & Huang, 2019; Heckert Bastos, Vicente, Correa dos Santos, de Carvalho, & Garcia-Rojas, 2020; Soares, Siqueira, de Carvalho, Vicente, & Garcia-Rojas, 2019).

Currently, a large number of reported microcapsules are fabricated by adjusting pH to pH_{opt} which was identified at a low biopolymer concentration. This is under the assumption that pH_{opt} is independent of biopolymer concentrations but only mass ratio with regards to the formation of complex coacervates (Bakry, et al., 2019; Eratte, Wang, Dowling, Barrow, & Adhikari, 2014; Heckert Bastos, et al., 2020; Kaushik, Dowling, McKnight, Barrow, & Adhikari,

2016). For example, the pH_{opt} for fish myofibrillar protein–carrageenan (protein to polysaccharide ratio of 4:1) at 0.2 wt% of total biopolymer concentration was pH 5.0 according to turbidimetric method. This pH (5.0) was subsequently employed to encapsulate tuna oil at 5.0 wt% of total biopolymer concentration (Bakry, et al., 2019). Nevertheless, our previous study showed that both pH range and pH_{opt} of protein–polysaccharide complex coacervates formation were appreciably affected by total biopolymer concentrations (Lan, Chen, & Rao, 2018). Moreover, pH_{opt} of complex coacervate formation has become the widely accepted pH condition for the preparation of microcapsules (Bakry, et al., 2019; Heckert Bastos, et al., 2020; Kaushik, et al., 2016; Soares, et al., 2019). Intriguingly, our recent work showed that coacervates formed at the late stage of coacervates formation pH ($pH_{\varphi 2}$) afforded well organized and smooth microstructures compared with that obtained at the pH_{opt} in pea protein isolate (PPI)–sugar beet pectin (SBP) system (Lan, Ohm, Chen, & Rao, 2020). As very little information is available in terms of the impact of complex coacervates formation pH on physicochemical properties of microcapsules, we questioned if pH_{opt} is always the optimal pH condition for the purpose of microencapsulation by means of complex coacervation.

Furthermore, the majority of microencapsulated bioactive compounds are achieved using animal proteins, which may constrain their applications. Recently, plant proteins have gained popularity because of number of reasons such as low cost, health benefit to the consumers, sustainable resources and so on (Vainio, Niva, Jallinoja, & Latvala, 2016). Among all the plant proteins, pea protein is one of promising encapsulating materials due to their good emulsification properties and thermal stability (McCarthy, et al., 2016; Shevkani, Singh, Kaur, & Rana, 2015). In this study, PPI was selected as protein part of wall material to microencapsulate HSO. The PPI-SBP complex coacervates was chosen to be as wall material to encapsulate HSO because it

is a continuous study of PPI-SBP complex coacervation on the basis of our recent results (Lan, et al., 2020). The overall objective of this study was to understand the influence of pH during complex coacervates formation and the wall/core ratio on the physicochemical properties of microcapsules such as the encapsulation yield, efficiency, and microstructure of encapsulates, as well as the oxidative stability of encapsulated HSO.

Materials and methods

Materials

Yellow pea flour was purchased from Harvest Innovations (Indianola, Iowa, USA). Freeze-dried PPI was prepared from yellow pea flour based on alkali extraction–isoelectric precipitated method, and the protein content of PPI is ca. 79.50% (wet basis; conversion factor of 6.25%) (Lan, et al., 2018; Lan, et al., 2020). Sugar beet pectin (SBP) (Betapec RU301) was provided by Herbstreith & Fox KG (Neuenbürg, Germany) and used without any modification/purification. As stated by manufacturer, the pectin has degree of esterification (DE) and galacturonic acid content of 55% and 65%, respectively. Hempseed oil was solvent extracted using non-dehulled seeds from the crop year 2019. Nile red, Bodipy, polyethylene glycol (PEG, molecular weight of 400), and other chemicals (reagents) were of analytical grade and purchased from MilliporeSigma (St. Louis, MO). Ultrapure water was used for the preparation of all solutions (18.2 MΩ·cm, Thermo Fisher Scientific Inc., USA). All percent concentrations in this work were weight concentration (wt%) and all ratio between ingredients were on a basis of mass ratio unless stated otherwise.

Preparation of microencapsulated hempseed oil in PPI–SBP complex coacervates

Preparation of stripped hempseed oil (HSO) and biopolymer stock solution

The crude hempseed oil prepared by n-hexane extraction was further processed to strip off the minor constituents and impurities using column chromatograph following the previous reported method without any modification (Chen, McClements, & Decker, 2014). PPI stock solution (1.20%) and SBP stock solution (2.00%) were prepared by dissolving PPI or SBP powder, respectively, in phosphate buffer solution (pH 7, 10 mM) following a published procedure (Lan, et al., 2020).

Preparation of HSO-in-water (O/W) emulsions

HSO-in-water (O/W) emulsions were prepared using high pressure homogenization. In brief, PPI and SBP stock solutions were first mixed to achieve PPI to SBP mixing ratio of 5:1, and the total amount of biopolymer mixture was fixed at 1.20%. The different amount of stripped HSO (1.20%, 0.60%, or 0.30%) was added to the biopolymer mixtures to maintain the wall/core ratio of 1:1, 2:1, and 4:1, respectively. Subsequently, the mixture was pre-homogenized for 2 min at 8,000 rpm using a high-speed blender (M133/128–0, Biospec Products Inc., Switzerland), which was then further homogenized using a two-stage homogenizer at 5,500 psi for two passes (LAB 2000, APV–Gaulin, Wilmington, MA). The control emulsions were prepared which consisted of 1.00% PPI as wall material with various HSO contents (1.00%, 0.50%, and 0.25%) to achieve PPI/core ratio of 1:1, 2:1, and 4:1, respectively.

Optimizing the pH conditions for complex coacervation

The boundary pH range for the formation of PPI–SBP complex coacervate and the pH condition (pH_{opt}) of maximum coacervate yield were identified using state diagram and viscoelastic properties of coacervates, respectively, as described previously with a slight

modification (Lan, et al., 2020). In brief, 0.1% (w/v) Nile red was added into HSO-in-water emulsions to facilitate visualization of oil distribution in phase separation. The pH of the emulsion was adjusted from 5.0 to 2.0 with 0.5 decrement by the addition of HCl with various concentrations (0.1–2 N). The state diagram of complex coacervates was constructed in accordance to the visual observation after 24 h static stand at 4℃. Viscoelastic properties of complex coacervates were measured using a rheometer (DHR-2, TA Instruments Ltd., DE, USA) according to our previous work (Lan, et al., 2020). The pH_{opt} was defined as the pH condition where the highest G' was observed (Lan, et al., 2020).

Complex coacervation

To prompt complex coacervation between PPI and SBP, the pH of PPI–SBP stabilized emulsions were adjusted to pH 3.5 and 2.5, respectively, by applying 0.1–5 N HCl. Afterwards, emulsions were left to stand static for 24 h at 4 °C to allow phase separation and equilibrium. The control emulsions were adjusted the pH 7.0. The complex coacervates formation pH were determined according to result of previous section (Optimizing the pH conditions for complex coacervation).

Microencapsulation

In total, nine microcapsules (**Table 5-1**) were obtained by spray drying liquid complex coacervates and PPI controls. For the complex coacervates, the phase separation was observed and the supernatant was decanted after 24 h of equilibrium. The sediments were collected and concentrated by centrifuging at 153×*g* for 10 min (J2–HS, Beckman Inc., IN, USA) and the resulting supernatant was decanted. The residues were collected and magnetically stirred for 10 min, prior to feeding into a spray dryer (Büchi mini B–290, New Castle, DE, USA). PPI stabilized HSO-in-water emulsions at pH 7.0 were used as a control. The optimized drying

operation parameters were set as follows: air temperature of inlet (130 °C) and outlet (55 °C), peristaltic pump rate of 18% (about 0.39 L/h), nozzle diameter of 0.7 mm, and aspirator flow of 40 L/h. These spray-dried microcapsules and controls were collected and stored in glass bottles at 4 °C for further characterizations. The powder yield (PY) was calculated as shown below to determine the solid loss during spray drying (Kaushik, et al., 2016)

$$PY\% = (Wp)/(Ws) \times 100\%$$

Where Wp and Ws are the weight of powder collected after spray drying and the initial weight of solids in the dispersion prior to spray drying processing, respectively.

Table 5-1. Formulation and code of microcapsules.

Microcapsule formulation number	Mass ratio of wall to core	Wall materials (wt%)			Core materials (wt%)	Coacervation pH
		PPI	SBP	Total		
F1	1:1	1.00	0.20	1.20	1.20	3.5
F2	2:1	1.00	0.20	1.20	0.60	3.5
F3	4:1	1.00	0.20	1.20	0.30	3.5
F4	1:1	1.00	0.20	1.20	1.20	2.5
F5	2:1	1.00	0.20	1.20	0.60	2.5
F6	4:1	1.00	0.20	1.20	0.30	2.5
F7	1:1	1.00	–	1.00	1.00	–
F8	2:1	1.00	–	1.00	0.50	–
F9	4:1	1.00	–	1.00	0.25	–

Physiochemical properties of microcapsules

Encapsulation efficiency and pay load

The encapsulation efficiency (EE) and pay load (PL) were determined according to previous methods with some modifications (Timilsena, Adhikari, Barrow, & Adhikari, 2016; Xiao, Yu, & Yang, 2011). In order to precisely calculate the surface oil (Wso) content, 2.5 g of powder microcapsules was placed on a filter paper (Whatman No.1) within a funnel (diameter of 90 mm). Subsequently, the powder was thoroughly washed with 5 mL of n-hexane and the

filtrate was collected in a clean flask, which was subjected to an evaporation under vacuum using a Rotavapor (Buchi, Germany) and a further drying in an oven (100 °C for 30 min). The Wso was calculated by weight differences of the flask before and after filtrate in flask. Meanwhile, the oil content in the dried filtration residues (on the filter paper) was determined using an accelerated solvent extraction unit as reported previously without any modification (ASE 350, Dionex Corp., CA, USA) (Lan, Zha, et al., 2019). The total oil content of microcapsules was the sum of the measured Wso and the oil in the residues. The EE and PL was calculated as follows:

$$EE\% = (Wto-Wso)/Wto\times100\%$$

$$PL\% = (Wto/Wms)\times100\%$$

Where Wto, Wso, and Wms are the total oil content, the surface oil content, and the mass of microcapsule, respectively.

Moisture content and water activity

Moisture content was gravimetrically measured by heating 2.00 g of freshly spray-dried microcapsule in an oven at 105 °C until constant weight was reached. Water activity (A_w) of freshly spray-dried microcapsules were measured using a water activity meter (AquaLab, Decagon Devices Inc., WA, USA) at 25 °C.

Particle size

The particle size and size distribution of spray-dried microcapsules were measured using Mastersizer 3000 equipped with Hydro LV (Malvern Instrument, Worcester, UK) according to the method reported by Timilsena et al. with slight modifications (Timilsena, et al., 2016). In short, microcapsule powder was dispersed in a measuring chamber filled with water to reach an obscuration of 20%, followed by adjusting the stir speed to 3,500 rpm for 1 min to eliminate any

possible particle aggregation. The stir speed was then reduced to 1,050 rpm prior to measurement. The particle size and size distribution were recorded by the integrated software.

Fourier transform infrared spectroscopy (FTIR)

FTIR spectra of PPI, SBP, HSO, and selected microcapsules were collected using a Varian FTIR spectrophotometer equipped with an attenuated total reflectance accessory (Pike Technologies, Madison, WI, USA) following the procedure without any changes (Lan, Xu, Ohm, Chen, & Rao, 2019). Characteristic wavenumbers were selected for comparison study.

Morphological properties of microcapsules

Surface morphology of selected microcapsules was recorded using a scanning electron microscope (SEM) (JEOL Model JSM–6490LV, MA, USA) as reported previously (Lan, Xu, et al., 2019). Images at magnification of 5,000 × were selected as a representative for each sample. The oil distribution in microcapsules was observed using a confocal laser scanning microscope (CLSM) (LSM 700, Carl Zeiss Microscopy Ltd., Jena, Germany). Briefly, Rhodamine B (10 µg/mL) and Bodipy (1 µg/mL) solutions were prepared by dissolving in PEG. The spray-dried microcapsules were then placed at the bottom of micro-plate wells (µ-Plate 96 well, ibidi USA, Inc., Wisconsin). Subsequently, Bodipy and Rhodamine B solution with a same volume (100 µL) were pipetted into each well to label oil and protein, respectively. Finally, samples were observed at objective lens of 40 ×. The excitation wavelength of Bodipy and Rhodamine B were 488 nm and 555 nm, respectively. Images were acquired in 1024 × 1024 pixels. Z–stacks with a 16 µm penetration depth were applied to generate a three-dimensional (3-D) structure of microcapsules.

Mineral content

Copper and iron ions are two naturally occurring elements in pea protein and hemp seed oil. However, they are both transition metals which could accelerate lipid oxidation

(Mozuraityte, Kristinova, Standal, Carvajal, & Aursand, 2016). Therefore, copper and iron content in microcapsules were determined by atomic absorption spectroscopy. After an ash pretreatment, the samples were digested with perchloric acid and nitric acid. The digest solution was further analyzed on an atomic absorption spectrophotometer (ICAP 6300duo, Thermo Scientific Inc., USA). The mineral content was reported in ppm.

The oxidative stability of microencapsulated hempseed oil

Both hexanal and propanal were selected as the secondary oxidation product markers to quantitatively evaluate the oxidative stability of microencapsulated HSO since they are the major secondary oxidation products of linoleic acid and α-linolenic acid in HSO. Glass vials (20 mL) containing 0.5 g of samples were tightly closed with aluminum caps and PTFE/silicone septa. The samples were stored at 37 °C in an incubator (Isotemp, Fisher Scientific Inc., USA) for 15–25 day. The concentration of markers as a function of time was determined using Agilent 7890B GC-FID according to the method of Zha, Dong, Rao, and Chen (2019) with some modifications. Vials were preheated (55 °C, 10 min and 350 rpm) in an autosampler heating block (PAL RSI 85, CTC Analytics, Zwingen, Switzerland). Next, SPME fiber needle was injected in glass vials to absorb the volatiles for 50 min at 55 °C, followed by desorption of the volatiles at GC injector port (250 °C) for 3 mins in splitless mode. Thereafter, the volatiles were separated in a ZB-Wax column (60 m×0.25 mm i.d., 0.25 μm film thickness) with following temperature program: initial temp 40 °C, to 85 °C (45 °C/min), to 200 °C (9 °C/min), to 250 °C (45 °C/min), then held for 3 mins. The temperature of FID detector was set at 250 °C. The concentration of hexanal and propanal were calculated based on peak areas and linear regression equation and expressed as ppm (mg/kg sample). The standard calibration curves were prepared by following a previous method (Hillen, 2016) with slight modification. The standards were spiked in corn starch within

a concentration range of 1–25 ppm. The lag phase was determined by a sudden increase of the oxidation markers as a function of storage time.

Statistical analysis

The experiment was arranged in a completely randomized design with three replicates. All measurements were carried out in triplicate using freshly prepared samples and values were expressed as means ± standard deviation. Differences between means were significant at $p < 0.05$ according to t test, one–way analysis of variance (ANOVA), and F–protected LSD using SAS software (Version 9.3, SAS Institute Inc., NC, USA).

Results and discussion

Optimum pH for complex coacervation between PPI and SBP

Previous research strongly indicated that state diagram is a practical and plausible means to distinguish boundary pH range for complex coacervate of biopolymers such as PPI and SBP at concentrated solutions (2.0 wt%) (Lan, et al., 2020). Consequently, state diagram was applied in the current study to determine the impact of HSO concentrations (varied wall/ core ratio) on the boundary formation pH of PPI–SBP complex coacervates and their phase behaviors (**Fig. 5-1**). To better visualize the HSO distribution during phase separation, 0.1% (w/v) Nile red was added in HSO-in-water emulsion prior to pH adjustment. It should be noted that the total biopolymer concentration and the mass ratio of PPI to SBP were fixed at 1.20% and 5:1, respectively, in the entire experiments. Therefore, any ratio mentioned afterwards were wall/core ratio unless otherwise stated.

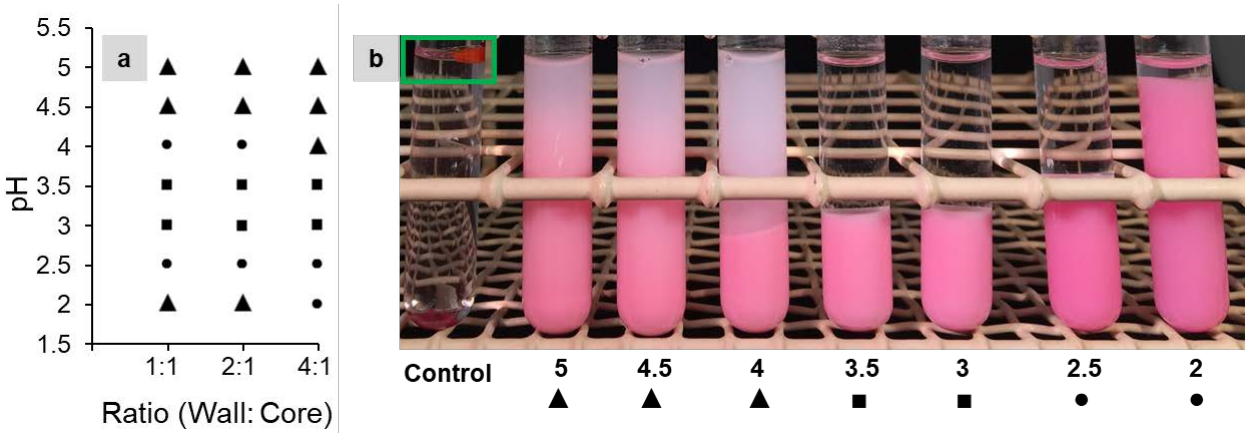

Figure 5-1. (a) State diagram of pea protein isolate (PPI)–sugar beet pectin (SBP) mixtures as function of pH (5.0–2.0) and wall/core mass ratios (4:1 to 1:1). (b) The appearance of PPI–SBP mixture (at wall/core ratio of 4:1) as function of pH observed after 24 h static standing at 4 °C. For all mixtures, PPI to SBP mixing ratio and the total biopolymer concentration was fixed at 5:1 and 1.20 wt%, respectively. Nile red (lipophilic dye) was added into both water &hem seed oil (HSO) mixture (control) and the microencapsulated HSO in PPI–SBP complex coacervate (pink color tubes) to aid for visualizing oil distribution during phase separation. Three symbols ▲, ■, and ● represents (i) precipitation & cloudy solution, (ii) precipitation & clear solution, and (iii) precipitation & clear solution containing higher volume of precipitation than ■, respectively.

Three different phase behaviors and appearances were observed in PPI–SBP mixtures at a wall/core ratio of 4:1 in the pH range of 5.0 to 2.0 (**Fig. 5-1b)**. These phase behaviors (▲, ■, and ● in **Fig. 5-1**) were all considered as complex coacervates bearing different structures as reported previously (Lan, et al., 2020). In the control sample where Nile red was simply mixed with water and HSO, a recognizable red color of ring was observed on the top of the test tube (**Fig. 5-1b as highlighted by green rectangle**). This is reasonable as Nile red is a lipophilic stain which only associates with oil floating on top of the mixture. By contrast, the image of biopolymer test tubes indicated that the majority of Nile red stayed at the bottom phase of coacervates, demonstrating the successful entrapment of HSO in complex coacervate phase rather than in solvent phase, which was consistent with the previous report (Timilsena, et al., 2016). This also suggested that Nile red is an appropriate indicator to visualize oil distribution during biopolymer phase separation. Using Nile red stain, the wall/core ratio dependent effect on the pH range of HSO–PPI–SBP complex coacervate formation was identified (**Fig. 5-1a**). For instance, the mixtures at

wall/core ratio 4:1 (the core HSO concentration was at 0.3%) showed same phase behaviors throughout the pH range (pH 5 to 2) with the PPI–SBP complex coacervates without added oil as reported previously (Lan, et al., 2020). This implied that a small amount of added oil (0.3%) had no effect on the phase behaviors of this tertiary system. Regarding the impact of added HSO concentration on phase behaviors of PPI-SBP coacervates, phase behaviors of coacervates changed at pH 4.0 (from ▲ to ●) and at pH 2.0 (from ● to ▲) as the wall/core ratio decreased from 4:1 to 1:1 by increasing the HSO concentration to 1.2%, suggesting the phase behaviors of complex coacervation was oil content dependent. This phenomenon could be explained by the conformational changes of SBP and/or PPI when exposed to hydrophobic species such as oils. Researchers have reported that proteinaceous moieties of SBP acted as anchors to attach at the oil–water interface upon the addition of oils, which resulted in conformational changes of SBP (Alba & Kontogiorgos, 2017). Such wall/core ratio dependent effect, which has not been previously discussed, might have potential impacts on the physicochemical properties of microcapsules by means of complex coacervation.

Microencapsulation of bioactive oils by complex coacervation were habitually prepared by adjusting pH to pH_{opt} that was identified at a lower biopolymer concentration system using spectrophotometer (Bakry, et al., 2019; Heckert Bastos, et al., 2020; Kaushik, et al., 2016; Soares, et al., 2019). The state diagram constructed for high concentration biopolymers does not provide the information about pH_{opt}. Alternatively, storage modulus (G′) and loss modulus (G″) of complex coacervates can be applied to predict the pH_{opt} of a concentrated biopolymer mixture. It is generally accepted that the values of G′ and G″ are proportional to the strength of electrostatic interaction between protein and polysaccharide (Raei, Rafe, & Shahidi, 2018). Higher values of G′ and G″ represent stronger electrostatic interaction, thus corresponding to the

greater coacervates yield. As such, viscoelastic properties of encapsulated HSO by complex coacervates at the pH range of 2.5–4.0 and under different wall/core ratio were measured (**Fig. 5-2**).

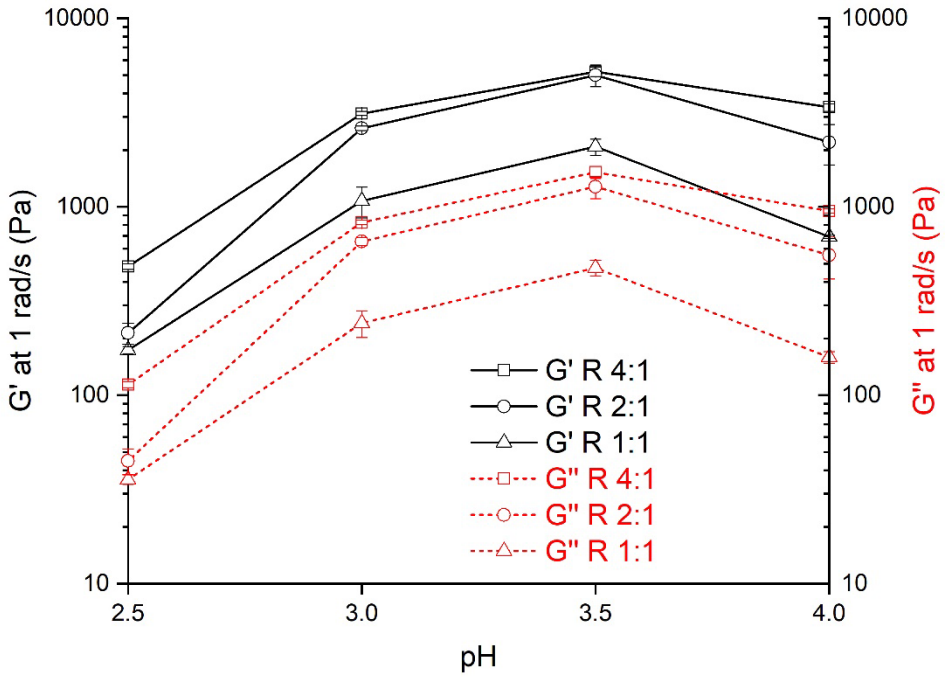

Figure 5-2. Impact of wall/core ratios on storage modulus (G′) and loss modulus (G″) of hemp seed oil (HSO) microcapsules by means of PPI–SBP coacervates at 1 rad/s frequency as a function of pH.

As one can see in **Fig. 5-2**, storage modulus (G′) of all coacervates at 1 rad/s was higher than loss modulus (G″), indicating a gel-like structure of coacervates with higher elasticity (Raei, et al., 2018; Rocha, Souza, Magalhaes, Andrade, & Goncalves, 2014; Ru, Wang, Lee, Ding, & Huang, 2012). In terms of impact of pH on viscoelastic properties of coacervates, the coacervates prepared at pH 3.5 had the highest G′, being independent of wall/core ratio (1:1 to 4:1). This result implied that the maximum electrostatic attraction between PPI and SBP was achieved and coacervates with strongest gel-like network structure were formed at pH 3.5 (Liu, Shim, Shen, Wang, & Reaney, 2017). Hence, pH 3.5 was defined as the pH_{opt} for the current ternary system and applied in the following microencapsulation study. Moreover, the lowest G′ of coacervates

appeared at pH 2.5 regardless of wall/core ratio (**Fig. 5-2**), suggesting that the coacervates prepared under this pH had a weaker gel-like network structure. Considering the distinct phase behaviors and viscoelastic properties of coacervates formed at different pH, both pH 3.5 and 2.5 were selected to compare the influence of coacervate structures on microencapsulation efficiency and oxidative stability of the encapsulated HSO.

The wall/core ratio also affected the viscoelastic properties of PPI–SBP complex coacervates (**Fig. 5-2**). In particular, both G′ and G″ reduced at the tested pH as the ratio reduced from 4:1 to 2:1 by increasing core HSO from 0.3% to 0.6%. They dropped dramatically when the ratio further reduced to 1:1 (HSO concentration increased to 1.2%). In other words, the more the HSO was encapsulated in PPI–SBP complex coacervates system, the lower the gel strength was. Similar observations were noticed in the previous study which was explained by the interference incurred by the presence of oil droplet on protein–polysaccharide electrostatic attraction in the gel matrix (Gani & Benjakul, 2018).

Encapsulation efficiency of microcapsules and their physicochemical properties

Physical properties of microcapsules are critical parameters determining their functional properties such as dispersibility, wettability, and the protective effect for bioactive compounds against environmental stress (Timilsena, et al., 2016). As such, moisture content, water activity (a_w), particle size and their distribution of the HSO microcapsules obtained after spray drying process were determined. In addition, the key indicators for the efficiency of spray drying process including powder yield (PY), encapsulation efficiency (EE), and pay load (PL), were also calculated.

Overall, powder yield of spray-dried HSO microcapsules ranged from 34.9% to 70.0% (**Table 5-2**), which was slightly higher than the previous report (35–52%) (Kaushik, et al., 2016).

The solid loss which determines the powder yield is inevitable and can occur in three parts during spray drying process including fine powder in cyclone, powders adhering to walls of drying chamber, and sediments to the bottom of the chamber (Tan, Chan, & Heng, 2005). Interestingly, the PY decreased as the wall/core ratio increased, indicating a positive correlation between PY and HSO concentration. For example, as the ratio rose from 1:1 to 4:1, the PY decreased from 47% to 35% for microcapsules prepared at pH 3.5 (F1-F3). This can be explained by the fact that HSO–PPI–SBP coacervates became sticky and congregated together with the increased oil content and the partial removal of water during spray drying process. For this reason, the powder easily stuck to the surface of dryer chamber (Tan, et al., 2005).

Table 5-2. Powder yield (PY), encapsulation efficiency (EE), pay load (PL) and physical properties of hemp seed oil (HSO) microcapsules.

Microcapsule formulation number	PY (%)	EE (%)	PL (%)	Moisture (%)	Water activity (A_w)	Particle size D_{50} (μm)
F1	47.3±6.6^{b}	79.65±5.99^{e}	34.44±3.18^{b}	1.97±0.22^{de}	0.14±0.003^{a}	12.80±2.17^{c}
F2	48.8±5.2^{b}	87.15±6.71^{ad}	23.39±2.14^{c}	1.92±0.26^{a}	0.14±0.002^{a}	14.02±1.53^{c}
F3	34.9±1.0^{c}	95.83±0.33^{a}	13.14±1.58^{d}	2.72±0.11^{ab}	0.13±0.001^{a}	23.70±1.23^{a}
F4	70.0±6.4^{a}	87.12±4.36^{ae}	35.65±3.45^{ab}	2.77±0.09^{e}	0.14±0.004^{a}	15.88±1.24^{b}
F5	66.1±5.0^{a}	92.43±4.40^{ab}	22.45±2.52^{c}	2.06±0.27^{c}	0.14±0.006^{a}	16.73±2.83^{b}
F6	60.0±4.2^{a}	94.42±6.63^{a}	11.98±1.03^{d}	2.50±0.33^{bc}	0.13±0.001^{a}	15.69±1.47^{b}
F7	60.1±2.1^{a}	83.05±1.72^{bde}	39.44±2.47^{a}	0.81±0.21^{e}	0.13±0.002^{a}	0.34±0.18^{d}
F8	46.9±8.8^{b}	81.58±3.47^{cde}	21.94±2.05^{c}	1.88±0.11^{cd}	0.15±0.001^{a}	0.28±0.05^{d}
F9	43.4±0.4^{bc}	89.88±7.77^{ac}	11.45±1.42^{d}	2.70±0.19^{ab}	0.13±0.003^{a}	0.20±0.05^{d}

† The values with different superscript letters within a column are significantly different (p<0.05).
‡ F1-F9 represent nine formulations listed in Table 5-1.

With respect to the coacervation formation pH, coacervates prepared at pH 3.5 (F1-F3) exhibited lower PY than did at pH2.5 (F4-F6). The possible explanation was that coacervates prepared at pH 3.5 yielded greater viscoelasticity than those prepared at pH 2.5 (**Fig. 5-2**). As a result, the condensed and high viscous coacervates was more prone to deposit on the bottom of spray drying chamber during the drying process. The encapsulation efficiency (EE) measures the

percentage of oil that is encapsulated inside the PPI–SBP coacervates matrix compared with total oil including surface oil and encapsulated oil, and a higher EE is preferable. Overall, HSO microcapsules formed by PPI–SBP coacervates (F2-F6) presented a higher EE compared with the control samples (F7-F9). Obviously, the wall/core ratio significantly affected the EE which raised dramatically upon the escalating of the wall/core ratio. For example, EE of microcapsules F1-F3 increased from 80 % to 96 % as the wall/core ratio rose from 1:1 to 4:1. A similar trend was also observed by other researchers. For example, by applying flaxseed protein–flaxseed gum coacervates to encapsulate flaxseed oil, Kaushik et al (Kaushik, et al., 2016) found that the EE increased from 73% (at a ratio of 2:1) to 87% (at a ratio of 4:1). Regarding the complex coacervate formation pH on EE, the coacervates F4 and F5 showed improved EE compared with F1 and F2, respectively. In our previous study, we examined the morphology of PPI–SBP complex coacervates obtained at pH 2.5 in the absence of oil using SEM which displayed homogeneous large pore size and smooth inner surface. We speculated it might have greater encapsulation capacity than that prepared at pH 3.5 (Lan, et al., 2020). The current results seem to corroborate the speculation that microstructure of complex coacervates is one of the critical factors contributing to the EE of microcapsules. Although there was no significant difference ($p>0.05$) between formation pH on EE at the ratio of 4:1 (F3 *versus* F5), this was understandable inasmuch as the small amount of oil (0.3%) could be adequately encapsulated by PPI–SBP coacervate matrix regardless of the microstructure. The pay load (PL) measures the percentage of oil content in total spray-dried microcapsules powder. The PL was in the range of 11–39% and was dependent of the wall/core ratio (**Table 5-2**). There was no significant difference among samples and controls at a same ratio. For example, at a wall/core ratio of 2:1, the PL of microcapsules F2, F5 and F8 were 23.39%, 22.45%, and 21.94%, respectively. This result

suggested that the centrifugation step for removing extra solvent prior to spray drying process does not cause any remarkable loss of HSO.

The moisture content and A_w ranged from 0.81–2.72%, and 0.13–0.15, respectively, which was consistent with other spray-dried microcapsules (Kaushik, et al., 2016; Timilsena, et al., 2016). The particle size and size distribution of microcapsules were also measured (**Table 5-2 and Fig. 5-3**).

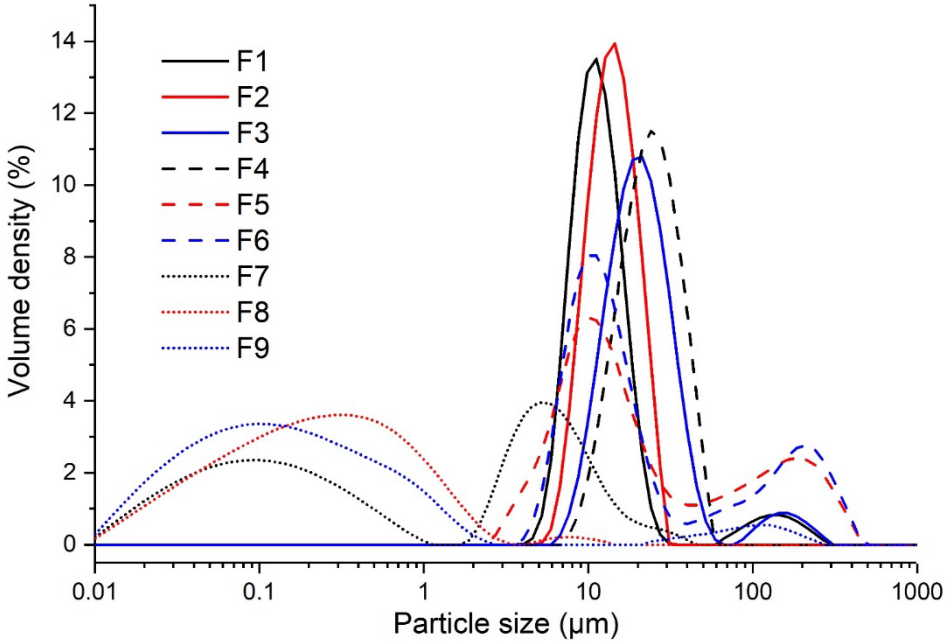

Figure 5-3. Particle size distribution of spray-dried hemp seed oil (HSO) microcapsules. F1-F9 represent nine formulations listed in Table 5-1.

As expected, microcapsules prepared by a single wall material PPI (F7-F9) had very small particle size compared to those produced by PPI–SBP coacervates. For instance, the particle size (D_{50}) of PPI encapsulated microcapsules fell in a narrow range of 0.20–0.34 μm, whereas the size of PPI–SBP coacervates formed microcapsules diverged from 12.80 to 23.70 μm (**Table 5-2)**. It has been reported that the particle size of microcapsules made by complex coacervate was higher than that of protein microcapsules (Bakry, et al., 2019), which can be

ascribed to the molecular weight difference between PPI–SBP coacervates and PPI. The liquid coacervates consisted of biopolymer PPI and SBP and thus had higher molecular weight and bulk density than PPI itself. In consequence, the liquid coacervates generally produce larger particle size of powder through spray drying (Timilsena, et al., 2016). It should be noted that the influence of the wall/core ratio and coacervation formulation pH on the particle size of microcapsules was not significant. Intriguingly, all HSO microcapsules by complex coacervates approach displayed a single or bimodal pattern with narrow curved particle size distribution. By contrast, PPI encapsulated HSO showed a wider particle size distribution containing three peak curves (**Fig. 5-3**), suggesting inhomogeneous droplet size of the powder, presumably because of the aggregation of PPI stabilized HSO-in-water emulsion droplets during spray drying process. The particle size distribution results manifested that SBP–PPI coacervates had greater protective effect against droplet aggregation during spray drying than that of PPI itself.

Additionally, FTIR spectra of controls (individual HSO, PPI, and SBP) and microcapsules (F1, F4, F7) were recorded to shed light on the interactions among oil, PPI, and SBP. The spectra of microcapsules prepared at different wall/core ratio showed great similarity (data was not shown). For this reason, only the spectra of microcapsules prepared at the wall/core of 1:1 was selected and reported in **Fig. 5-4**.

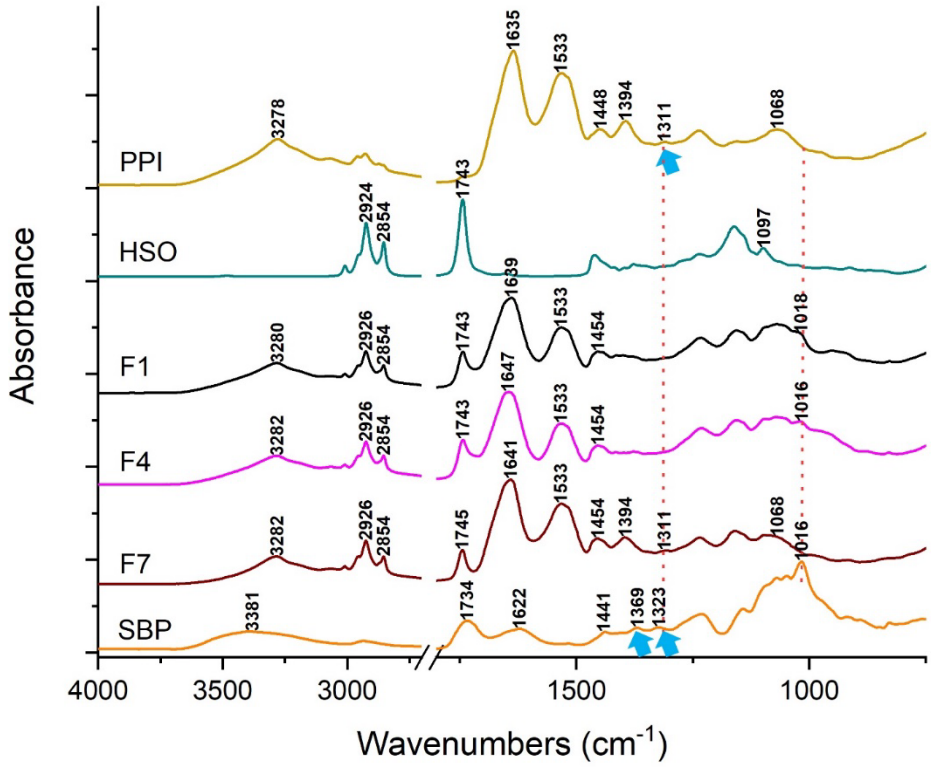

Figure 5-4. ATR–FTIR spectra of the hemp seed oil (HSO), PPI, SBP, PPI–SBP microcapsules (F1 and F4) and PPI microcapsules (F7). F1, F4, and F7 represent formulations listed in Table 5-1.

As shown in **Fig. 5-4**, the spectra of PPI and SBP were identical to our previous study (Lan, Xu, et al., 2019). The spectrum of HSO exhibited the featured C–H stretching vibrations of methyl and methylene groups at three wavenumbers of 3008, 2924, and 2854 cm^{-1}, C=O stretching of ester functional groups of lipids and fatty acids at 1743 cm^{-1}, and CH_2 out-of-plane deformation at 1161 cm^{-1} (**Fig. 5-3**) (Wang, Adhikari, & Barrow, 2019). The spectra of selected microcapsules (F1, F4, F7) presented all distinct wavenumbers of HSO, indicating the oil was successfully incorporated into microcapsules (**Fig. 5-3**). The spectrum of HSO microcapsule encapsulated by PPI as the sole wall material (F1) exhibited similar signals to that of PPI powder alone, except the former had the signals from HSO. Although the spectra of PPI–SBP coacervate microcapsules (F1 and F4) were dominated by the PPI, some peaks (e.g., N-H and C-N bending/stretching of PPI at 1311 cm^{-1}, and CH3 asymmetric stretching vibrations of SBP at

1369 and 1323 cm^{-1}) were disappeared, evincing the formation of complex coacervates between PPI and SBP (Mallamace, et al., 2015; Muhoza, et al., 2019). Additionally, the asymmetric and symmetric $–COO^-$ stretching vibrations of SBP (1620 and 1441 cm^{-1}) were disappeared as well in microcapsules fabricated by coacervates (F1&F4) and the peak of amide I in coacervates shifted towards the higher wavenumbers compared to that of the native PPI (**Fig. 5-3**). These changes occurred in carbonyl–amide region, suggesting that electrostatic interactions between the amino groups of PPI ($–NH_3^+$) and carboxylic groups of SBP ($–COO^-$) participated in the formation of complex coacervates (Espinosa-Andrews, Sandoval-Castilla, Vázquez-Torres, Vernon-Carter, & Lobato-Calleros, 2010; Souza & Garcia-Rojas, 2017; You, Liu, & Zhao, 2018). Furthermore, the "fingerprint region" of PPI–SBP coacervates showed a broad band (1010–1080 cm^{-1}), possibly because of signal superposition of PPI (peak at 1068 cm^{-1}, C–O stretching vibration) and SBP (peak 1016 cm^{-1}, C–O–C stretching vibration). These results again suggested that electrostatic interaction was involved in PPI–SBP coacervates formation (Bastos, de Carvalho, & Garcia-Rojas, 2018).

Morphological properties of microcapsules

The surface morphological properties of HSO microcapsule powders encapsulated by PPI or PPI–SBP complex coacervates as wall materials under variable pH were presented in **Fig. 5-5**. In the formulation F3 and F6, the small amount of oil (0.3%) in microcapsules did not impact on the surface morphology of the microcapsules compared with control according to our preliminary experiment results. As such, samples containing wall/core ratio of 1:1 and 2:1 were selected to evaluate the impact of pH (3.5 and 2.5) and the ratio on morphological properties of HSO microcapsule.

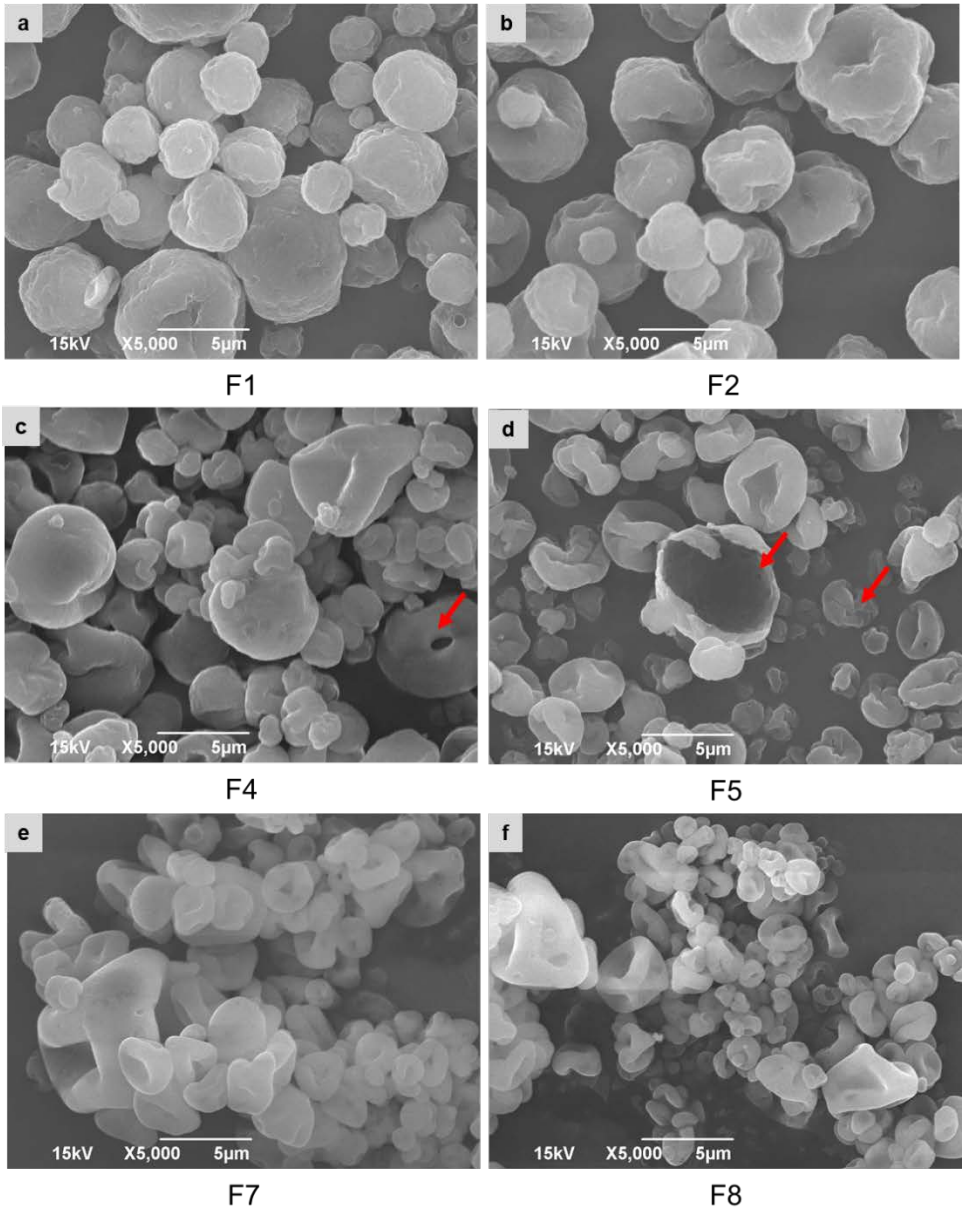

Figure 5-5. SEM of spray-dried HSO microcapsules by means of PPI–SBP coacervates (a–d) and HSO microcapsules by means of PPI as wall material (e–f). Bar represents 5 μm. Arrow was pointed as hollow and uncompleted particles. F1-F8 represent formulations listed in Table 5-1.

All microcapsules exhibited spherical shape with more or less dents on the surface (**Fig. 5-5**). The formation of dent on the surface of spray-dried powders is common and originates from the rapid evaporation of water during drying process, resulting in uneven shrinkage of particles (Cui, Kimmel, Zhou, Rao, & Chen, 2020). Overall, the wall/core ratio studied here had no remarkable impact on the surface morphology of microcapsules, agreeing with a previous

study (Kaushik, et al., 2016). However, wall materials exerted substantial effects on the surface features of the microcapsules. Comparing with microcapsules produced by complex coacervates, PPI microcapsules presented noticeable particle agglomerations with obvious dent surface morphology (**Fig. 5-5e & f**). This observation was also supported by the particle size distribution results where the boarder and multimodal particle size distributions of PPI microcapsules were obtained (**Fig. 5-3**).

With respect to the complex coacervates formation pH, microcapsules F4 prepared at pH2.5 (**Fig. 5-5c & d)** exhibited relative smooth surface with more dents on each particle; while F1 fabricated at pH3.5 showed less dent but more wrinkles and rough surface morphological properties (**Fig. 5-5a & b)**. In addition, some microcapsules with holes and/or unclosed particles were also found (**Fig. 5-5c & d**). These holes and non-integrity of particles were also reported in morphological properties of spray-dried whey protein isolate–gum arabic coacervates at pH 3.7, suggesting the interaction strength of PPI–SBP at pH 2.5 was weaker than that at pH 3.5 (Rojas-Moreno, Cardenas-Bailon, Osorio-Revilla, Gallardo-Velazquez, & Proal-Najera, 2018). Besides, higher viscoelasticity of liquid complex coacervates at pH 3.5 (**Fig. 5-2**) may also account for the compact structure with increased wrinkle surface of microcapsules since more condensed structure was built under this pH.

CLSM was applied to evaluate whether HSO was microencapsulated in SBP–PPI coacervate matrix, and to further understand the distribution of HSO droplets in spray-dried microcapsules.

The PPI (labelled red color) and HSO (labelled green color) in microcapsules were stained by Rhodamine B and Bodipy, respectively (**Fig. 5-6**). It should be noted that yellow to orange color in **Fig. 5-6** indicated the overlap of green and red signal. Each image is a 3-D

construction of microcapsules, which means a number of cross section images of microcapsules (around 15 µm depth) were recorded and stacked simultaneously as one z-axis of 3-D image. Hence, the overall percentage of green color in CLSM image and the brightness of green color perform as an indicator to illustrate the distribution of oil droplet in the microcapsules. For example, the brighter green color suggests the oil droplets are mainly located on the surface of microcapsules, as opposed to dimmer green color which indicates the oil droplets is buried in the microcapsules. In this experiment, the microcapsules prepared with the wall/core ratio of 1:1 and 2:1 of samples were selected to examine the impact of the formation pH and the wall/core ratio on HSO distribution in the microcapsules.

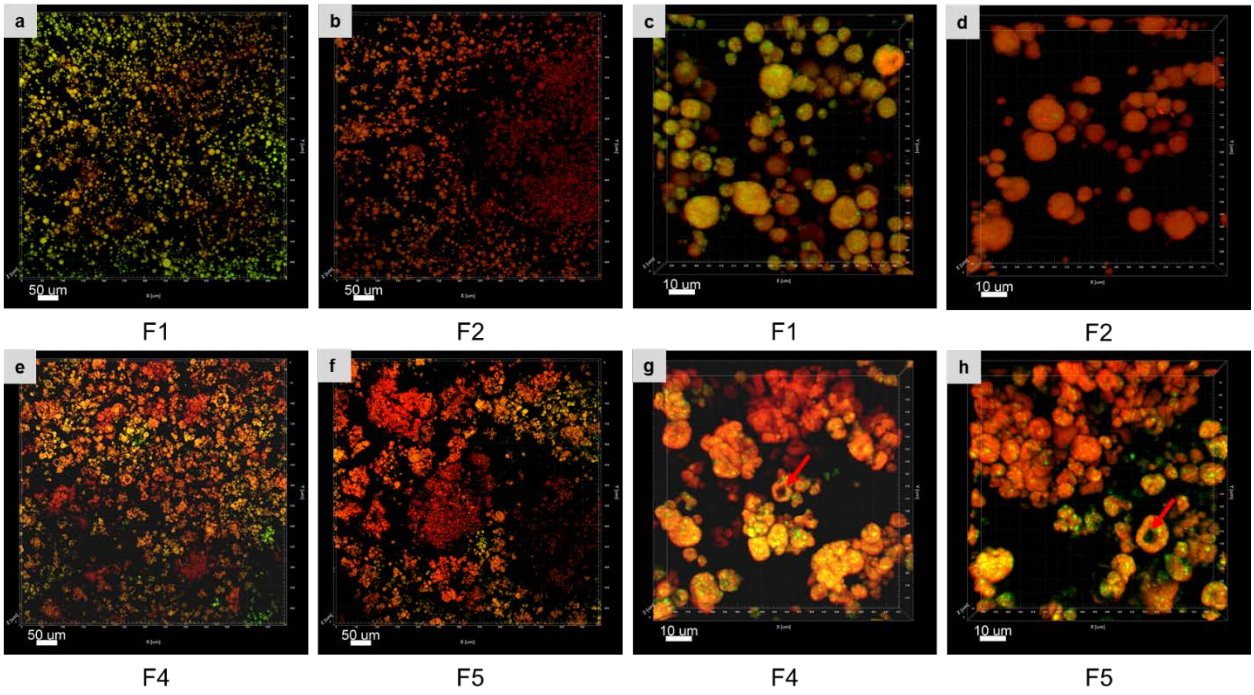

Figure 5-6. Three-dimensional confocal images of HSO microcapsules by means of PPI–SBP coacervates presented in full size (abef; size of 650×650×15 µm in x, y and z directions respectively) and smaller size (cdgh; 90×90×15 µm in x, y and z directions respectively). PPI and HSO were labelled as red and green color, respectively. Arrow was pointed as hollow and uncompleted particles. F1, F2, F4, and F5 represent formulations listed in Table 5-1.

Overall, both formation pH of complex coacervates and wall/core ratio greatly influenced the location of oil droplet within PPI–SBP coacervates matrix. Clearly, the wall/core ratio is a

predominant factor in determining the oil distributions in microcapsules. Compared to the microcapsules prepared at a wall/core ratio of 2:1 (**Fig. 5-6b**), a large amount of brighter green color appeared on microcapsules prepared at a lower wall/core ratio (1:1) (**Fig. 5-6a**). This result indicated that a higher percentage of oil droplets in F1 was located on the surface of microcapsules, which is in consistent with our EE% result (**Table 1**), the lower EE% was observed in F1 microcapsules. This was not surprising, given that more HSO was present and needed to be encapsulated in the matrix as the wall/core ratio decreased. The image observed in CLSM was also in accordance with our EE results (**Table 5-2**) where F1 had the lowest EE among all formulations. With regards to pH, dimmer green color of oil droplets was observed in microcapsules F2 prepared at pH 3.5 (**Fig. 5-6d**) than in F5 formulated at pH 2.5 (**Fig. 5-6h**). Furthermore, agreeing with our SEM results, some hollow centers were observed clearly in smaller size image of microcapsules F4&F5 (**Fig. 5-6g & h)**. Among all the tested samples, microcapsules F2 prepared at pH 3.5 and wall/core ratio of 2:1 presented the homogeneous orange appearance and dimmest green color (**Fig. 5-6b & d**), indicating HSO was encapsulated in the inner PPI–SBP matrix rather than being exposed on the surface.

Oxidative stability of HSO in microcapsules

Oxidative stability of microencapsulated polyunsaturated fatty acid is the principal quality parameter to evaluate the ability of wall material for protecting lipid oxidation of the core material. For this reason, the oxidative stability of microencapsulated HSO was evaluated by quantitatively measuring secondary oxidation products (hexanal and propanal) as a function of storage time during the elevated storage temperature (37 °C). For the purpose of differentiate oxidative ability among samples, the lag phase of hexanal and propanal formation was determined from the oxidation product markers measurements as the inflection point in the

concentration of markers versus storage time (day), and the lag phase was further plotted as the inserted table shown in **Fig. 5-7**. Generally, the higher oxidative stability is proportional to the longer lag phase (Cadenas & Sies, 1998).

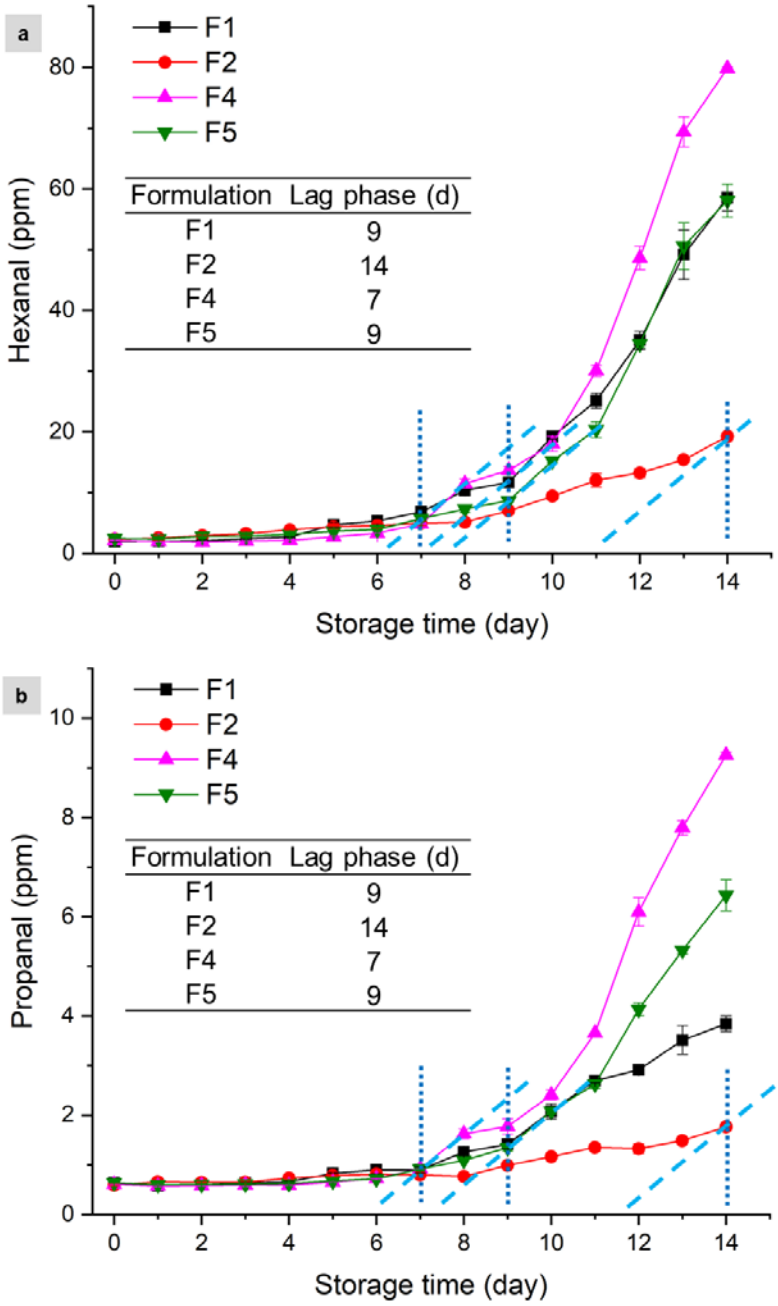

Figure 5-7. Formation of secondary oxidation product hexanal (a) and propanal (b) in HSO microcapsules by means of PPI–SBP coacervate as a function of storage time during storage at 37 °C. Some of standard error bars are within the data points. The lag phase of variants was calculated and inserted as table. F1, F2, F4, and F5 represent formulations listed in Table 5-1.

In general, similar kinetics were registered for the formation of both hexanal (**Fig. 5-7a**) and propanal (**Fig. 5-7b**) over the course of 14 days storage for all the tested formulations. The only contrasting difference was that the concentration of hexanal (0–80 ppm) was considerably higher than that of propanal (0–10 ppm) at a given time, which can be attributed by the higher percentage of n-6 PUFA in HSO (e.g., 53% of LA) as compared to n-3 ones (e.g., 12% of ALA) (Lan, Zha, et al., 2019). In comparison with coacervates prepared at different pH, the microcapsules prepared from coacervates at pH 3.5 (pH_{opt}) had longer lag phase than at pH 2.5. For example, the lag phase of F5 (pH 2.5) was 9 days, whereas 14 days of lag phase was measured in F2 (pH 3.5). The mineral analysis results precluded the possible impact of transition metals as both formulations had the same concentrations of copper and iron (**Table 5-3**). We therefore surmised that the oxidative stability of microencapsulated oil was primarily determined by viscoelastic and morphological properties of PPI–SBP complex coacervates formed at different pH. For SEM and CLSM results, coacervates formed at pH 3.5 featured condensed structure due to neutral aggregates of PPI and the extra hydrophobic interaction between PPI and SBP, which might have slowed down permeation of air passing through wall to core material. Apart from this, spray-dried microcapsules prepared from aggregates at pH 3.5 exhibited completed core–wall structure with homogeneous lipid distribution within coacervates matrix. As a result, the longer lag phase of encapsulated HSO was observed. On the other hand, holes and non-integrity of particles were observed in the spray-dried microcapsules (F4&F5) prepared from complex coacervates at pH 2.5. By applying these hollow and incomplete morphologies of particles for the purpose of microencapsulation, the oxygen could be easily diffused into the broken microcapsules to promote oxidation of encapsulated bioactive compound (Bakry, et al., 2019). As a result, the oxidative stability of HSO in those microcapsules might be reduced.

Table 5-3. Copper and iron content in microcapsules as determined by ICP–OES.

Formulation number	Cu ppm	Fe ppm
F1	2.33±0.17[c]	105.06±11.32[b]
F2	3.26±0.08[b]	126.85±6.63[a]
F4	2.79±0.33[bc]	87.89±4.64[c]
F5	2.96±0.15[b]	117.03±0.55[ab]
F8	4.20±0.10[a]	125.84±2.10[a]

† The content of each mineral was calculated on a dry basis.
‡ F1, F2, F4, F5 and F8 represent formulations listed in Table 5-1.

With regards to the wall/core ratio, the lag phase of microcapsules prepared at a ratio of 1:1 (1.2% of HSO) was shorter than those at 2:1 (0.6% of HSO). This result was reasonable because higher HSO concentration was subject to a faster lipid oxidation. Interestingly, the lag phase of F1 (1.2% of HSO) had the same lag phase as F5 (0.6% of HSO), and again it indicated that the coacervation formation pH strongly affected the oxidation stability of encapsulated oil. Besides, the lower EE and higher surface oil as observed through CLSM in F1 might also give rise to the shorter lag phase as compared with F5. On the ground of morphological properties of HSO microcapsules, microcapsules prepared by PPI–SBP complex coacervates at a wall/core ratio of 2:1 and pH 3.5 (F2) could be the best candidate to prevent the encapsulated bioactive lipids against lipid oxidation.

Conclusions

In this work, microencapsulation of HSO was successfully fabricated in PPI–SBP by means of complex coacervation. State diagram was constructed to determine the pH_{opt} of complex coacervation. The phase behaviors of complex coacervation was oil content dependent and a small amount of oil (0.30%) had no effect on the phase behaviors of PPI–SBP system as compared to the ones in the absence of oil. PPI–SBP complex coacervation formation pH (3.5 *vs*

2.5) and wall/core ratio (1:1, 2:1, and 4:1) drastically affected the physicochemical properties of the finished spray-dried HSO microcapsules. The higher wall/core ratio was associated with the higher viscoelastic properties of PPI–SBP coacervates. Meanwhile, the microstructure of coacervates were greatly influenced by the coacervation formation pH. As a result, technical parameters of microencapsulation such as powder yield (PY), encapsulation efficiency (EE), and oil distributions in microcapsules, as well as the oxidative stability of encapsulated HSO showed distinct outcomes. The microcapsules spray-dried from PPI–SBP coacervates at pH 2.5 showed improved EE than from the ones at pH 3.5. This was because homogeneous larger pore size and smooth inner surface of coacervates was constructed at pH 2.5. However, holes and/or partially broken particles were observed in spray dried microcapsules prepared at pH 2.5 due to the rupture of the weaker strength of electrostatic interaction between PPI–SBP during spray drying process, as evidenced by SEM and CLSM. Hence, the resulting microcapsules may not be a great candidate to protect labile bioactive compounds from oxidation as compared to these prepared at pH 3.5. The selection of wall/core ratio and coacervation formation pH is thus utmost important and should be determined considering the balance between the technical performance and the oxidative stability of the core material.

References

Alba, K., & Kontogiorgos, V. (2017). Pectin at the oil-water interface: Relationship of molecular composition and structure to functionality. *Food Hydrocolloids, 68*, 211-218.

Bakry, A. M., Huang, J. J., Zhai, Y. Y., & Huang, Q. L. (2019). Myofibrillar protein with kappa- or lambda-carrageenans as novel shell materials for microencapsulation of tuna oil through complex coacervation. *Food Hydrocolloids, 96*, 43-53.

Bastos, L. P. H., de Carvalho, C. W. P., & Garcia-Rojas, E. E. (2018). Formation and characterization of the complex coacervates obtained between lactoferrin and sodium alginate. *International Journal of Biological Macromolecules, 120*, 332-338.

Behrouzain, F., Razavi, S. M. A., & Joyner, H. (2020). Mechanisms of whey protein isolate interaction with basil seed gum: Influence of pH and protein-polysaccharide ratio. *Carbohydrate Polymers, 232*, 115775.

Cadenas, E., & Sies, H. (1998). The lag phase. *Free Radical Research, 28*(6), 601-609.

Chang, P. G., Gupta, R., Timilsena, Y. P., & Adhikari, B. (2016). Optimisation of the complex coacervation between canola protein isolate and chitosan. *Journal of Food Engineering, 191*, 58-66.

Chen, B., McClements, D. J., & Decker, E. A. (2014). Impact of diacylglycerol and monoacylglycerol on the physical and chemical properties of stripped soybean oil. *Food Chemistry, 142*, 365-372.

Cui, L., Kimmel, J., Zhou, L., Rao, J., & Chen, B. (2020). Combining solid dispersion-based spray drying with cyclodextrin to improve the functionality and mitigate the beany odor of pea protein isolate. *Carbohydrate Polymers, 245*, 116546.

Eratte, D., Wang, B., Dowling, K., Barrow, C. J., & Adhikari, B. P. (2014). Complex coacervation with whey protein isolate and gum arabic for the microencapsulation of omega-3 rich tuna oil. *Food & Function, 5*(11), 2743-2750.

Espinosa-Andrews, H., Sandoval-Castilla, O., Vázquez-Torres, H., Vernon-Carter, E. J., & Lobato-Calleros, C. (2010). Determination of the gum arabic–chitosan interactions by Fourier Transform Infrared Spectroscopy and characterization of the microstructure and rheological features of their coacervates. *Carbohydrate Polymers, 79*(3), 541-546.

Gani, A., & Benjakul, S. (2018). Impact of virgin coconut oil nanoemulsion on properties of croaker surimi gel. *Food Hydrocolloids, 82,* 34-44.

Heckert Bastos, L. P., Vicente, J., Correa dos Santos, C. H., de Carvalho, M. G., & Garcia-Rojas, E. E. (2020). Encapsulation of black pepper (*Piper nigrum* L.) essential oil with gelatin and sodium alginate by complex coacervation. *Food Hydrocolloids, 102,* 105605.

Hillen, C. (2016). *Sensory and quality attributes of deodorized pea flour used in gluten-free food products.* Unpublished Master of Science, North Dakota State University.

Kaushik, P., Dowling, K., McKnight, S., Barrow, C. J., & Adhikari, B. (2016). Microencapsulation of flaxseed oil in flaxseed protein and flaxseed gum complex coacervates. *Food Research International, 86,* 1-8.

Lan, Y., Chen, B., & Rao, J. (2018). Pea protein isolate–high methoxyl pectin soluble complexes for improving pea protein functionality: Effect of pH, biopolymer ratio and concentrations. *Food Hydrocolloids, 80,* 245-253.

Lan, Y., Ohm, J. B., Chen, B. C., & Rao, J. J. (2020). Phase behavior and complex coacervation of concentrated pea protein isolate-beet pectin solution. *Food Chemistry, 307,* 125536.

Lan, Y., Xu, M., Ohm, J.-B., Chen, B., & Rao, J. (2019). Solid dispersion-based spray-drying improves solubility and mitigates beany flavour of pea protein isolate. *Food Chemistry, 278,* 665-673.

Lan, Y., Zha, F., Peckrul, A., Hanson, B., Johnson, B., Rao, J., & Chen, B. (2019). Genotype x environmental effects on yielding ability and seed chemical composition of industrial hemp (*cannabis sativa* L.) varieties grown in North Dakota, USA. *Journal of the American Oil Chemists' Society, 96*(12), 1417-1425.

Lee, M. J., Park, S. H., Han, J. H., Hong, Y. K., Hwang, S., Lee, S., Kim, D., Han, S. Y., Kim, E. S., & Cho, K. S. (2011). The effects of hempseed meal intake and linoleic acid on Drosophila models of neurodegenerative diseases and hypercholesterolemia. *Molecules and cells, 31*(4), 337-342.

Liang, J., Appukuttan Aachary, A., & Thiyam-Holländer, U. (2015). Hemp seed oil: Minor components and oil quality. *Lipid Technology, 27*(10), 231-233.

Liu, J., Shim, Y. Y., Shen, J. H., Wang, Y., & Reaney, M. J. T. (2017). Whey protein isolate and flaxseed *(Linum usitatissimum* L.) gum electrostatic coacervates: Turbidity and rheology. *Food Hydrocolloids, 64*, 18-27.

Mallamace, F., Corsaro, C., Mallamace, D., Vasi, S., Vasi, C., & Dugo, G. (2015). The role of water in protein's behavior: The two dynamical crossovers studied by NMR and FTIR techniques. *Computational and Structural Biotechnology Journal, 13*, 33-37.

McCarthy, N. A., Kennedy, D., Hogan, S. A., Kelly, P. M., Thapa, K., Murphy, K. M., & Fenelon, M. A. (2016). Emulsification properties of pea protein isolate using homogenization, microfluidization and ultrasonication. *Food Research International, 89*, 415-421.

Mozuraityte, R., Kristinova, V., Standal, I. B., Carvajal, A. K., & Aursand, M. (2016). Chapter 5 - Oxidative Stability and Shelf Life of Fish Oil. In M. Hu & C. Jacobsen (Eds.), *Oxidative Stability and Shelf Life of Foods Containing Oils and Fats* (pp. 209-231): AOCS Press.

Muhoza, B., Xia, S. Q., Cai, J. B., Zhang, X. M., Duhoranimana, E., & Su, J. K. (2019). Gelatin and pectin complex coacervates as carriers for cinnamaldehyde: Effect of pectin

esterification degree on coacervate formation, and enhanced thermal stability. *Food Hydrocolloids, 87*, 712-722.

Raei, M., Rafe, A., & Shahidi, F. (2018). Rheological and structural characteristics of whey protein-pectin complex coacervates. *Journal of Food Engineering, 228*, 25-31.

Rocha, C. M. R., Souza, H. K. S., Magalhaes, N. F., Andrade, C. T., & Goncalves, M. P. (2014). Rheological and structural characterization of agar/whey proteins insoluble complexes. *Carbohydrate Polymers, 110*, 345-353.

Rojas-Moreno, S., Cardenas-Bailon, F., Osorio-Revilla, G., Gallardo-Velazquez, T., & Proal-Najera, J. (2018). Effects of complex coacervation-spray drying and conventional spray drying on the quality of microencapsulated orange essential oil. *Journal of Food Measurement and Characterization, 12*(1), 650-660.

Ru, Q. M., Wang, Y. W., Lee, J., Ding, Y. T., & Huang, Q. R. (2012). Turbidity and rheological properties of bovine serum albumin/pectin coacervates: Effect of salt concentration and initial protein/polysaccharide ratio. *Carbohydrate Polymers, 88*(3), 838-846.

Shevkani, K., Singh, N., Kaur, A., & Rana, J. C. (2015). Structural and functional characterization of kidney bean and field pea protein isolates: A comparative study. *Food Hydrocolloids, 43*, 679-689.

Soares, B. D., Siqueira, R. P., de Carvalho, M. G., Vicente, J., & Garcia-Rojas, E. E. (2019). Microencapsulation of sacha inchi oil (*Plukenetia volubilis* L.) using complex coacervation: Formation and structural characterization. *Food Chemistry, 298*, 125045.

Souza, C. J. F., & Garcia-Rojas, E. E. (2017). Interpolymeric complexing between egg white proteins and xanthan gum: Effect of salt and protein/polysaccharide ratio. *Food Hydrocolloids, 66*, 268-275.

Tan, L. H., Chan, L. W., & Heng, P. W. S. (2005). Effect of oil loading on microspheres produced by spray drying. *Journal of Microencapsulation, 22*(3), 253-259.

Timilsena, Y. P., Adhikari, R., Barrow, C. J., & Adhikari, B. (2016). Microencapsulation of chia seed oil using chia seed protein isolate-chia seed gum complex coacervates. *International Journal of Biological Macromolecules, 91*, 347-357.

Vainio, A., Niva, M., Jallinoja, P., & Latvala, T. (2016). From beef to beans: Eating motives and the replacement of animal proteins with plant proteins among Finnish consumers. *Appetite, 106*, 92-100.

Wang, B., Adhikari, B., & Barrow, C. J. (2019). Highly stable spray dried tuna oil powders encapsulated in double shells of whey protein isolate-agar gum and gellan gum complex coacervates. *Powder Technology, 358*, 79-86.

Xiao, J. X., Yu, H. Y., & Yang, J. A. (2011). Microencapsulation of sweet orange oil by complex coacervation with soybean protein isolate/gum arabic. *Food Chemistry, 125*(4), 1267-1272.

You, G., Liu, X. L., & Zhao, M. M. (2018). Preparation and characterization of *hsian-tsao* gum and chitosan complex coacervates. *Food Hydrocolloids, 74*, 255-266.

Zha, F., Dong, S., Rao, J., & Chen, B. (2019). Pea protein isolate-gum arabic Maillard conjugates improves physical and oxidative stability of oil-in-water emulsions. *Food Chemistry, 285*, 130-138.

OVERALL CONCLUSION

Protein–polysaccharide complexes including soluble complexes and complex coacervates are the promising technology for improving protein functionality and protecting bioactive compounds, respectively. Previously, factors influenced on protein–polysaccharide complexes formation have been examined extensively in low biopolymer concentrations. Very limited information is available on concentrated biopolymer system of protein-polysaccharide complexes. However, to fulfill abovementioned applications, it generally requires high concentration of protein–polysaccharide solution. As such, the overall objective of this work was to investigate the phase behavior and physicochemical properties of protein–polysaccharide complexes. In our study, pea protein and pectin were chosen as protein and polysaccharide, respectively. In this work, pH (3–7), PPI–pectin mixing ratio (1:1 to 20:1), pectin type (HMP *vs* LMP) and biopolymer concentrations on phase behaviors of PPI–pectin mixtures were investigated. The microstructure, thermodynamic behavior, and non-covalent bonding of PPI–pectin soluble complex and complex coacervates were studied by SEM, ITC, and FTIR. In the end, the applications of improving PPI functionality by PPI–HMP soluble complexes and microencapsulation of HSO by PPI–SBP complex coacervates were explored.

The results indicated that pHs (pH_c, $pH_{\varphi 1}$ and $pH_{\varphi 2}$) of co-solubility, soluble complex and complex coacervate could be identified using the combination of state diagram and ζ–potential measurement at concentrated biopolymer solution. The pH_{opt}, a particular pH condition to maximize the formation of complex coacervates, could be recognized at the net charge neutrality of the mixed biopolymer solutions or the highest viscoelastic behaviors of biopolymer mixtures. The pHs shifted towards higher pH values as PPI–pectin mixing ratio increased from 1:1 to 20:1 and as PPI concentration increased from 0.05 % to 1.00 wt%. With regard to charge density of

pectin (HMP *vs* LMP), LMP showed earlier initial electrostatic interaction (higher pH_c and $pH_{\varphi 1}$) and lower dissolution pH for coacervates ($pH_{\varphi 2}$) than that of HMP due to higher overall charge density of LMP. Both ITC and FTIR analyses indicated that both soluble complexes and complex coacervates were formed through the electrostatic interaction between the nonspecific amine groups of PPI (NH_3^+) and the carboxyl groups of pectin ($–COO^-$), and hydrogen bonding was also involved in PPI–pectin complexation. Moreover, the microstructure of PPI–SBP complex coacervates showed that smooth inner pore surfaces with homogeneous large pore size distribution of complex coacervates could be formed at the late stage of coacervation when the environmental pH is near the $pH_{\varphi 2}$.

Ultimately, applications of PPI–pectin soluble complexes and complex coacervates were investigated. Firstly, we demonstrated that PPI–HMP soluble complexes expanded pH dependent solubility profile of PPI towards more acidic pH values. In addition, thermal stability of PPI slightly increased through the formation of PPI–HMP soluble complexes. Regarding the rheological properties, the PPI–HMP soluble complexes presented a shear thinning flow behavior and possessed slightly higher values than that of HMP or PPI alone. As for the microencapsulation by means of PPI–SBP complex coacervates, PPI–SBP complex coacervation formation pH (3.5 *vs* 2.5) and wall/core ratio (1:1, 2:1, and 4:1) significantly affected the physicochemical properties of the spray-dried HSO microcapsules. The microcapsules obtained from PPI–SBP coacervates formation pH 2.5 showed improved encapsulation efficiency (EE) than that of pH 3.5. However, holes and/or partially broken particles were observed in spray dried microcapsules prepared at pH 2.5 due to the rupture of the weaker strength of electrostatic interaction between PPI–SBP during spray drying process, as evidenced by SEM and CLSM. Hence, the resulting microcapsules may not be a great candidate to protect highly oxidized

bioactive compounds as compared to these prepared at pH 3.5. The selection of wall/core ratio and coacervation formation pH are thus the utmost important parameters for determining technical performance of complex coacervates.

Overall, this work could provide guidelines for understanding phase behaviors and structures of pea protein–polysaccharide complexes in a concentrated biopolymer system.

FUTURE WORKS

Our project developed some alternative methods (state diagram combining with zeta–potential and rheological measurements) to identify critical soluble complex and complex coacervation formation pHs at concentrated binary biopolymer system. The factors influencing pulse protein isolate–polysaccharide complex coacervates formation (e.g., pH, biopolymer ratio, and concentrations) and physiochemical properties of complexes were characterized. We also demonstrated the potential application of complexes. However, there is lack of information on mechanism of action of complexation between pea protein and polysaccharide. It is worth noting that the protein–polysaccharide complex coacervates are reversible as the change of environmental condition. For example, when the ionic strength or pH in the system are changed, the complex coacervates might be dissociated. Obviously, this limits the utilization of complex coacervates in the area of microencapsulation. Therefore, better understanding of the mechanism involving pea protein–polysaccharide complexation and cross linker type will help facilitate application of pea protein–polysaccharide complex coacervates in the area of microencapsulation. The future research directions are highlighted below:

(1) State diagram in conjunction with zeta–potential and rheological measurement were developed to identify critical transition pHs of complexes based on concentrated PPI–pectin system. But we do not know if these methods can be applied in diverse protein–polysaccharide systems. Therefore, one of our future work would test these methods in different plant protein–polysaccharide systems.

(2) Recently, Mession, Assifaoui, Cayot, and Saurel (2012) reported that different phase behaviors of the sodium alginate and pea globulin were observed by using different type of globulin from pea protein. For example, legumin–alginate and globulins–alginate had similar

phase boundary formation pH, but vicilin/convicilin–alginate system showed distinct phase behaviors compared with above-mentioned two biopolymer systems. As a result, different protein composition in pea protein might affect the formation and functional properties of pea protein–polysaccharide complexes. Thus, it is necessary to purify the protein fractions from pea proteins and study phase behaviors of pea protein fraction–polysaccharide system.

(3) By adding covalent bonds, it makes the complex coacervates more stable against environmental changes and during the food processing. Therefore, the other future research direction would be creating PPI–pectin complexes using food grade cross linking agent.

References

Mession, J. L., Assifaoui, A., Cayot, P., & Saurel, R. (2012). Effect of pea proteins extraction and vicilin/legumin fractionation on the phase behavior in admixture with alginate. *Food Hydrocolloids, 29*(2), 335-346.